POLITECNICO DI MILANO

II Facoltà di Ingegneria

Corso di Laurea in Ingegneria Fisica

Dipartimento di Fisica

Role of Oxygen Vacancies in EuO Thin Films

Relatore: Prof. Giacomo Claudio Ghiringhelli
Correlatore: Prof. Dr. Liu Hao Tjeng

Tesi di Laurea di
Valerio Oliana
Matricola 736843

Anno accademico: 2010-2011

to my parents

Contents

List of Figures

List of Tables

Abstract

Europium Oxide (EuO) is a ferromagnetic semiconductor with a Curie Temperature (T_C) of 69 K and a band gap of 1.2 eV at room temperature. Upon electron doping it shows spectacular metal-insulator transition (MIT) at T_C and colossal magnetoresistance (CMR), whereas the change in resistivity can exceed 13 orders of magnitude. The exchange splitting of about 0.6 eV of the conduction band in the ferromagnetic phase leads in Eu-rich EuO thin films to obtain 100% spin polarized conduction current, thus making of EuO a promising material for spintronics applications. The Curie temperature can be enhanced by doping with rare earths, e.g. Gd, and by exerting hydrostatic pressure.

The present thesis describes the work I carried out in the group of Prof. Liu Hao Tjeng at the II Institute of Physics of the University of Cologne in cooperation with the Max Planck Institute of Dresden (Germania). It deals with the growth of Europium Monoxide thin films and in particular with the correlation of temperature dependent transport and magnetic properties with the oxygen deficiency concentration in electron-doped Eu-rich EuO thin films. The films were prepared on YSZ(100) substrates using the Molecular Beam Epitaxy (MBE) techinique under Ultra High Vacuum (UHV) condition, which allows to grow single-crystalline EuO films with fine-tunable stoichiometry. A wide range Eu-rich EuO samples with different stoichiometry were grown, by systematically varying the oxygen pressure and substrate temperature. The quality of the films was monitored by means of surface sensitive electron diffraction techniques, i. e. Reflection High Energy Electron Diffraction (RHEED) and Low Energy Electron Diffraction (LEED). Subsequently the spectroscopic, transport and mangetic of each film were analyzed by means of X-Ray Photoemission Spectroscopy (XPS), resistance and Superconducting Quantum Interference Device (SQUID) measurements, respectively. Those properties were then related to the oxygen vacancy concentration, in order to find out the limiting concetration leading to MIT to occurr.

L'Ossido di Europio (EuO) appartiene alla rara categoria dei semiconduttori ferromagnetici. Presenta un band gap pari a 1.2 eV e una temperatua di Curie (T_C) di 69 K, al di sotto della quale si osserva una transizione della magnetizzazione dallo stato paramagnetico a quello ferromagnetico. La magnetizzazione in funzione della temperatura M(T) segue fedelmente l'andamento della funzione di Brillouin derivata dalla teoria di Campo Medio secondo il modello di Weiss. Per via della forte localizzazione degli stati atomici $4f$ inoltre l' EuO è considerato un modello perfetto di ferromagnete di Heisemberg. A seguito del dopaggio tramite donori tale materiale presenta effetti spettacolari: una transizione da semiconduttore a metallo (MIT) al di sotto di T_C ed una colossale magnetoresistenza (CMR), mentre la resistività può variare fino a 13 ordini di grandezza. Lo splitting della banda di conduzione pari a 0.6 eV, in seguito al forte effetto Zeeman nella fase ferromagnetica, porta i film di Eu-rich EuO ad avere una corrente di conduzione completamente polarizzata. Questo rende l' Ossido di Europio un promettente materiale per lo studio e lo sviluppo di applicazioni nella spintronica. La temperatura di Curie può essere aumentata tramite dopaggio con terre rare, in particolar modo con il Gadolinio, che presenta la stessa configurazione elettronica $4f^7$ e non comporta pertanto disordine nell'allineamento ferromagnetico.

Il presente lavoro descrive l'attività svolta presso il gruppo del Prof. Liu Hao Tjeng presso il II Instituto di Fisica dell'università di Colonia in collaborazione con il Max Planck Institute di Dresda (Germania).

Esso riguarda la crescita di film sottili di Ossido di Europio, le cui proprietà generali sono brevemente illustrate nel Capitolo 1. In particolare il lavoro svolto riguarda la correlazione delle proprietà di trasporto e magnetizzazione in dipendenza della temperatura con la concentrazione di vacanze di ossigeno in campioni di Eu-rich EuO. La preparazione dei film, descritta ampiamente nel Capitolo 2, è stata realizzata crescendoli su substrati di YSZ(100) tramite Molecular beam Epitazy (MBE) in condizioni di vuoto estremo (UHV), tecnica che permette di crescere film di EuO a struttura cristallina singola e di regolarne precisamente la stochiometria. In particolar modo per la crescita di film stochiometrici viene utilizzata la tecnica di *distillazione* la quale, per via dell' elevata temperatura del substrato, permette agli atomi di Europio in eccesso di rievaporare dal substrato fintanto

che non incontrano un atomo di ossigeno con cui reagire e formare l'ossido divalente $Eu^{2+}O^{2-}$ in rapporto 1:1.

I capitoli 3 e 4 descrivono le tecniche di caratterizzazione, *in-situ* ed *ex-situ* rispettivamente, dei campioni. La qualità dei film viene monitorata per mezzo di tecniche con sensitività superficiali quali Reflection High Energy Electron Diffraction (RHEED) e Low Energy Electron Diffraction (LEED). La prima viene impiegata durante la crescita del film e permette di monitorarne la crescita, mentre la seconda viene impiegata solo in un secondo momento e fonrisce inforazioni sulla struttura cristallina.

Successivamente per ogni campione vengono analizzate le proprietà spettroscopiche, magnetiche e di trasporto per mezzo di tecniche specifiche: Photoemissione a Raggi X (XPS) per le prime, Superconducting Quantum Interference Device (SQUID) per le seconde, e misure di resistività per le ultime.

Il capitolo 5 riporta invece i risultati sperimentali ottenuti in relazione ai set di campioni cresiciuti. Sono stati preparati una serie di campioni variandone sistematicamente le condizioni di crescita, quali la pressione dell'ossigeno P_{O2} e la temperatura del substrato T_S, e con esse la stochiometria e quindi la concentrazione di vacanze di ossigeno nella struttura cristallina.

Dall'analisi delle proprietà di trasporto e correlandole con la concentrazione di vacanze di ossigeno siamo stati in grado di identificare la concentrazione limite di drogaggio che permette il verificarsi della transizione metallo-isolante nei film di Eu-rich EuO. Tale concentrazione si è rivelata essere pari al 20%, come riportato in dettagli nel capitolo conclusivo.

Chapter 1

Introduction

In this chapter, the main features of the ferromagnetic semiconductor europium monoxide (EuO) are presented. Far from being a complete and detailed description of this compound, attention will be paid on those properties that are being investigated in the following chapters, and attracted quite a number of researchers since the very beginning of its discovery.

Europium Monoxide is a fascinating compound in which dependence of macroscopic properties on electronic structure is especially manifest, as it experiences a phase transition at which a change in electronic structure is accompained by tremendous changes in magnetic, optical and transport properties[25]. Besides these spectacular effects, it can be also considered as a model for ionic ferromagnetic semiconductors, being a clear realization of the Heisemberg ferromagnet. Additionally is one of the simplest representatives of a ferromagnetic material where the transition from paramagnetic to ferromagnetic state at the Curie temperature is accompained by a change from a semiconducting to metallic behaviour, also known as Metal-Insulator transition (MIT). This change in conductivity is also linked with a spin polarization of the conduction carriers in the ferromagnetic state, that, together with it colossal magneto-resistance effect, makes EuO an interesting material for applications in spin-based electronics.

Its properties were widely investigated in the last fourty years , but even though a large amount of work has already been done, some mechanism are still not fully understood and some controverse opinions exsist about them. For istance the effect of doping on increasing T_C or the physical nature of the metal insulator transition remain under debate.

However it is meant to realize that one of the main challenges with this compount is its creation, since it does not exist in nature and easily reacts in air. Therefore it has to be grown in thin film form using techniques like Molecular Beam Epitaxy, and kept under ultra-high vacuum conditions to avoid its oxidation into non stochiometric EuO compunds, giving rise to many defective physical properties.

1.1 Overview of the Properties of EuO

Stochiometric Europium Oxide is a paramagnetic semiconductor, with a band gap of 1.2 eV at room temperature [2] [3] and becomes ferromagnetic below a Curie temperature T_C of 69 K [7]. Here the magnetism originates from the Eu^{2+} ions. In the ferromagnetic state, there exist a spin splitting of the conduction band, resulting in a decrease and increase of the spin-up and spin-down band gap, respectively.

The existence of a material of this type, a *ferromagnetic semiconductor*, was severely disputed in the mid fifthies, since the localized nature of electrons in insulators and semiconductors could not explain the ferromagnetic state by exchange mechanism via free electrons as it is in metals. When EuO was discovered by Matthias *et. al* [4] in the sixties, it opened the door also for the other members of Eu chalcogenides group to be recognized as magnetically ordered semiconductors. However it was in 1964 that Wachter [2] and Bush [8] *et. al* gave experimental evidence that Eu calchogenides remained semiconductor also below their respective magnetic ordering temperatures, by means of optical absorption measurements. These experiments gave first also evidences of a magneto-optical phenomena, namely the red-shift of the absorption edge upon cooling below T_C.

1.1.1 Crystal Structure and Growth

EuO crystallizes in a rocksalt structure with a lattice constant of 5.144 A at room temperature, which reduces to 5.127 A below 10 K. In Rocksalt structure, as can be seen in Figure 1.1, each of the two species forms a face-centered cubic crystal lattice, interpenetrating one each other and shifted by an amout of half of the lattice parameter. In this configuration, the Eu^{2+} ions are octaedrally surrounded by divalent O^{2-} ions, and the density of Eu atoms is 44% higher than in Eu metal.

It was shown that homogeneous EuO single crystals can be grown at temperature of around 1800 ℃, and the stochiometry of the compound depends significantly on the growth temperature, and the starting composition.A slight deviation from the required conditions results in the formation of either oxygen-rich or europium-rich compounds, Eu clusters, Eu_3O_4 or Eu_2O_3 phases, as it is shown in the pahse diagram by Shafer *et. al* [14] in Figure1.2.

More recently attempts to grow EuO thin films were made, and different vacuum deposition techniques were employed, like heating bulk EuO using an electron beam, simultaneous evaporation of Eu and Eu_2O_3, and reactive evaporation in oxygen athmosphere.
In the last decades thin films preparation technologies, in particular Molecu-

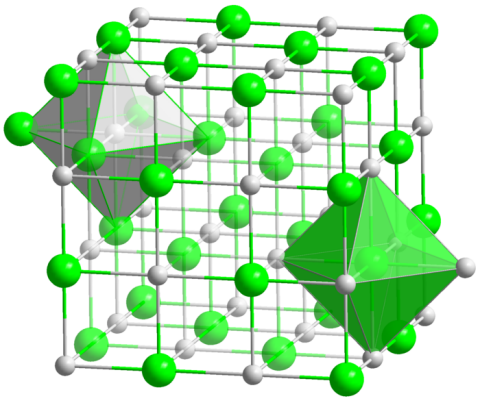

Figure 1.1: Rocksalt crystal structure of EuO. In this ionic bond alloy, Eu^{2+}(green) atoms ar surrounded by 8 O^{2-}(white) atoms.

lar Beam Epitaxy (MBE) under Ultra High Vacuum (UHV) conditions, have developed enormously. In MBE the Eu metal is evaporated from a crucible heated-up at around 400℃, generating a flux of atoms directly incident on the substrate, in oxygen atmosphere. However here the system operates at a base pressure of $10^{-10} \div 10^{-9}$ mbar. This technique therefore enables the preparation of thin films in a much cleaner and precise way, allowing a much better control of stochiometry. In this way Eu-rich or doped Europium can be grown with the desired rates of vacancies or dopants. Epitaxy, single crystallinity, and stochiometry of EuO film depends indeed critically on growth conditions, namely substrate selection, substrate temperature T_S, oxygen pressure P_{O_2} and Eu flux rate Φ_{Eu}.

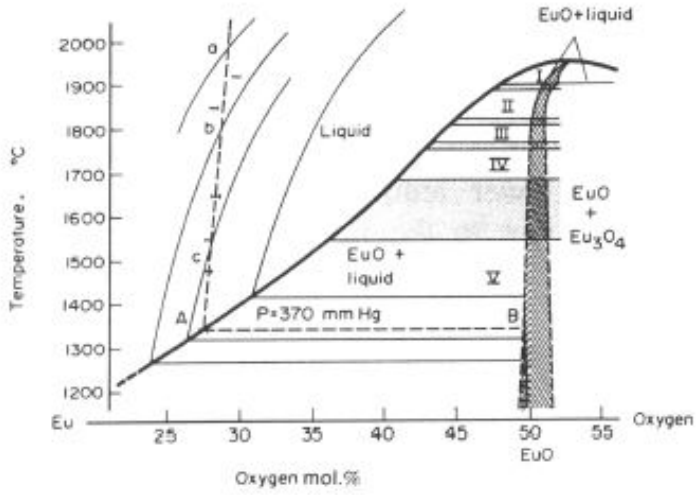

Figure 1.2: Phase diagram of Eu-O from Shafer[14]

Epitaxial and single crystalline Europium Oxide can be achieved using different type of substrates, like Yttria-stabilized cubic Zirconia (YSZ), MgO, BaO-buffered $SrTiO_3$, BaO buffered Si, $YAlO_3$, SrO-buffered Si and SrO-buffered GaN, all of them offering a quite good matching of the lattice parameter. In particular YSZ, with a lattice constant of 5.142 A, is almost perfectly matching the one of EuO. Moreover, depending on the orientation of the substrate, i.e. the surface of the crystal on which the film will grow, one can achieve different type of alloys. For istance, when using a YSZ(111), that means cut along the x,y,z=1 direction, EuO film will present polar surfaces. This can be see by cutting the crystal structure of Figure1.1 along the (111) direction, and thinking the film growing in layers made of Eu^{2+} and O^{2-} ions, one next to the other. In this way the surface of the film ends up with the last monolayer strongly polarized with a positive or negative charge if Eu or O terminated, respectively. While usinge YSZ(100) this phenomena does not occur, since the planes along the (100) direction of EuO crystal structure show an alternating composition of Eu and O atoms in 1:1 ratio.

1.1.2 Electronic Structure

Europium monoxide has a ionic $Eu^{2+}O^{2-}$ character, such that electrons from the outer atomic shell of the cation (Eu), are transferred to the anion (O) thus forming completely filled p^6 shells. As the atomic electronic configurations of Eu and O atoms are

$$[Eu] = [Xe]4f^7 6s^2 \qquad [O] = 1s^2 2s^2 2p^4$$

respectively, transferring two electrons produces the ions Eu^{2+} and O^{2-} to be in the following electoronic configuration

$$[Eu] = [Xe]4f^7 6s^0 \qquad [O] = 1s^2 2s^2 2p^6$$

The energy levels which are important for the low energy features, i.e. those near the chemical potential, are the O 2p and Eu 4f orbitals, and the Eu 5d - 6s conduction band. The electronic structure of EuO has been well studied using modern electron spectroscopy techniques[25], and a proposed version by Wachter[1] is shown in Figure1.4.

For the paramagnetic state above T_C, the typical valence band spectra consists of Eu^{2+} 4f band at $\sim$ 2 eV and O 2p band at 4 - 7 eV binding energy. The charge density distribution of the 4f electrons is to a large part well inside the $5s^2$ and $5p^6$ shells of the [Xe] configuration, so direct overlap of 4f wavefunctions is negligable and its electrons are well electrostatically screened against external perturbations, conserving thus their atomic character. Moreover from Hund's first rule, we know that the groung state configuration of Eu $4f^7$ electrons will be ${}^8S_{\frac{7}{2}}$ with $L = 0$ and $S = 7/2$. Analysis

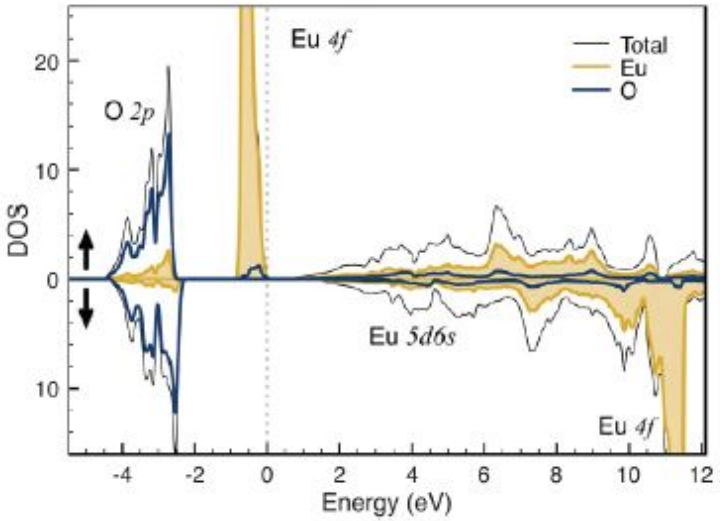

Figure 1.3: Spin resolved density of states for bulk EuO in the ferromagnetic phase calculated by Ingle and Elfimov[34].

by XPS and spin-resolved photoemission[25] measurements indicates that it costs =6.5 eV to flip one 4f spin, showing that the high-spin configuration is very stable and the spin polarization of the 4f levels is nearly 100%.
The typical conduction band spectra are composed of Eu 5d – 6s band. Now, the cubic crystal field acts only on the 5d states and splits them into 6 fold degenerate $5d_{t_{2g}}$ levels, situated 1.2 eV above the top of the Eu 4f valence band, and 4 fold $5d_{e_g}$ levels at 3-4 eV above the Eu $5d_{t_{2g}}$ band. It is also well estabilished that in EuO the bottom of the 6s conduction band is slightly higher in energy than the one of 5d band.

Below T_C the conduction band for spin-up and spin-down split due to the indirect exchange interaction between the Eu 4f moments and the 5d – 6s conduction electrons. Although the 4f - 5d transfer integrals are quite small, the exchange interactions between these orbitals is still significant and leads to an exchange splitting of about Δ_{ex}=0.3 eV[28]. The difference in total is about 0.6 eV. As a result the band gap for spin-up is reduced to $\sim$ 0.9 eV, while the band gap for spin-down is increased to $\sim$ 1.5 eV. Moreover, the role of d - f exchange and spin-orbit coupling can be see in the interplay between 4f spins and spin-polarization of the conduction band, having a substantial influence on the optical, magnetic and transport properties of this compound.

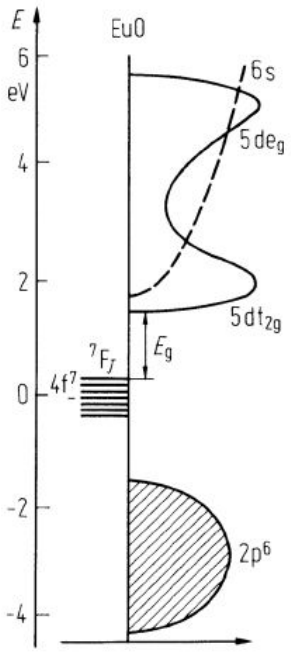

Figure 1.4: Electronic structure of EuO proposed by Wachter *et al.* [1]

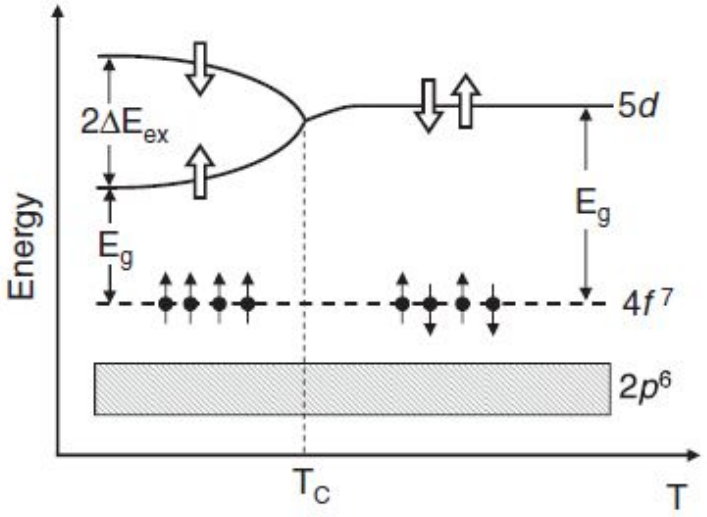

Figure 1.5: Schematic of the energy gap of EuO, showing the exchange splitting in the *5d* conduction band for $T < T_C$, lowering the spin-up sublevel from the spin-down sublevel by $2\Delta E_{ex}$[28].

1.1.3 Optical Properties

EuO and EuO-based materials shows spectacular optical properties that have generated much interest, not only because they can probe the electronic structure, but also because they change upon lowering the temperature or applying a magnetic field. The most impressive effect is the *red shift of the optical absorption edge* when decreasing the temperature below T_C. This shift is a result of the indirect exchange interaction between Eu 4f spins and the conduction electrons, which pushes the spin-down band to higher energies, and the spin-up band to lower energies, thus reducing the gap. The exchange splitting parameter is $\Delta_{ex} = 0.3$ eV, thus lowering the band gap from 1.15 eV at room temperature to 0.9 eV below T_C. The same effect can also be seen as a splitting of the O K edge x-ray assorption spectrum (XAS), see Figure 1.6, and the corresponding transition is probably from the 4f orbitals to the $5d_{t_{2g}}$ conduction band states.

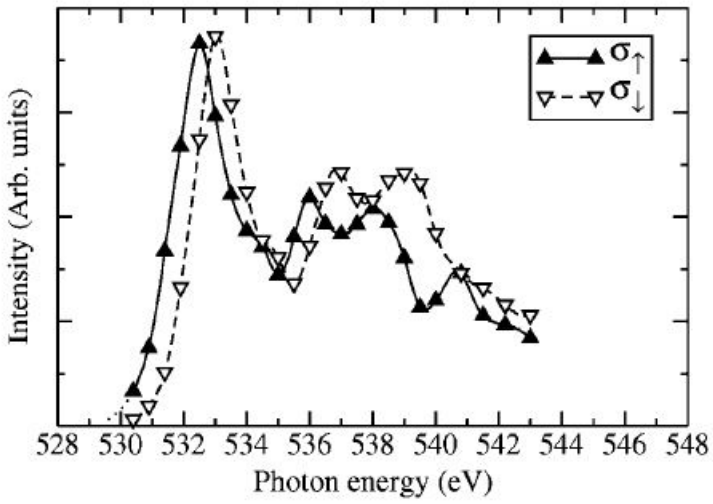

Figure 1.6: Spin respolved O K XAS of EuO taken at 20 K[28].

The refractive index n of EuO at the absorption edge also reduces with temperature. it has a value of 2.25 at room temperature and increases sharply around T_C untill a value of about 2.45 at low temperature.

Connected to the optical properties, effect such as large *Kerr* and Faraday rotation are observed[10] for EuO: this effect consist of the rotation of polarization upon reflection and transmission respectively from a magnetized medium. For example, in EuO single crystal was observed a polar Kerr rotation of 7.1 degree at a photon energy ($h\nu$) of 1.4 eV at T=10 K, and a specific Faraday rotation of $5\text{x}10^5$ degree cm^{-1} at $h\nu \sim 1.9$ eV and T=5 K.

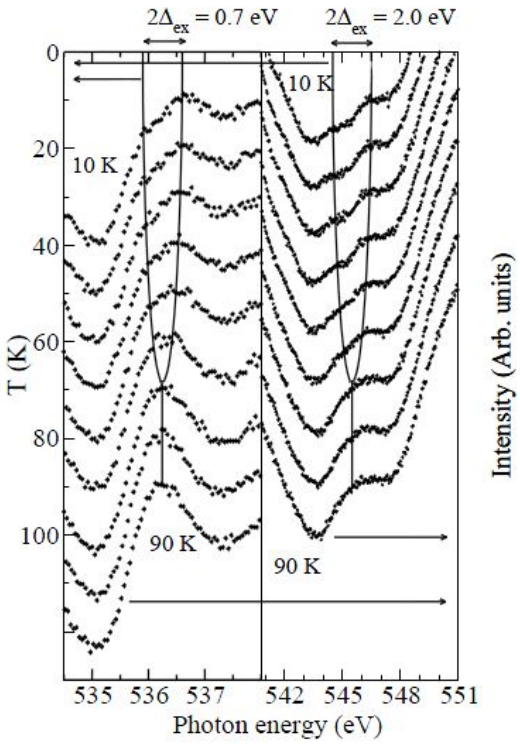

Figure 1.7: Two energy regions of the O K XAS spectra of EuO at temperatures from 10 to 90 K, taken at intervals of 10 K. Solid lines are split proportional to the magnetization in a mean field model to show the exchange splitting below T_C. [1]

1.1.4 Magnetic Properties

Europium Oxides is one of the very rare ferromagnetic semiconductor[4, 7], a class of materials whose existance was severely disputed in the mid fifthies[1], because ferromagnetism was not considered to be possible in insulators. In ferromagnetic semiconductors the magnetic order is induced by indirect exchange interactions, which is quite different than the itinerant electron ferromagnetism of common ferromagnets.

In a first approach ferromagnetism in EuO is well described by the *Weiss mean-field model*, but for a better description of the mechanism leading to the ferromagnetic coupling in this compound the *Heisemberg model* is widely applied.

Weiss model

The molecular (mean) field model, developed by Piere Weiss in 1907[40], considers only the interactions between a local magnetic moment and the effective magnetic field H_{eff} generated by the crystal. In Europium Oxide the Eu^{2+} ions carry a spin magnetic moment of $7/2\mu_B$ due to the spin parallel aligned electrons of the $4f$ band. The effective field instead is proportional to the magnetization M and is supposed to couple the localized moments sitting on Eu atoms.

Moreover the temperature dependent spontaneus magnetization of the crystal is noticed to follow a classical Brillouin function, which is derived from the Weiss model and expressed as follows

$$M(T) = M(0)B_S\left(\frac{3S}{S+1}\frac{M}{M(0)}\frac{T_C}{T}\right) \tag{1.1}$$

where

$$B_S(x) = \frac{2S+1}{2S}\coth\left(\frac{2S+1}{2S}x\right) - \frac{1}{2S}\coth\left(\frac{1}{2S}x\right) \tag{1.2}$$

is the Brillouin function, $M(0)$ the saturation magnetization at T=0K, and S the spin angular momentum. For EuO $S = 7/2$ and $T_C = 69$ K is the transition temperature.
The expression of the reduced magnetization is then given by

$$\sigma = \frac{M(T)}{M(0)} = 1 - \frac{1}{S}\exp\left(-\frac{3S}{S+1}\frac{T_C}{T}\right) \tag{1.3}$$

close to the zero temperature, and by

$$\sigma \propto (T_C - T)^{\beta}, \qquad \text{with } \beta = 1/2 \tag{1.4}$$

close to the transition temperature T_C. However it was found that the low temperature trend diviates significantly from this model, and that the exponent β is not exactly 0.5 for Europium Oxide. This lead us to explore another model to provide a better description of EuO ferromagnetism.

Heisemberg Model

The Heisenberg model is a statistical mechanical model used in the study of critical points and phase transitions of magnetic systems which suggests that spontaneous magnetization arises from the *exchange interaction* between spin moments of neighburing atoms in the crystal. The exchange interaction J_{ex} originates from the overlap of the charge distribution of two orbitals centered in different sites as a consequence of Pauli exclusion principle and Coulomb repulsion between weakly interactin electrons. The sping Hamiltonian employed by the model is of the form

$$H = -\sum J_{ex}\mathbf{S_i}\cdot\mathbf{S_j} \tag{1.5}$$

where J_{ex} is the exchange integral related to the overlap of the atoms at sites i and j with spin moment S_i and S_j, respectively. For a Heisemberg ferromagnet the spin parallel configuration is favoured by a positive exchange integral value, and the maximum coupling is reached at zero temperature with the atoms in the ground state.

In EuO the ground state of ${}^8S_{\frac{7}{2}}$ is in spherical symmetry, so that the exchange interactions are essentially isotropic, and can be well described by the Heisemberg Hamiltonian. Experimental results indeed seems to support this choice in describing the ferromagnetism of EuO. The reduced magnetization[19, 42] is then found to be well described by the Bloch $T^{\frac{3}{2}}$ law

$$\sigma = \frac{M(T)}{M(0)} = 1 - \frac{0.0587}{SQ}\left(\frac{k_B T}{2J_{ex}S}\right)^{3/2}, \qquad Q = \begin{cases} 1 & \text{sc structure} \\ 2 & \text{bcc structure} \\ 4 & \text{fcc structure} \end{cases} \tag{1.6}$$

where Q is 4 for EuO fcc structure, and k_B the Boltzman constant. Moreover, the 3D Heisemberg model is able to predict well the reduced magnetization just below the magnetic phase transition[41], which is given by

$$\sigma \propto (T_C - T)^{\beta}, \qquad \text{with } \beta = 0.36 \tag{1.7}$$

Moreover, the Heisemberg model provides a good description of EuO temperature-dependent magnetization not only at low temperatures and close T_C but also in between, following a sharp Brillouin-like shape curve. For this reason EuO is considered a clear realization of the three-dimensional Heisember ferromagnet model.

Tough there is no exact solution to the Heisemberg model, in first approximation a simpler model can be obtained by restricting the interaction over the nearest and next-nearest neighbur, as proposed by Mauger and Godart[21]

$$H = -J_1 \sum_{i,\Delta_1} \mathbf{S}_i \cdot \mathbf{S}_{i+\Delta_1} - J_2 \sum_{i,\Delta_2} \mathbf{S}_i \cdot \mathbf{S}_{i+\Delta_2} \tag{1.8}$$

The main issue remains however to determine the microscopic origin of the exchange mechanism. In the case of an insulator exchange mechanism via free electrons,i.e. Stoner band model, of course do not work. As proposed by Kasuya *et al.*[12] several competing exchange mechanism exist in EuO.

Nearest neighbor Eu-Eu exchange interaction $\mathbf{J_1}$ This term represents the mechanism in which the overlap between the wavefunction of the Eu^{2+} cations nearest neighbour is most significant and neglect the role of O anion bands. In this case of *indirect exchange*, a $4f$ electron is excited and transferred from valence band to the $5d$ or $6s$ conduction

band. Here experiences an $s-f$ or $d-f$ exchange interaction with the $4f$ spin on a nearest neighbor and returns to the initial state. This virtual excitation seems important because of the small activation energy needed, and leads to ferromagnetic coupling. It was experimentally determined that the strenght of this interaction is $J_1 = 5.22$–$5.39 \times 10^{-}5$ eV[18, 20].

Next-nearest neighbor Eu-O-Eu exchange interaction J_2 In this term, on the contrary, the indirect exchange mechanism includes the p state of the O^{2-} anion, which are involved to create various competing exchange paths between the next-nearest Eu atoms. Three different mechanism are included in this cathegory:

- *Kramers-Anderson superexchange* It consist of an effective coupling of Eu f electrons of next-nearest neighbor sites which are transferred via the oxygen anion. The coupling in this case is antiferromagnetic. Because of the small overlap of O $2p$ bands and the $4f$ states however, this mechanism gives a too small value for J_2 (negative).
- *Superexchange via the d-f interaction* Here oxygen electrons are transferred to the $5d$ or $6s$ orbitals of neighboring Eu atoms where they align with the $4f$ spins through $d-f$ exchange interaction. The 180° Eu-O-Eu bond angle leads to a substantial antiferromagnetic coupling, and due to the larger overlap between $2p$ and $5d$ states this mechanism seems to be important in determining the value of J_2 (negative).
- *Cross-term between the formers* This term results from an interference between the Kramers-Anderson mechanism and the d-f exchange mechanism described above. The $5d$ and$2p$ orbitals form bonding and antibonding molecular orbitals via hybridization. An oxygen electron is then ecited from the bonding to the antibonding $5d-2p$ molecular orbital, which has exchange interaction with both Eu spins. Its palce is taken by a $4f$ electron while the $5d$ one fills the $4f$ hole. This mechanism, in contrast with the previous ones could lead to ferromagnetic coupling, and would explain why J_2 is positive in EuO, in agreement with experimental findings.

The net J_2 exchange from all the mentioned contribution is thus ferromagnetic, but its strenght however is much smaller than J_1. Experimental values are determined to be J_2=1.03–1.09$\times 10^{-5}$ eV[18, 20].

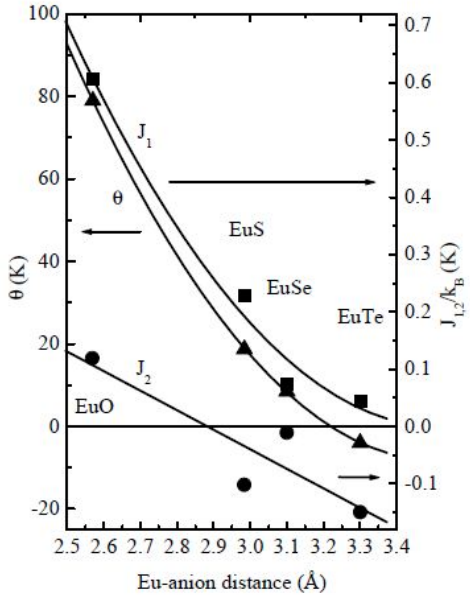

Figure 1.8: Curie-Weiss temperature θ and Heisemberg nearest and next-nearest neighbor exchange parameters J_1(squares) and J_2(circles) versus Eu-anion distance in Eu chalchogenides, from [1]

Effect of Doping

EuO can be doped in several ways: by substitution of a Eu^{2+} with Gd^{3+} rare earths ions, or by supplying excess of Eu atoms in the compound, resulting in a departur from stichiometry. In the both case an n-type doping is achieved.

In particular Gd-doping has been widely investigate in Tjeng's group, as it represents one of the most used way to increase the Curie temperature of Europium Oxide. This is because its in the same $4f^7$ electronic configuration, with sipin S=7/2, of Eu. Therefore the magnetic system is fully preserved, and spin disorder effects are expected to be negligible with respect to the long range magnetic interaction mediated by free carriers. A model extension is needed in this case to explain the physical effect of doping on magnetic interactions, and a further indirect exchange mechanism between localized spins, mediatet via low density of free carriers, must be taken into account. As result of Gd-doping one can achieve enchancement of T_C up to 125 K[43], corresponding to an optimum Gd concentration of about 7%[50], but at the same time a remarkable deviation from the classic Brillouin curve is observed.

In the case of Eu-rich doped EuO instead, several studies reported of enchancements of T_C up to 150 K, which is attributed to the increase in the indirect exchange interaction between Eu^{2+} spins via conduction eletrons.

However, this enchancements occurs as the appearing of a magnetization tail extending the curve from T=70 K up to T=150 K only at high external fields. This feature strongly deviates from the Brillouin curve and could be more likely ascribed to Europium metal clusters magnetically aligning in strong fields.

1.1.5 Transport Properties

The most fashinating phenomena of Europium Oxide are related to the transport properties. Those are highly sensitive to oxygen stoichiometry, chemical doping, external magnetic field, pressure and illumination of light.

Upon electron doping, i.e. by oxygen vacancies or chemical doping, indeed, the ferromagnetic phase transition is simultaneusly followed by a semiconductor to metal transition, namely the *metal-insulator transition* (MIT). This spectacular phenomena consist of a abrupt drop in resistance, of about 8 to 13 orders of magnitude, below the Curie temperature, with nearly 100% of the conducting carriers fully polarized. This corresponds to a spin splitting of the conduction band below T_C of about 0.6 ev, which is also related to the reduction of the bandgap from 1.2 eV at room temperature to 0.95 eV at 20 K. The earlies study of this phenomena were carried by Oliver *et al.* who measured resistivity as function of several parameters. In examining the temperature dependance they found that stoichiometric EuO samples were showing a typica semiconductor-like curve, with resistance decreasing while rising the temperature. Whereas those samples which were grown with excess Eu in the mixture were showing a large resistance peak in the vicinity of T_C and a subsequent decreas below the same. However it was not easy to control the amount of Eu excess in single crystal compounds. Later, specific studies on EuO thin films allowed the characterization in terms of transport properties with a higher concentration of oxygen vacancies and a better control of stoichiometry, like as in Tjeng's group, and how will be better discussed in the present work.

A second spectacular effect in Eu-rich EuO occurs upon the application of a magnetic field: the resistivity changes up to 6 order of magnitude, resulting in a huge *colossal magneto-resistance effect* (CMR) concomitant with the metal insulator transition. While increasing the intensity of the external magnetic field the shape of the resistance curve around T_C becomes more gradual, and MIT shifts considerably to higher temperatures. Some example of the measurements of these phenomena, both MIT and CMR, are shown in Figure 1.9.

Furthermore, it remarkable that resistance can be varyed and metal-insulator transition can also be induced in stoichiometric EuO, by the application of high pressure or under the illumination of light, respectively. In

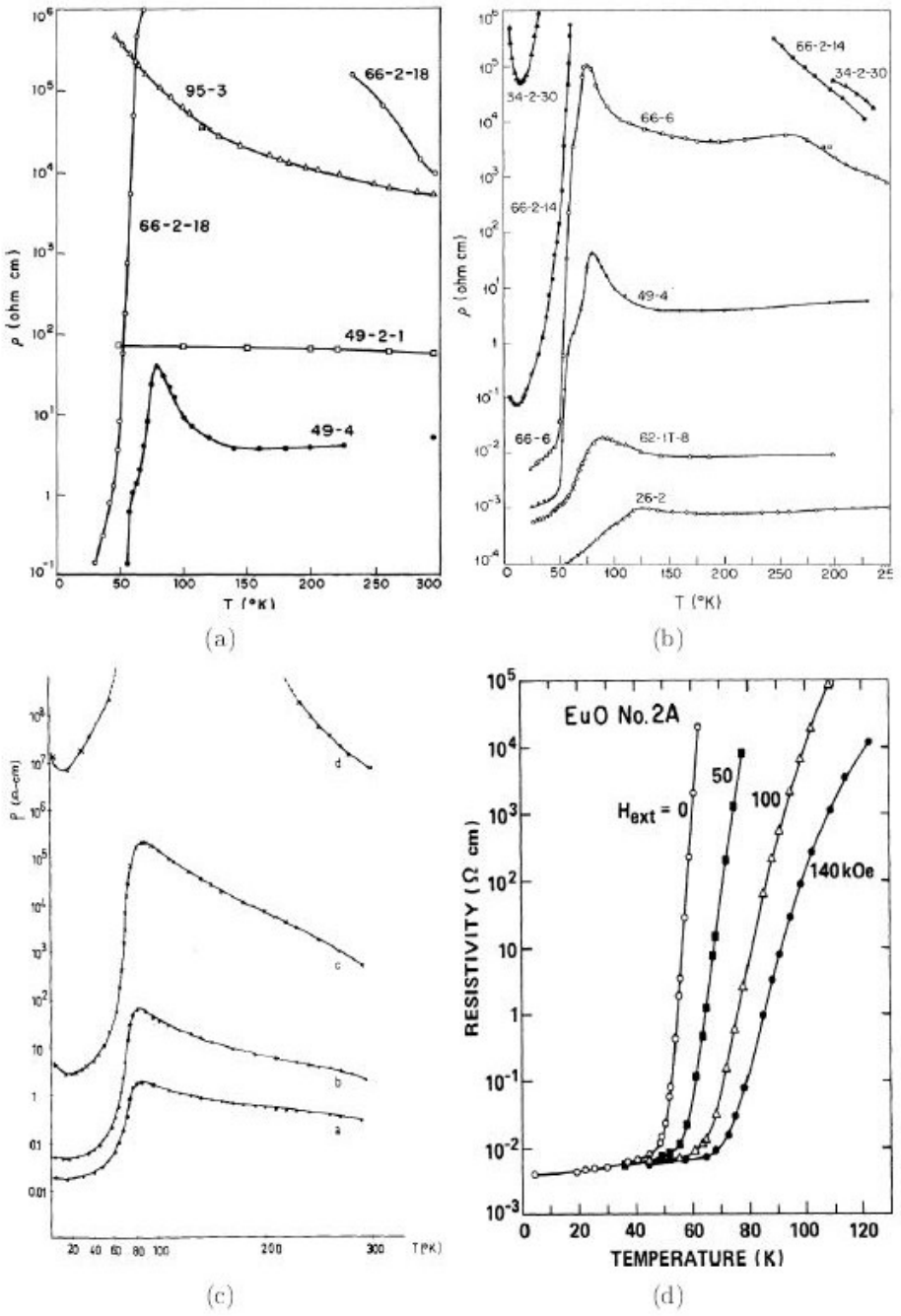

Figure 1.9: Transport properties of EuO. (a–c) $\rho(T)$ of $EuO_{1\pm x}$ from Oliver[15][17]. (d) Magnetoresistance of EuO crystal from Shapira[24].

the former case, the resistivity at room temperature strongly reduces under high pressures, together with the decrease of the bandgap. A huge change of resistivity of about 10 orders of magnitude was instead observed at 200 K by exerting a quasi-hydrostatic pressure up to 250 kbar. In the latter case, strong illumination by He-Ne lasers is able to change resistivity of about 1 order of magnitude in the samples which also show MIT under illumination, whereas the conductivity in the dark shows oly semiconducting behaviour.

Although the origin of this metal-insulator transition is still object of discussion, several theoretical models have been proposed to explain it. In the erliest models[11, 39] electrical conductivity at high temperature was ascribed to thermally activated hopping process, while the large change below T_C and under applied magnetic field was related to changes in electron mobility. Later it was discovered by pressure dependent measurements that the conductivity variation near and below the Curie temperature is due to a change in carrier density. What is remarkable is that the exchange splitting of the conduction band can account for the large increase in the free carrier concentration and corresponding metal-insulator transition that is observer entering the ferromagnetic state[25]. Experimental results were found to be better in agreement with the latter considerations and the most widely accepted theoretical models are the He model[13], the Trap level model[16], and Bound magnetic Polaron (BMP)[5].

According to the He- and trap model, above T_C the exceeding electrons are bounded in the oxygen defect levels which are located in the gap with fixed energy. In this situation the compound behaves as an insulator. Below T_C, the cunduction band splits up and the parallel spin band lowers in energy crossing the defect level and thus the vacancy electrons are emptied in the conduction band. This results in high carriers density in the fully polaryzed conduction band leading a ferromagnetic metal. As each oxygen vacancy can bind two electrons, hence comes the name of the model.

Many authors instead ascribe the metal-insulator transition to the bound magnetic polaron (BMP) model. A BMP consisto of an oxygen vacancy, or doped impurity ion, which binds electrons by its Coulomb potential. Those electrons increase the ferromagnetic coupling w of the surrounding Eu moments via indirect exchange, thus resulting in an increased local magnetization which binds the electrons to the vacancy sites. This is true above T_C, where the electron gains magnetic free energy by localizing and concentrating on ordering a smaller number of Eu spins, thus formin the BMP. Belove T_C instead, all the Eu ions are ordered and the magnetic part of the binding disappears while the Coulomb part of the bound is not large enough to localize the electrons. The MIT is then attributed to the occurence of a Mott or Anderson transition of the randomly distributed BMP upon magnetic ordering.

The main difference between these two models is basically how they consider to be aligned the two electrons of the vacancy sites: in the He-

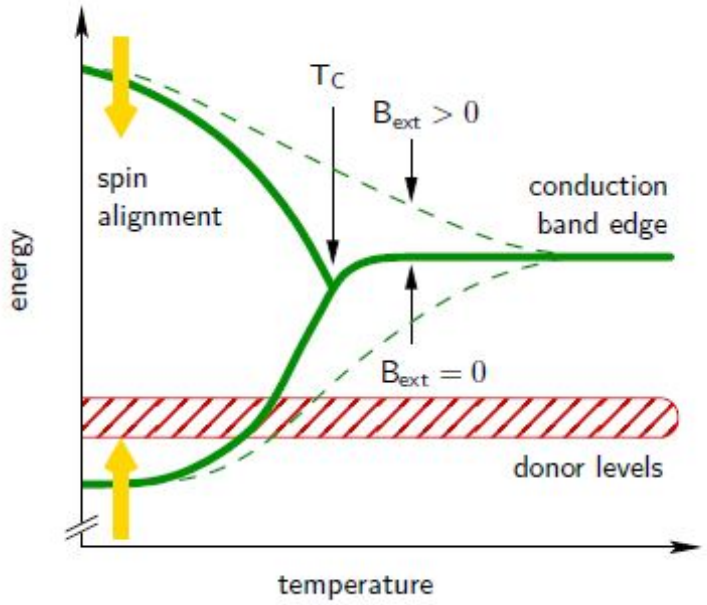

Figure 1.10: Temperature dependent energies of the conduction band of Eu-rich EuO, according to the He-model. An applied magnetic field enhances the spin-splitting at higher temperatures. Adapted from Wachter[1].

model they have antiferromagnetically aligned spins and all the Eu^{2+} spins are disordered; in the BMP model, on the contrary, the two electronic spins are ferromangetically aligned, as are the Eu^{2+} spins neighboring the oxygen vacancy. Moreover the BMP model seems to be in agreement with the fact that the Curie temperature in Eu-rich EuO could be higher than of undoped EuO, while the HE-model does not. Anyway as the attempts to quantitatively compare these models to trnsport experiments have been quite few, it is still unresolved which of the proposed mechanism describes the properties of EuO most accurately. What is largely agreed instead is that the metal insulator transition is solely driven by a change in the magnetic configuration of the crystal.

1.2 Motivation and Scope

1.2.1 EuO as a Promising Material

Thanks to these fashinating propertis, Europium Oxide has been, since its ts discovery in the mid fifthies, one of the most throughly investigated materials in every respect. In the last decade we assisted to a strong renewed interest in EuO due to the progress in preparation technologies, e.g. MBE under UHV, and to the availability new analysis methods such as synchrotron based spectroscopies.

Moreover many research groups attempted to utilize those extraordinary properties for device applications. Stoichiometric EuO indeed is a ferromagnetic insulator with a large exchange splitting of its conduction band, magneto-opica response and magnetic moment of 7 μ_B per Eu atom, characteristics that makes of it an attractive material for spintronic devices.

Spintronics is an emerging technology that exploits both the intrinsic spin of the electron and its associated magnetic moment, in addition to its fundamental electronic charge, in solid-state devices.
The ongoing miniaturization of semiconductor devices is approaching the technological-physical limits to preserve transport and magnetic properties necessary to the development of electronic circuits. Further lowering the length scales requires therefore to exploit the spin degree of freedom of conduction electrons in order to open new possibilities for semiconductor-based data processing and memory applications[47]. The development of spintronic devices crucially depends on the ability to create, transfer and detect coherent spin states. This, in turns, requires:

- efficient electrical spin injection
- long spin lifetimes in semiconductors

It has longer been demonstrated that Si should have significatly longer spin-lifetimes, compared to GaAs, due to the presence of indirect band-gap, inversion symmetry, and lower spin-orbit coupling. however it is hard to inject spins into Si using conventional magnetic metals because of its propensity for silicide formation and the so called conductivity mismatch at the interface[49].

For this reason the integration of a magnetic insulator, such as EuO, with semiconductors is important for developments in the field, since semiconductors ar the mainstay of current electronics industry[46]. With its very pronounced exchange splitting in the ferromagnetic phase below T_C, and a fully polarized conduction band, EuO results indeed an ideal candidate for

the fabrication of proof-of-concept spintronic devices. Many studies were performed on this spectacular effect, revealing that the spin polarization in both stoichiometric and Eu-rich EuO exceeds 90% demonstrating that EuO is a half-metal[1] even when highly doped.

As a first attempt stoichiometric EuO thin films have been succesfully grown on III-IV semiconductors, e.g. GaAs and GaN, and eve on Si, using the EuO as a tunnel barrier for effective spin filtering[44, 46, 48]. Spin polarization (P) in this case originats from the different barrier height for spin-up(lower) and spin-down(higher) electrons. Since the tunnel current is exponentially increased as the barrier height is lowered, EuO effectively filters out the spin-down electrons from an unpolarized current of a nonferromagnetic electrode, thereby resulting in spin-polarized current revealing that effective spin injection can be achieved. However, while such an approach can succesfully overcome the conductivity mismatch problem, the tunnel barrier limits significantly the spin current.

In more recent works instead an effective alternative to spin filtering is found in the use of a nearly 100% spin-polarized material conductively matched with silicon. A perfect example of such a material is Eu-rich EuO (EuO_{1-x}), which has been demonstrated growing epitaxially and termodynamically stable on Si. Moreover the carrier densities of lightly doped EuO_{1-x} match those of doped Si very well, which is the key of achieving efficient coherent spin injection into a semiconductor with long spin lifetimes such as silicon. On the contrary of stoichiometric one, Eu-rich EuO exhibits a metal-insulator transition (MIT) close to T_C which leads the compound to a metallic behaviour in the ferromagnetic hase. Due to the already mentioned exchange splitting in this phase a 100% spin polarized current is obtained below the Curie temperature, thus making of Eu-rich EuO one of the most promising materials for the efficient spin injections into Si.

Although the rather low Curie temperature makes EuO unsuitable for common household application, it represents an extremely good model compound for the study of basic principles that determine the performance of spintronic devices. To manufacture this kind of devices is therefore fundamental to achive full control in the preparation of high quality epitaxial EuO thin films with desired stoichiometry.

[1] A half metal is a material, that for electrons(holes) of one spin-orientation $|\uparrow|$ acts as an insulator for, while for the other spin-orientation $|\downarrow|$ as a conductor. As a consequence of this current transport ideally occurs only by one spin channel.

1.2.2 Scope of this Work

The quality and the control of stoichiometry of EuO thin films have always been serious issues. Many works indeed reported of Eu^{3+} contaminations, oxygen vacancies or metal clusters in their films. In Tjeng's group Sutarto *et.al*[50] have already carried out a lot of progress in this direction, succeding in the preparation of single crystalline, stoichiometric EuO thin films free of contaminats. Moreover several studies report conficting results about the properties of doped EuO films. In particular the metal-insulator transition and the possibility to enhance T_C in Eu-rich EuO have always been object of discussion. To resolve those debates it is necesary to deeply investigate that factor which give rise to these fashinating effects: the oxygen vacancy concentration.

In order to achieve full control of the growth of Eu-rich EuO thin films, the focus of this work will be oriented to the properties of this spectacular material under different stoichiometric composition. In particular we are going to investigate the transport properties in relation to the oxygen vacancy concentration of the growing films. Although it is very difficult to determine the absolute value of the oxygen vacancies concentration in the films, we will try to overcome the issue by a systematic analysis through X-Ray Photoemission Spectroscopy. This will allow us to determine the limiting condition for metal-insulator transition to occurr and the related oxygen vacancy concentration.

In the following chapters this thesis work will be investigate in detail: Chapter 2 describes the experimental techniques used for the growth of the films, whlie Chapter 3 and Chapter 4 contain information of the *in-situ* and *ex-situ* cheracterization techniques used to investigate the properties of the films. Chapter 5 will present the main results of the work, in particular the effect of pressure, and of substrate temperature on Eu-rich EuO thin films, while Chapter 6 outlines the final conclusions.

Chapter 2

Experimental Techniques

In this chapter a detailed description of the experimental techniques we used to grow EuO thin films and to study its properties is given.

The first part, i.e. chapter 2.1 and 2.2, will start with a general overview of the principles of Molecular Bam Epitaxy (MBE), as one of the most fundamental techniques to grow thin films. Subsequently the specific oxide MBE chamber and the UHV tools used for the growth of the samples will be presented, followed by a detailed description of the entire process of fabrication of the films, from the choice of the substrate, the preparation of the samples and the growth mechanism itself.

In the second part of the chapter the analyzing techniques used for the characterization of the films are explained, divided into *in-situ* and *ex-situ*. The first include Reflection High-Energy Electron Diffraction (RHEED), Low-Energy Electron Diffraction (LEED), Transport measurements and X-Ray Photoemission Spectroscopy (XPS). While the latter consists mainly of magnetic characterization by Superconducting Quantum Interference Device (SQUID).

2.1 Molecular Beam Epitaxy

2.1.1 General considerations of MBE

Molecular Beam Epitaxy was invented in the early 1960s and has developed as one of the main and fundamental technique for the growth of thin films. Due to its versatility it can be used for growing any type of natural or artificial material, e.g. metal, insulators or semiconductor thin films, both at research and industrial level. MBE under ultra-high vacuum (UHV) conditions offers indeed capacity of high quality single crystalline thin films production in an epitaxial manner with monolayer control.

In MBE the elements of desired materials are evaporated onto a substrate where they crystallize as thin film. Additionally, gaseous constituents can be supplied directly in the chamber to perform the growth in the desired athmosphere. The growth process can be described into three steps:

- The *production of molecular beams*. In solid-source MBE, ultra pure elements are heated up in separate Knudsen effusion cells. A Knudsen cell consist of a ceramic crucible containing the solid material (Eu in our case) which is heated by a tungsten filament. Rising up the temperature they begin to slowly evaporate, so that a flux of atoms in gaseus state generates. The stability of the molecular beam flux determines the uniformity of the film thickness and its composition. Therefore it is important to choose appropriate effusion cells with good temperature control, as well as to set appropriate geometry between the source and the substrate.

- The *transport of molecular beams* to the substrate. Once generated, the flux of gaseus atoms has to traverse a certain path before sticking on the substrate. However, on the way to the substrate, the molecular beam may suffer scattering with other atoms or molecules of the residual gas present in the chamber. This will degradate the directionality and uniformity of the mass flow, thus leading to a non-uniform arrival of the atoms to the surface of the substrate. To avoid these undesired process, it is necessary to have a good vacuum in the MBE chamber in order that the atoms of the flux do not interact with each other an with other contaminats. It is derived that pressure in the range of $10^{-3} \div 10^{-4}$ mbar is adequate to ensure a satisfactionary value of the mean free path of the particles composing the beam, so that the uniformity of the mass transport is mantained.

  $$l = \frac{k_B T}{\sqrt{2}\pi p d^2} \geq 20cm \tag{2.1}$$

  Nevertheless, UHV conditions of 10^{-9} - 10^{-10} mbar are required to keep the chemical composition of each layer of the film without impurities of the residual gases.

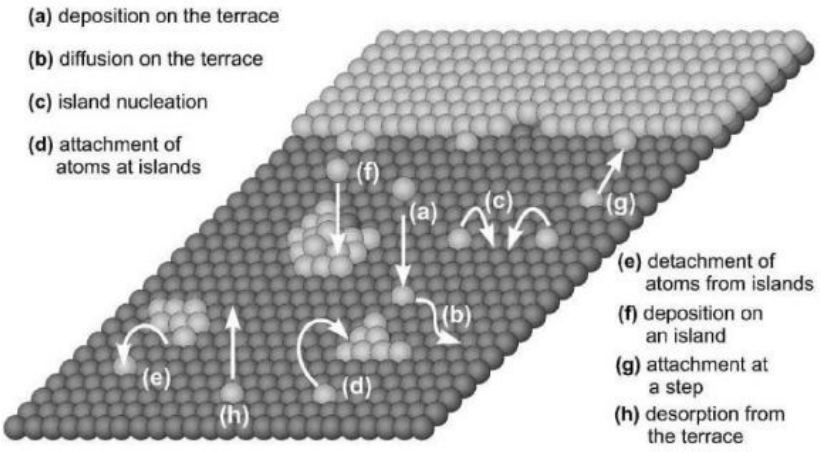

Figure 2.1: Surface elementary process in molecular beam epitaxy. Reproduced from[29].

- The *deposition of the molecular beams* onto the substrate. In MBE, flat substrates are employed, i.e. smooth surfaces having large terraces with monoatomic steps. So when the impinging beam arrives on the substrate surface different physical and chemical process may occurr, as it is represented in Figure 2.1. The adsorbed atoms can meet other adatoms and nucleate into two-dimensional clusters (c), or, if they find an island, attach to it (d). It is also possible that they propagate on the surface until they find a step edge (g) and, depending whether the step is rough or smooth there they can either attach or further migrate along it till they find a kink, respectively. Another important process is the thermal desorption (h) of an atom from the surface back to the vacuum, that happens especially when the temperature is high. We will see better in Chapter 3 how this process plays a crucial role in producing epitaxial and stochiometric EuO thin films.

The main advantage of molecular beam epitaxy is the precise control of the desired chemical composition of an epitaxial film. The stochiometric composition of the grown epilayer depends indeed on the relative arrival rates of the constituent elements on the surface. While the atomic structure and symmetry of the substrate plays a crucial role in epitaxial growth, as it directly influences the arrangement of the atomic species impinging on it.

Another important advantage of this technique is that, being realized in UHV enviroment, the growth of the films can be controlled *in-situ* by surface sensitive diagostic methods based on the scattering of electrons, like RHEED and LEED, as well as various kind of electron spectroscopies like X-Ray Photoelectron Spectroscopies, as shown more in detail in the later sections of this chapter.

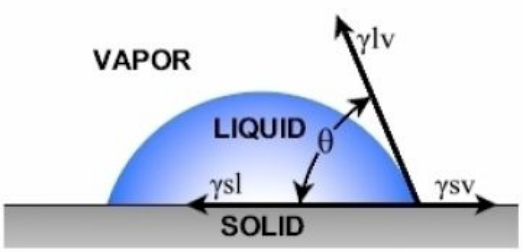

Figure 2.2: Surface free energy (or *tension*) between different phases.

Growth Modes

In this work we will focus on heteroepitaxy growth, which occurs when a crystalline material is deposited on a crystalline substrate of a different material. In this case two important parameters have to be considered since they strongly influence the growth mode of the film: the *lattice mismatch* (2.2) between the substrate and the film, and the *surface tension* energy of the substrate γ_s, of the film γ_f, and between substrate and film $\gamma_{s,f}$.

$$f = \frac{a_s - a_f}{a_s} \tag{2.2}$$

There exist three basic modes of thin film growth:

- the *3D islands* (or *Volmer-Weber*) mode. Islands growth happens when adatoms are more strongly bound to each other than to the substrate. So when impinging on the substrate, they start nucleating immediately resulting in the formation of three dimentional agglomerate. This growht mode is energetically favorable when

  $$\gamma_s > \gamma_f + \gamma_{s,f}$$

  and, as depicted in Figure 2.3, it occurs even when there is no lattice misfit between film and substrate. Nevertheless its range of dominace expands when the lattice mismatch increases.

- the *layer-by-layer* (or *Frank-van der Merwe*) mode. Diametrically opposed situation to the island mode is the layer-by-layer growth, where the adsorbed atoms are more likely wetting the substrate than binding to each other. In terms of surface tension it is energeticaly favorable when

  $$\gamma_s < \gamma_f + \gamma_{s,f}$$

  This growth mode leads to the smoothest surfaces since it is governed by the nucleation of two-dimensional islands, which expand to complete each monolayer. In principle each monolayer has to be complete

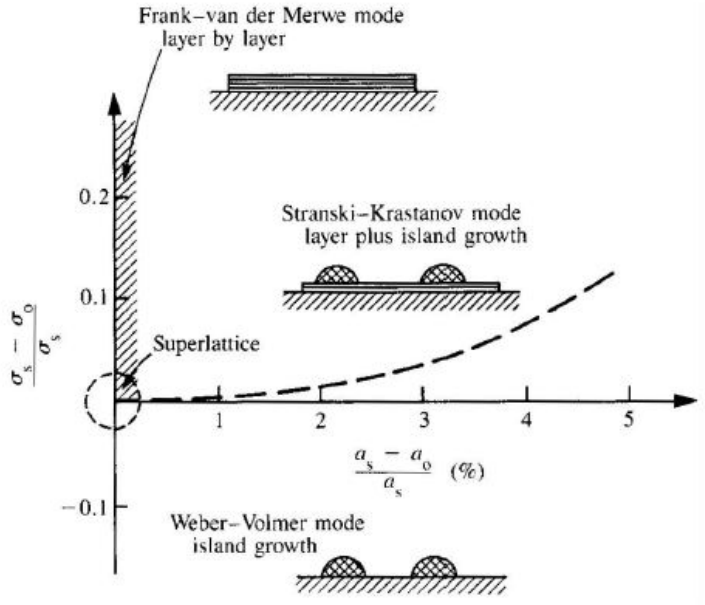

Figure 2.3: Schematic diagram that illustrates stability regime of the three basic thin film growth modes. Surface tension difference is plotted on [x] axis as function of the lattice mismatch. The dashed line denotes the separation between the *island* and *layer plus island* modes.

before the growth of the following one takes place. However, as the growht proceeds the surface becomes rougher, due to the limited diffusion leght of the adsorbate atoms. Since the diffusion length is directly related to the substrate temperature this effect is more pronounced at low T_S. Remarkably the layer-by-layer growth is also possible in presence of a slightly mismatch, meaning that strained-layer epitaxy is also feasible.

- the *layer plus islands* (or *Stranski-Krastanov*) mode. In between the previous two modes, a mix of them can be possible. In the layer plus island mechanism a formation of one or few monolayers is favorable in the beginning. After, due to the weaker interaction between the substrate and deposited atoms, they tend to nucleate together and 3D island growth becomes dominant. This mode is favoured when the surface tension condition is similar to the layer-by-layer growth but with a larger lattice mismatch.

2.2 Experimental Setup

The purpose of this section is to describe briefly the experimental setup used to carry out the experiments in the group of Prof. Tjeng in Cologne. The cluster UHV system, i.e. where the samples are grown and *in-situ* characterized, is composed by six vacuum chambers connected together.

- The mini-MBE chamber, on the right side in the picture. This chamber, described in detail later, is the place where substrates are annealed, the EuO films are grown and the first RHEED characterizations is taken.
- The XPS chamber on the opposite side. In this chamber the chemical and structural characterization takes place, i.e. X-ray photoemission spectroscopy (XPS) and Low Energy Electron Diffraction (LEED).
- The MOKE chamber for transport measurements. This chamber was designed to measure *in-situ* Magneto-Optical Kerr Effect on the samples, and lately adapted in order to perform conductivity measurements by the addition of a contact clamp on the manipulator. The latter will be better explained in Section 3.4.
- The load-lock chamber on the front side. Here is the place where samples are stored and capped for *ex-situ* characterization, i.e. for Superconducting Quantum Interference Device (SQUID).
- Another MBE chamber on the back side, which is dedicated to the growth of various oxides thin films in Tjeng's group.
- The UFO chamber in the middle. This chamber provides the only and indispensable task to transfer the samples from one chamber to the other. This has to be done in a safe and fast way, by keeping them in UHV condition to prevent films from contamination or further oxidation.

All the chambers operate in Ultra High Vacuum (UHV) conditions, mantained by a complex pumping system always working in standard experimental condition. Each of the chamber has its own pumping system. For those chambers like UFO, mini-MBE and XPS where a better vacuum is required, a cryo-pump is used, that can reach pressures in the range of 10^{-9}– 10^{-10} mbar. Whereas for those that are smaller or those which needs to be often opened, like load locks or the capping chamber, it is chosen a turbo-pump system (P $\simeq 10^{-8}$ mbar) . Both the cryo and the turbo pumps needs to be connected to separate scroll pump to initially reduce the pressure to 10^{-3}–10^{-4} mbar and for the final pumping of the gases. The chambers are isolated from the other by vacuum-proof valves, that can be opened to permit the

sample transferring, but which are afterwards immediately closed to prevent that departure from UHV condition in one of them will contaminate the others.

XPS and MOKE are provided with a rotative 4 axis vertical manipulator, where the sample is mounted for further characterizations. Moreover, each manipulator has a flow cryostat which allows measurements at low temperature, down to 4K (He) thanks to liquid-helium cooling system. Liquid He is passed through an external pumping system till to the manipulator channel, after which it is removed by means of an outlet channel. By flowing in the circuit the liquid helium cooles down the mechanical part by thermal conduction and remove the heat excess.

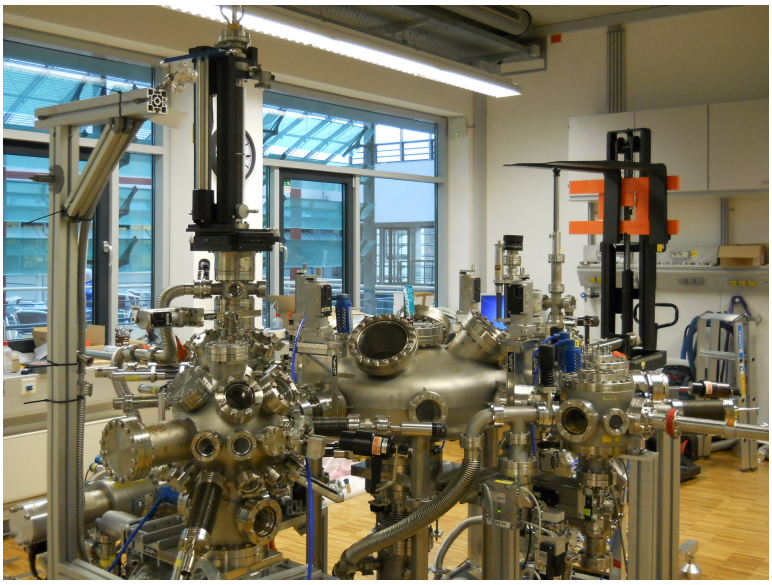

Figure 2.4: Experimental chamber setup in Dresden.

2.2.1 Mini-MBE Chamber

The growth of Europium Oxide thin films was carried out in Cologne in the so called Mini-MBE chamber. It is an oxide MBE chamber designed and built exclusively for the preparation of EuO samples. A copy of the same chamber is located at the NSRRC Synchrotron in Hinchu, Taiwan, in order to reproduce samples with the same growth conditions from in-house experiments for the beam measurement time. The chamber has a cylindrical shape and consists of 3 circles of flanges connected toghether as can be seen in Figure.

The first circle, on the left side, is where the deposition of the film takes place. At the flanges, the equipment for the growth process: two effusion cells, a RHEED gun and its phosphor screen for detection of the

electrons, and a water cooled thickness monitor. The Eu effusion cell is located on the bottom, perpendicular to the substrate surface at the growth position. It is a Knudsen type effusion cell Veeco EPI-1-S-SM single filament source with an Al_2O_3 crucible heated up by a tungsten filament and with a temperature controller, as depicted in Figure 2.5. The Gd effusion cell (Luxel RADAK I Knudsen type) is at an angle of 40°from the normal to the surface, and is provided with an external water cooling system, due to the higher temperature needed for Gd evaporation. The RHEED gun (Staib EK-35) is located parallel to the sample position and the Al-coated phosphor screen diametrically on the opposite side. While the Sycon-100/MF quartz crystal microbalance thickess monitor is mounted on the top flange. It can be lowered to reach the growth position for the monitoring of the flux rate.

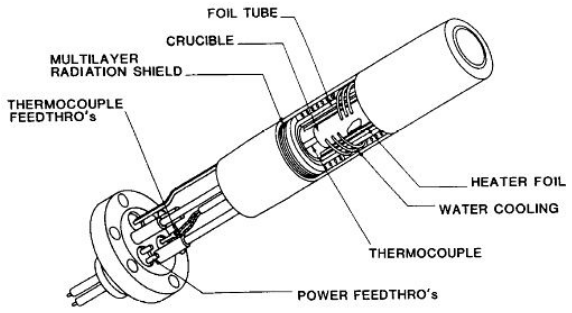

Figure 2.5: Schematic of a Knudsen-cell.

On the middle flange circle a parking lot and a wobble stick are mounted. The third flange circle is equipped with a heating stage for the annealing of the substrate and a leak valve for oxygen source with a nozzel directed towards the heating stage. Connected to this part of the chamber is also the load-lock from where substrates are inserted, and a heatable manipulator where the samples are mounted for the thin film deposition. The manipulator has three degrees of freedom and it is used to bring the substrate in the growth position.

On the left side the chamber is connected to a smaller one, that serves as a connection to the so called UFO chamber[1]. On this chamber is mounted a MKS quadrupole mass-spectrometer, used to monitor the oxygen partial pressure during growth and the presence of residual gases in the chamber.

The mini-MBE operates under UHV condition, where a pressure of $P \leq 3 \times 10^{-10}$ mbar is mantained by a cryopump. The load lock is pumped by a turbo-pump connected to a scroll pump.

[1]UFO is a big circular 5-flanges chamber with a rotable and extensible sampleholder used to transfer the samples in between the chambers

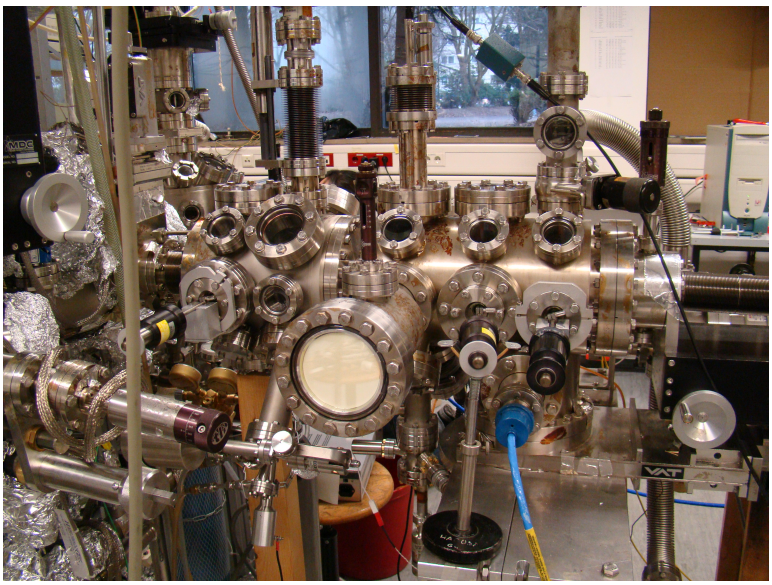

Figure 2.6: Picture of the mini-MBE chamber during mouting in Cologne.

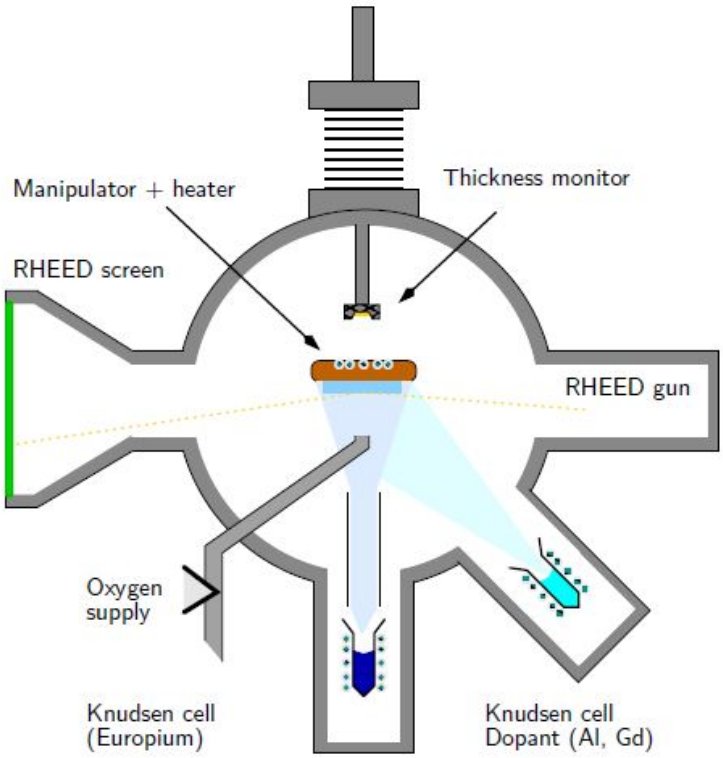

Figure 2.7: Section of the mini-MBE chamber at the growth flange position circle, from [32].

2.3 Thin Film Growth

In order to produce Europium Oxide thin films is necessary to select an apropriate substrate and prepare it for the growth process. In the following sections we will explain the choice of the YSZ(100) substrate, the process to prepare it for the various sets of measurements and the way to mount it before inserting it into the mini-MBE chamber load-lock. Later we will describe in detail the growth process.

2.3.1 Substrate Preparation

The choice of the substrate material is crucial in determining the growth mode, as already discussed in Section 2.1, and consequently the crystalline properties of the resulting film. The *misfit* or *lattice mismatch* f, between the substrate and the growing film lattice constants, is the crucial parameter that has to be taken into account for this choice. It is defined as follows

$$f = \frac{a_s - a_f}{a_s}$$

and the higher its value is, the higher will be the elastical deformation that the EuO film will undergo while growing on the substrate. This can be due to a compressive ($f < 0$) or tensile ($f > 0$) strain that increases proportionally to the film thickness. In presence of a slight mismatch after some layers it can result the formation of dislocation, i.e. empty spaces (or extra atoms) in the lattice to adapt the size of the film to the substrate. Only when the film reaches a critical thickness, such that the relaxation elastic energy overcomes the cost for the creation of a dislocation, it can keep growing with the expected lattice parameter. This would turn in some disordered structure in the very first layer of the film. Moreover if the lattice mismatch is too big ($> 10\%$) epitaxial growth becomes very difficult and policrystalline films are obtained.

In the previous works made by Tjeng's group different types of substrates were used as can be seen in Table 2.1. On YSZ and MgO, despites the large mismatch, EuO is able to grow epitaxially. On Al_2O_3 growth of EuO results to be policrystalline.

In the present work the chosen substrate is epypoloshed single crystalline Yttria Stabilized Zirconia, in short YSZ. It is basically -ZrO_2 that is doped by 9.5% Y_2O_3 in order to have stable cubic structure with a Fluorite type structure and a lattice constant of $a_{YSZ} = 5.142$ Å. The outstanding matching of its lattice constant with the one of EuO motivates the choice, together with the one of using (100) surface in order to get epitaxial growth and non-polar surface. The YSZ(100) substrates are provided by SurfaceNet GmbH company, already clean and properly sized ($10 \times 10 \times 0.5$ mm^3).

Before being mounted, it is needed to grow chromium stripes on the substrates, in order to prevent charging of the samples and to allow proper

single crystal	structure	surface plane	lattice constant	lattice mismatch
EuO	rock-salt	(100)	5.144 Å	–
YSZ	Fluorite	(100) (111)	5.142 Å	0.3 %
MgO	rock-salt	(100)	4.213 Å	22 %
Al_2O_3	Corundum	$(1\bar{1}02)$	4.758 Å	8 %

Table 2.1: Crystal properties of EuO and different possible substrates.

transport measurements with better contact between the probe and the substrate itself. The pattern can be seen in Figure and it is created through a mask that is placed over the substrate and then growing Cr on it in a separate chamber also by evaporating it through a knudsen-cell crucible. The growth lasts 6 hours with temperature of the crucible set to 1225°. Diverse mask configuration were employed depending on the specific measurements to take on a specific sample, however the standard pattern is also shown in the 3D model of the sample in Figure 2.8. The big stripe serves to improve the contact between the substrate and the stainless steel stripe that holds it down, while the two chromium island in the middle are made for transport measurements. The 0.2 mm gap in between them is where the resistivity is measured as will be better explained in Section 3.4.

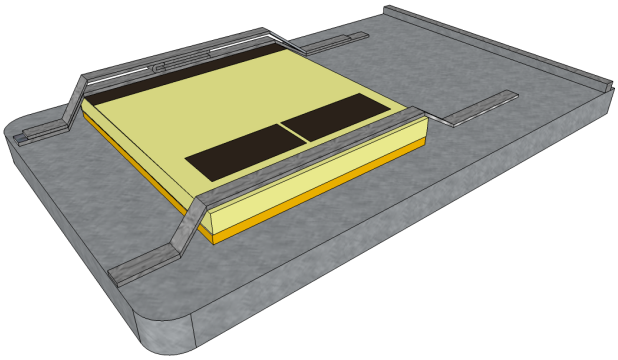

Figure 2.8: 3D model of the substrate(light yellow) mounted on the stainless steel plate. It can be noted the Au foil (dark yellow) below it and the Cr stripe and islands (black) on top of it.

The substrate is mounted on staninless steel (fron here SS) plates that serve as support for the insertion on the sample holders inside the chamber. Afterwards these can be fixed on it thanks to a pair screws mounted on the sides which push down two clamps on the plate. However, the previous step is to fix the substrate on the SSl plate, that is made by means of spot-welded thin stripes derived from a SS foil. On the Cr stripe side an additional SS

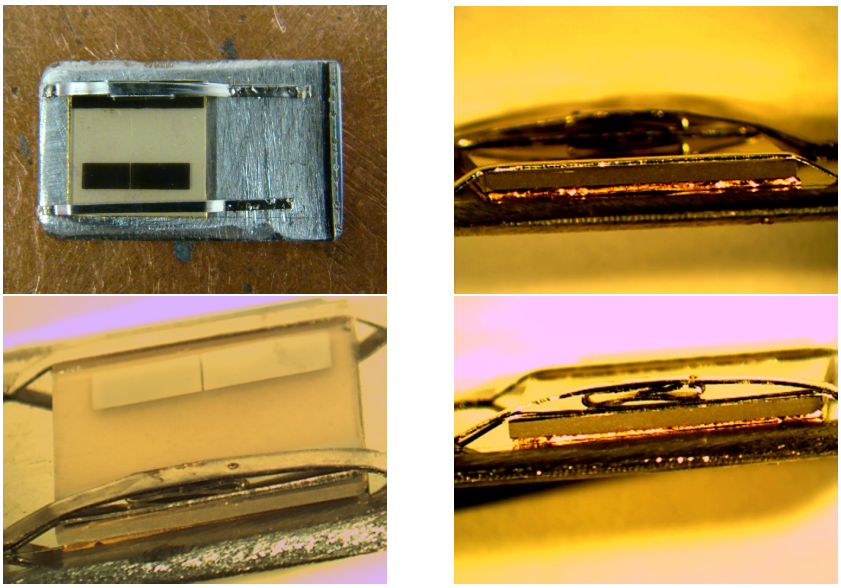

Figure 2.9: Pictures of the substrates already mouted on the stanium steel plate from different angles.

wire is used to push down the lower one to improve the electrical grounding of the substrate. It is also necessary to insert a 0.5 mm thick golden foil between substrate and plate in order to improve the thermal conductivity and thus the temperature uniformity of the substrate itself. Moreover a SS wire is added on one side of the plate in order to help the mechanical hands to grab it inside the chambers. All the SS holding parts, wires and Au foil are previously cleaned in aceton and through an ultrasonic bath, and demagnetized by inserting them in an external magnetic field back and forward many times.

The samples are then inserted in the load-lock and before the growth process takes place they are annealed at a temperature of 600°Cin oxygen athmosphere for 90 minutes. During the process pressure in the mini-MBE cheamber is kept at $P = 1 \times 10^{-7}$ mbar, corresponding to an oxygen partial pressure of $P = 1.1 \times 10^{-9}$ mbar, detected by the MKS mass spectrometer. The annealing procedure leads to atomically clean and well-ordered surface of the substrate as confirmed by RHEED pattern taken before growth.

2.3.2 Growth

Europium belongs to the class of rare earths, all of which have well known +3 oxidation state. Anyway few of them can also exist in +2 state, and this is the case of Eu, thus giving rise to the ionic $Eu^{2+}O^{2-}$ compound. However severe difficulties were encountered in the past years in synthesizing high quality single crystal EuO, such as: lack of reasonably pure Eu metal; high melting temperature and vapor pressure; and the high reactive nature of the divalent Europium Oxide.

Molecular Beam Epitaxy offers the way to overcome these difficulties in order to produce pure stoichiometric EuO thin films.This technique was first employed by Roesler *et al.*[22] in 1994, but an intensive study of the growth of EuO thin films by means of reactive evaporation of metallic Eu in oxygen atmosphere was first reported by Steeneken[25] in 2002.

The same technique and its recipe have been applied lately by Tjeng *et al.* group in Cologne, also redefining it in some aspects. In this section we will describe the general recipe and how it was used in the particular experimental of this work.

Control of stoichiometry: Distillation technique

The most important issue in growing Europium Monoxide thin films is the control of stoichiometry. In its PhD thesis, Steeneken[25] reports of a recipe to grow high quality epitaxial EuO thin films at a much lower temperature than before. It is called *distillation technique* and it is based on the fact that the temperature of the substrate can have big influence in determining the stochiometry of films prepared by evaporation.

The ratio (r) of europium to oxygen impinging on the substrate was found to be the determining factor in stochiometric growth of the layers.

$$r = \frac{\Phi_{Eu}}{\Phi_O}$$

It was indeed shown that a reduction in r was accompained by a slight reduction in the lattice constant, resulting from the incorporation of Eu^{3+} in the lattice, forming a metastable solid solution. It is hence mandatory a precise control of the flux rates of both europium and oxygen in order to obtain the desired combination of the two elements and thus the stochiometry of the final thin film.

Nevertheless Steeneken has shown that a substrate temperature regulated distillation effect permits a less strict tuning of the relative fluxes of the components, but keeping the stochiometry of the growth as well. According to experimental observations the proposed method is based on two main assumptions:

- due to their high reactivity, *oxygen* atoms have a sticking factor[2] S $\simeq$ 1 when they encounter an Eu atoms at the surface which is not yet fully oxidized. $S \leq 1$

- if the substrate temperature T_S is high enough, Eu vapor pressure is sufficient to ensure a complete re-evaporation of Eu metal atoms unless they react with oxygen.

So to clarify the concept, in the distillation condition, i.e. $T_S \geq 400$ ℃, when and Eu atom gets to the substrate surface can either react with an oxygen atom and thus stick on the surface, or, if no oxygen is available, being re-evaporated back to the vacuum. It is clear that being in this situation it means that europium flux rate impinging on the substrate has to be higher of the one of oxygen, i.e $\Phi_{Eu} \geq \Phi_O$. The proposed mechanism thus corresponds to an *oxygen limited* growth process, where stoichiometry of the EuO film is ensured by the lack of oxygen and the re-evaporation of Eu metal atoms unless other oxygen atoms are available, thus resulting in the formation of Europium Monoxide. On the contrary, if $\Phi_{Eu} \leq \Phi_O$, it is very likely that Eu vacancies or higer oxidation states will form, such as Eu_2O_3 or Eu_3O_4. The formation of these unwanted compounds will then affect the epitaxial growth together with the magnetic and transport properties of the thin films. On the other hand, if the substrate temperature is too low, the re-evaporation of Eu excess is no more ensured, thus resulting in the formation of oxygen vacancies and therefore Eu-rich EuO. The biggest consequences of the departure from stoichiometry in this latter direction results in the increasing of film conductivity, together with the appearing of a Metal-Insulator Transition (MIT) if above a certain level of oxygen vacancies. This process will be investigated and explained in detail in Chapter 5.

Distillation Technique		
Substrate temperature	Ts	400 ℃
oxygen pressure	P_{O_2}	4.0×10^{-8} mbar
Europium flux	Φ_{Eu}	8.1 Å/min

Table 2.2: Parameters of the distillation technique used by Sutarto *et al.*[50].

In the most recent work of Tjeng group in Cologne, Sutarto *et al.*[50] have found a recipe to prepare perfect stoichiometric EuO free of contamination, grown on YSZ and MgO substrates. The parameters are listed in Table 2.2 and they refer to the values detected in the mini-MBE chamber described

[2]the *sticking factor* expresses the probability that the impinging atom will be adsorbed on the substrate surface.

in the previous Section. In the present work this recipe is adopted and then slightly modified in order to explore the Eu-rich growth region.

Growth Process: stoichiometric EuO

Once the substrates are being mounted on the holders and properly annealed, they are ready for the growth process iteslf. The base pressure in the mini-MBE chamber is kept as low as possible, i.e. $P_{MBE} = 2^{-10}$ mbar in standard conditions, and $P_{MBE} \simeq 2 \div 3^{-9}$ during Eu evaporation, ensured by proper degassing of the Eu metal in the crucible.

The sample is then mounted and fixed on the manipulator, that is heated up to 400 ℃ in order to assure the complete re-evaporation of Eu excess atoms impinging the surface.

Before the growth takes place, Europium flux rate Φ_{Eu} is measured by means of the crystal thickness monitor that is lowered till the same height of the sample during growth. The temperature of the crucible is then adjusted to reach the desired value of about $8.0 \div 8.2$ Å/min. Since the quantity measured by the thickness monitor is the growth rate GR_{Eu} expressed in Å/min, the flux rate Φ_{Eu} [$cm^{-2}s^{-1}$] can be easily derived by some considerations on crystal structure: Eu metal has a bcc structure, so that a single primitive cell contains one Eu atom, with a lattice parameter $a_{Eu} = 4.581$ Å. The surface density is thus

$$\sigma = \frac{1}{4.581\text{Å}} = 4.765 \times 10^{14} cm^{-1} \tag{2.3}$$

A single monolayer of Eu has a thickness of half the lattice parameter. So let us define another constant ν, that represents the number of atoms per each Å of thickness

$$\nu = \frac{1}{2.2905\text{Å}} = 0.436\text{Å}^{-1} \tag{2.4}$$

It is thus straightforward to obtain the Eu flux rate from the following relation:

$$\Phi_{Eu} = \sigma \cdot \frac{1}{60} \cdot \nu \cdot GR_{Eu} \frac{\text{atoms}}{\text{cm}^2\text{s}} \tag{2.5}$$

The oxygen molecular flux instead, can be derived from considerations out of the kinetic theory of gases, using the following relation. The number of molecules hitting unit area of a surface is indeed estimated from the value of the measured partial pressure, in the framework on Maxwell-Boltzman energy (and velocity) distribution.

$$\Phi_{O_2} = \frac{P_{O_2}}{2\pi M_{O_2} k_B T} \simeq 2.685 \times 10^{20} \cdot P_{O_2} \frac{\text{atoms}}{\text{cm}^2\text{s}} \tag{2.6}$$

with P_{O2} (mbar) the partial pressure of molecular oxygen, M_{O2} the oxygen realtive molecular mass, k_B the Boltzmann constant and T=300 ℃ the room

temperature of the gas. Hence it is straightforward to derive the atomic flux rate, and thus the number of atoms impinging the surface, assuming it the double of the molecular flux

$$\Phi_O = 2 \cdot \Phi_{O_2} \simeq 5.37 \times 10^{20} \cdot P_{O_2} \frac{\text{atoms}}{\text{cm}^2\text{s}} \tag{2.7}$$

The parameters of growth used in this work are the following. For Eu flux rate, a typical growth rate of roughly 8.1±0.05 Å/min was kept constant fo all the growth processes, corresponding to a flux $\Phi_{Eu} = 2.774 \times 10^{13}$ atoms $\text{cm}^{-2}\text{s}^{-1}$. Whereas the oxygen pressure was varied between 3.5 and 7 $\times 10^{-8}$ mbar, corresponding to a flux of $\Phi_{Ox} = 1,88 \div 3.76 \times 10^{13}$ atoms $\text{cm}^{-2}\text{s}^{-1}$. It is easy to understand that oxygen limited growth condition is only ensured below a certain value of pressure, corresponding to about 5.1 $\times 10^{-8}$ mbar. the temperature of the substrate was also varied from sample to sample, with values in the range of 200 ÷ 400 ℃ in a way that distillation condition was not always completely fulfilled.

Growth Parameter		
Europium flux	Φ_{Eu}	$8.0 \div 8.2 \ \frac{\text{Å}}{min}$
oxygen pressure	P_{O_2}	$3.5 \div 7 \times 10^{-8}$ mbar
Substrate temperature	Tc	200 ÷ 400 ℃

Table 2.3: Range of the growth parameters of the set of samples of the present work.

Nevertheless it is the aim of the present work to explore a wider range of growth parameters also far from the distillation condition, basically varying T_C and P_{O_2}, simultaneously. Changes in transport and magnetic properties are hence expected, and investigated by means of transport and magnetization measurements, as will be discussed in chapter 5.

So, once Eu flux rate has been calibrated, and P_{O_2} is set to the desired value by gradually opening the leak valve, also the manipulator is heated up to the desired substrate temperature T_S. At this point the sample holder is rotated of 180°so that the substrate is facing down directly on top of Eu crucible. The shutter of the latter is then opened thus starting the growth of EuO thin film. The growth process lasts 90 minutes for each sample and during the whole time it is monitored by Reflective High Energy Electron Spectroscopy (RHEED) technique. Moreover, the growth was terminated by first closing the oxygen leak valve and then the Eu shutter after 60 seconds for some samples, while for the others by closing both of them simultaneously, and finally lowering the temperature of the substrate to room temperature. In the former case, an extra minute of Eu flux will compense the fact that pumps are not fast enough to pump out immediately the residual oxygen present in the chamber.

At the end of the growth process, the sample is transferred to the XPS and LEED chamber for determining th chemical composition and structural characterization, and later in the so-called MOKE chamber for transport measurements. The Eu flux rate is checked again immediately after growth by means of lowering again the thickness monitor, to ensure that no variations in the flux occured during the process.

2.3.3 Capping of EuO samples

Europium Oxide thinf films are very sensitive to air beacuse of their high reactivity with oxygen in the atmosphere, that may led to further oxidation states thus compromising their properties. For this reason, for *ex-situ* characterization, i.e. SQUID, it is necessary to protect the samples with an Aluminum capping layer before taking them out of vacuum. This process is performed in the UFO load-lock chamber after all *in-situ* characterizations, by means of an Al- evaporator Knudsen cell. Aluminum is evaporated onto EuO film at T_k=1180℃for 4 hours (2 hours perpedicular to the flux, 1 hour at 45° left ad 1 hour right, in order to be sure to cap the film properly). From XRR analysis of Sutarto *et al.*[50] it was revealed that the thickness of the Al capping layer in this condition was about 20÷40 Å.

Chapter 3

In-situ Characterization

In this section the techniques for *in-situ* characterization of the samples, i.e. which can be performed in the same environment where the samples are fabricated, are described. These are Reflection High Energy Electron Spectroscopy (RHEED), Low Energy Electron Spectroscopy (LEED), X-ray Photoemission Spectroscopy (XPS), and resistivity measurements for transport properties characterization. All the mentioned techniques are indeed employed on the samples directly either in the growth chamber, or in the specific chambers connected to it. What is important is that the UHV condition is mantained during the transferring of the samples, thus avoiding any contamination due to external factors.

3.1 RHEED

Reflection High Energy Electron Spectroscopy is one of the standard and most versatile techniques to characterize the surface structure and monitor the growth process itself. This is possible due to the high energy of the electron beam and the UHV vacuum condition, that permits to classify RHEED as an *in-situ* and *real-time* technique.

The primary electron beam is generated by an electron gun at an energy in the range of 10-30 keV. It is focused by a tunable multiple lens system and it impinges on the film surface at a grazing angles of about 3°. The elasticaly scattered electrons are reflected by the sample at a similar angle, and the produced diffraction pattern can be observed on a fluorescent screen on the opposite side of the gun. Due to the low incident geometry, the penetration depth of the beam is very limited ($\sim$ 10 Å), so that the information provided by the RHEED patterns are basically about the quality and morphology of the outermost atomic layers.

Kinematic theory and pattern

Even though more complex theories involving knowledge of the frequency dependent dielectric function could be possible, a geometrical interpretation of the diffraction pattern can be obtained by a much simpler treatment known as *kinematic theory*. In this context the diffraction process, that includes both *elastic* and *inelastic* scattering events, is based on the particle-surface single-scattering approximation, where the interaction between the incoming electrons and the periodic potential can be described using time-dependent perturbation theory.

So basically, monoenergetic electrons with energy E and wave vector $\mathbf{k}_0$ are incident on the surface and scattered into a state $\mathbf{k}$. So when only considering elastic scattering in the expression of the scattering probability, one then finds the diffraction, or *Laue condition*

$$K_{\parallel} = k_{\parallel} - k_{0\parallel} = G_{\parallel} \tag{3.1}$$

where $K_{\parallel}$ indicates the scattering vector component parallel to the surface, and must be equal to the surface reciprocal lattice vector $G_{\parallel}$, in order to heve constructive interference.

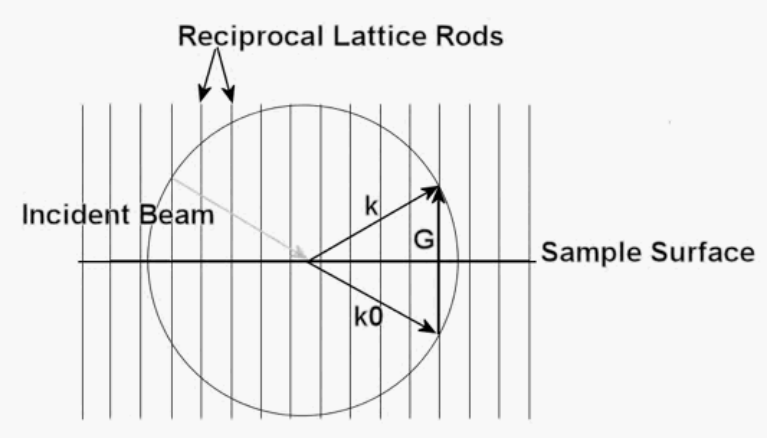

Figure 3.1: RHEED scheme of the Laue condition for constructive interference.

Due to the very high surface sensitivity of RHEED the periodical part beneath the surface can be neglected and the sample volume can be approximated to a 2D layer. The third Laue Condition perpendicular to the surface is then relaxed, and sharp streaks, spaced by $G_{\parallel}$ would originate in the reciprocal lattice along the z direction, instead of points as it is for the in-plane directions. Whereas the electron beam is represented in reciprocal space by the geometric construction of a sphere, the *Ewald Sphere*, centered on the incident point and with radius $\mathbf{k}_0$, related to the energy E of the

beam by the following relation:

$$k_0 = \frac{1}{\hbar}\sqrt{2m_0E + \frac{E^2}{c^2}} \tag{3.2}$$

So every time that this sphere intersect one of the reciprocal lattice streaks, it will originate a diffraction spot, corresponding to an intensity maxima on the fluorescent screen. In RHEED the Ewald sphere radius is much larger than the reciprocal lattice spacing, so that it makes an almost planar cut through the first Brilluine zones of the reciprocal lattice in the perpendicular direction to the beam. Moreover in real patterns both the ewald sphere and the streaks show a finite thickness, thus leading to a broadening of the spots into sharp streaks, as one would see in a typical smooth surface single-crystal RHEED pattern. This is due to the spread in energy and divergence of the incident electrons for the former while to surface disorder and termal vibration of the crystal for the latter.

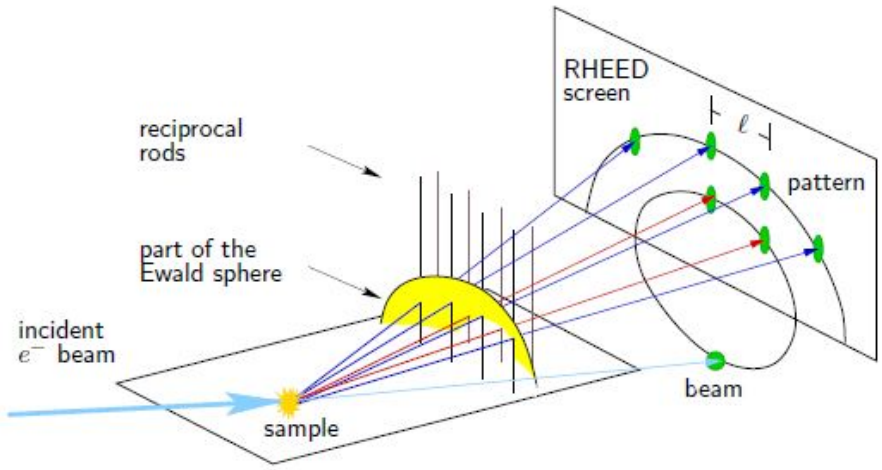

Figure 3.2: The principle of the formation of RHEED pattern, schematic.

Depending on the surface morphology and flatness one can distinguish between 3 general RHEED pattern:

- *smooth single-crystalline* surfaces. Generally associated to layer-by-layer growth mode, they produce a streak-like pattern, that indicates a very flat and smooth surface, with mono-crystalline thin film surface.
- *rough single-crystalline* surfaces, usually characterized by *island* growth. In this case the electrons impinging the surface feels the crystal periodicity also in the vertical direction in a way that also the 3rd Laue condition has to be fulfilled, resulting in the formation of a spot-like pattern. Modulated streaks pattern is also possible as intermediate situation between rough and flat surface.

- *polycrystaline* or*amorphous* surfaces, that is comparable to effect observable when an electron beam is passing through series of single crystals of different orientations. The diffraction pattern will then looks like the superposition of single-crystal spot patterns, resulting in a series of concentric rings features or in diffusive background only with no diffraction pattern at all.

RHEED Oscillations

If one considers only the first order reciprocal lattice spot, corresponding to the specularly reflected beam, periodic oscillations can often be observed. This effect is known as RHEED oscillations, and is one of the most powerful tool that provides in-situ and real time informations on the dynamics of the growth process, and in particular the total amount of material deposited with monolayer accuracy. In the case of layer by layer growth in fact, its intensity oscillates in a sine-like waveform as a function of time, where the period indicates the time for the formation of a complete single layer. In the case of layer-by-layer growth the origin of such RHEED oscillations can be explained through an approach based on dynamic/multiple scattering process[33]. According to this apporach the step density[1] of the 2D nucleation on the surface varies periodically. Thus a maximum in the 00 spot intensity occurrs when the step density is minimum, i.e. at the initial smooth surface of a complete growing layer, whereas a minimum intensity occur for a maximum in step density, in other words when the growing layer is half complete. The following formula shows the relation between the step density $\bar{\theta}$ and the intensity I of the reflected beam:

$$I \sim (1 - 2\theta)^2 \tag{3.3}$$

It is also possible to have layer-by-layer growth but without RHEED oscillations. This phenomenon is attributed to the fact that new adatoms do not nucleate in the position where they imping on the surface, but they migrate till to the step edge and only there nucleate. In this way the step density is always constant and no intensity oscillations of the reflected beam are expected. However the absence of RHEED oscillations may also be due to 3D island growth. In fact while islands nucleate the diffraction intensity due to multiple transmission and reflection processes is more dominant so that the intensity of the specular reflected beam is hidden. Nevertheless, the RHEED pattern may help in distinguish between the two situations. In the previous case, it still shows streaky features related to the two dimensional nucleation step-flow. Whereas in the latter case the corresponding RHEED pattern shows many spots, indicating the roughness of the surface.

Another frequently observed phenomena is the damping of the oscillations, that happens on a time scale much larger than the oscillation period.

[1] the direct cause of diffuse scattering

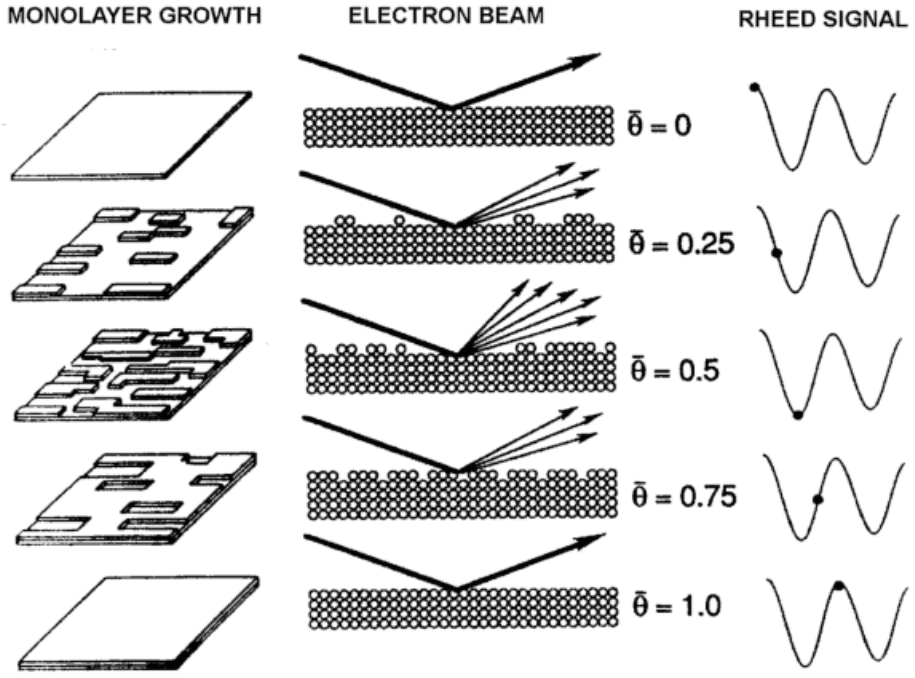

Figure 3.3: Representation of RHEED intensity oscillations taken from the corresponding morphology of the substrate.

This could be due to the roughening of the surface that approaches a steady state after some monolayers of growth, while a recovery after growth is related to an improvement of the surface smoothness towards the achievement of thermodynamic equilibrium. This is the case of EuO as shown for the first time by Sutarto *et al.*[50] in his work about initial and sustained growth. Moreover the experimental geometry could also influence this aspect influenced also by the experimental geometry. The flux density of an effusion cell indeed decreases with the distance as $1/r^2$, so the rate of arrival of the impinging atoms is not uniform over the surface. So, due to the finite diameter of the beam, the electrons impinge over 10 mm of the sample surface along the beam direction, thus sampling portion of the film with different growth rate, so that the net effect will damp out the oscillations in the final pattern.

EuO characterization

Our device is an EK-35-R RHEED type of STAIB Instruments. The energy of the beam is usually operated at 20 keV. The beam can be moved both horizontally and vertically and as initial step it is centered on the bottom

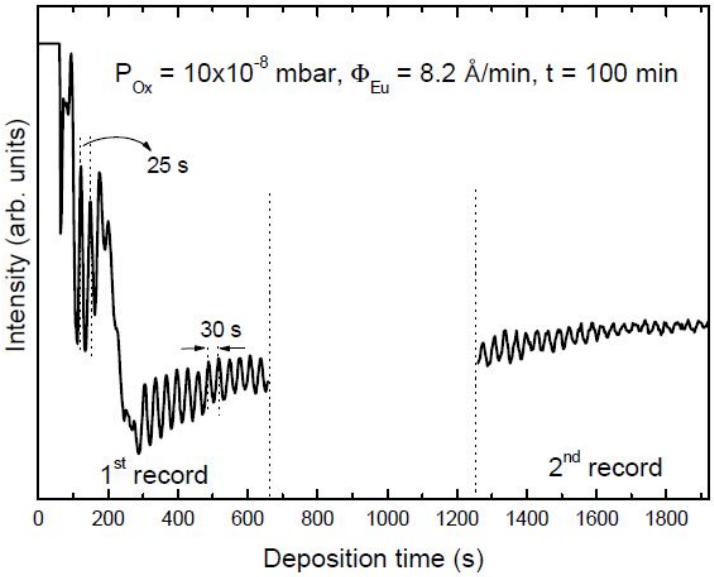

Figure 3.4: RHEED intensity oscillations of the specularly reflected electron beam recorded during EuO deposition on YSZ(001). Growth conditions: T_S=400℃, $P_{Ox} = 10 \times 10^{-8}$ and $\Phi_{Eu} = 8.2$ Å/min[50].

part of the phosphorus screen. Once the sample is placed in the growth position, the beam is slowly rised till the surface of the substrate, and the first diffraction pattern of the same appears on the screen. The focus and the shape of the electron beam can then be varied in order to get the best defined pattern, while a movable beam shutter can be lowered in order to get rid of background intensity by shadowing part of the beam that does not hit the sample. Before and during the growth process diverse images of the RHEED screen are recorded by means of a CCD camera which is interfaced to a computer. The program EE-2000 is the software used for the analisis, which permits also to record videos and monitor RHEED oscillations.

For each sample the same set of patterns (see Figure 3.5) is recorded: initially a first image of the annealed YSZ(100) substrate is taken to check the quality and to adjust the focus of the beam. After that a video of the first 10 minutes of growth is recorded. Nevertheless it is not trivial to find good RHEED oscillations for all of the films, since the most of them showed a slight shift of the reflected beam immediately after opening the shutter of the Eu effusion cell. Moreover during the whole deposition process, RHEED patterns of the growing film are recorded every 20-30 minutes, in order to provide a cronological recording of the film surface quality.

As can be seen in Figure 3.5(a), the pattern of YSZ(100) substrate shows marked Kikuchi lines at about 60°degree with respect to each other. These lines arise form inelastically scattered elctrons and their presence indicates a

crystal with perfect surface and bulk lattice, assuring thus the high crystallographic quality of the substrate. In the following patterns instead, related to the EuO growing film, Kikuchi lines disappear, meaning that the surface is getting less perfect. However streaks are still well defined and with the same distance, synonimus that the films is growing epitaxially with the lattice constant perfectly matching the one of YSZ substrate. At each time of the growth no marked spots are arising in the streak pattern, so that we can deduce that the deposition process is proceeding by layer-by-layer growth mode.

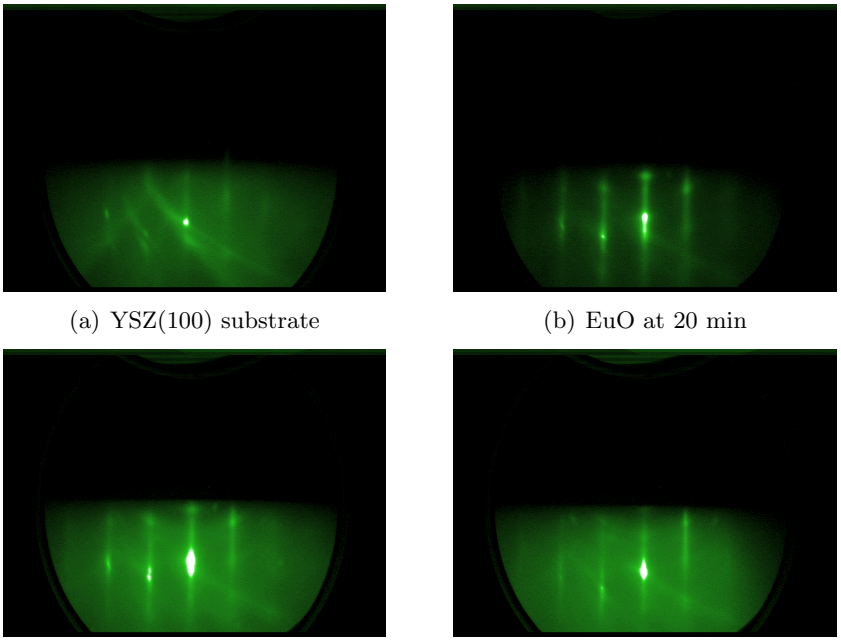

(a) YSZ(100) substrate

(b) EuO at 20 min

(c) EuO at 42 min

(d) EuO at 73 min

Figure 3.5: RHEED patterns of A337 sample recorded at different times.

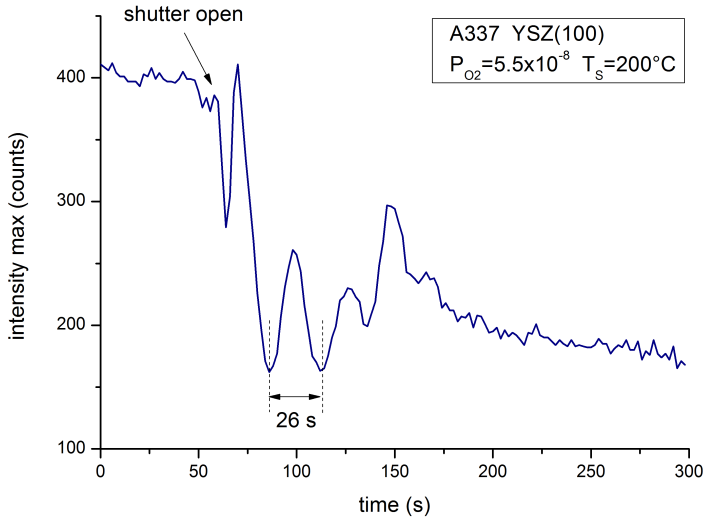

Figure 3.6: RHEED oscillations recorded during growth of A337 sample. The period is found by calculating the distance between two minima.

3.2 LEED

Low Energy Electron Diffraction is another surface-sensitive technique that allows surface characterization of the films in terms of lattice symmetry and crystal structural quality. As for RHEED it is based on the Kinematic theory but operates at much lower electron beam energy and the geometry of the experiment is also different: in LEED electrons with an energy between 50 an 500 eV impinges perpendicularly on the surface and they are collected on a fluorescent screen after back scattering. Even if the geometry is not the most suitable, the electrons penetrate only a few angstrom below the surface, due to their short mean free path, thus making of LEED a higly surface sensitive technique. The low energy electrons in fact interact strongly with the lattice, and only those which are scattered from near the surface can leave the surface and be detected.

The electron gun generates monochromatic electrons thanks to a heated filament that functions as cathod. The electrons are then focused into a beam by electrostatic lenses and accelerated by the potential between the cathode and the first aperture, which is at the same potential of the last, so that a field-free space is estabilished between the sample and the fluorescent screen. The latter is then biased positively in order to achieve a final acceleration of the back scattered electrons. An additional middle grid is set at negative bias, in order to prevent inelastically scatterd low energy electrons to reach the screen, which are the main cause of homogeneus background

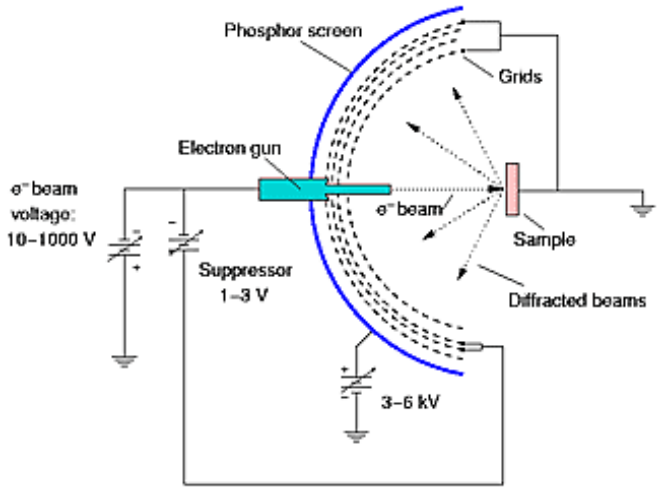

Figure 3.7: Schematic of the geometry of a LEED experimental setup.

illumination of the screen.

Patterns

Since the energy of electrons is low, and their **k** vector as well, in LEED the radius of the Ewald sphere is comparable with the reciprocal lattice constant. Therefore, instead of along their length, the Ewald sphere will intersect the lattice rods only in some points, where the two Laue diffraction conditions are fulfilled. The pattern will result then in an ordered arrangements of spots, corresponding to the 2D reciprocal lattice of the surface. Their position and separation thus give direct information about the in-plane lattice constant and the symmetry of the crystal. The relationship between reciprocal (a*,b*) and real (a,b) lattice constant is given by

$$|a^*| = \frac{2\pi}{a} \qquad |b^*| = \frac{2\pi}{b} \tag{3.4}$$

From the constructive interference for the in-plane directions

$$a(k - k_0) = \mathrm{h}\lambda \qquad b(k - k_0) = \mathrm{k}\lambda \tag{3.5}$$

where λ is the electron De Broglie corresponding wavelength, related to the the energy E of the beam

$$\lambda = \frac{h}{\sqrt{2mE}} \tag{3.6}$$

it follows the general *Laue condition*

$$k_{\|} - k_{0\|} = G_{\|} = \mathrm{h}a^* + \mathrm{k}b^* \tag{3.7}$$

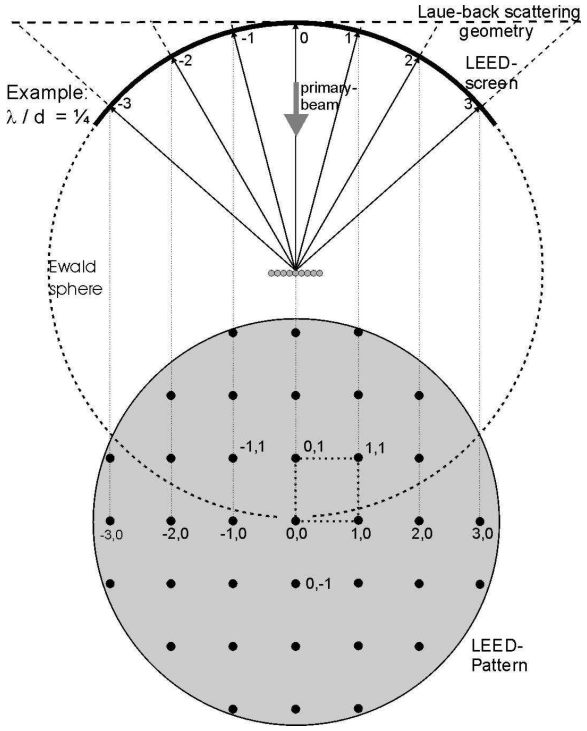

Figure 3.8: Expected LEED diffraction pattern of an fcc(100) crystal lattice surface.

Therefore in LEED, by changing the energy of the incident electron beam and thus increasing or decreasing the Ewald sphere radius, one can investigate different orders of the reciprocal space and not only the first Brilluin Zones. So sharp spots with low background intensity are expected in case of a well ordered crystalline lattice. on the contrary random defects or lattice imperfections broaden the spots and increase the background intensity.

EuO characterization

Our apparatus is the Rear View LEED with T191 Electronics form Thrmo Vacuum Generator Scientific, and is mounted on a side flange of the XPS chamber. The LEED patterns are taken right after the Photoemission measurements. Once the sample is placed in the right position, with the surface facing the electron gun, the LEED screen can be moved in to 4-6 cm far from the sample. The filament current is then rised to 2.6 A, and the high voltage immediately after to get the first pattern on the screen. Clear and sharp spots are obtained by operating on focus, retarding grid and mesh settings. As well as for RHEED, the images of the fluorescent screen is recorder with EE-2000 software by means of a CCD camera connected to a computer.

An example of LEED patterns taken at different electron energy is shown

in Figure 3.9. Here one can notice how at low energy, i.e. the first picture on top to the left, the patterns show only one or two reciprocal lattice unit cell. By increasing the energy instead, even more and more unit cell get into the patter, meaning that the Ewald sphere is intersecting a wider range of lattice rods.

Moreover at a first look all the spots look like having the same intensity, but one may notice that some are brighter and bigger, while others not. More exactly the brighter ones are disposed in a squared bigger cell oriented parallel with the axis of the camera, while the weaker ones are located in the middle of the high intensity spot cells. This phenomena can be explained by considerating a few aspects.
Europium Oxide has crystal structure composed by two interpenetrating fcc lattices, one made of Eu atoms andone of Oxygen. Since we are growing films on YSZ(100) we expect that also EuO film surface will be the (100), so that the surface structure will resemble a 2D square lattice composed of alternating Eu and O atoms, as shown in Figure 3.10. In the corresponding diffraction pattern 2 different unit cells are indicated, i.e. (a_1^*,a_2^*) and (b_1^*,b_2^*). The former is true if one considers as primitive cell in real space the square built by the (a_1,a_2) vectors. The latter if one considers only one speicemen, e.g. only Eu atoms, and the corresponding primitive cell built by the (b_1,b_2) vectors.

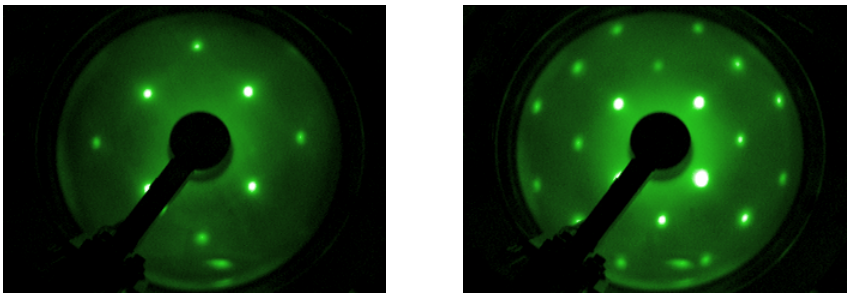

(a) E=65 eV (b) E=99 eV

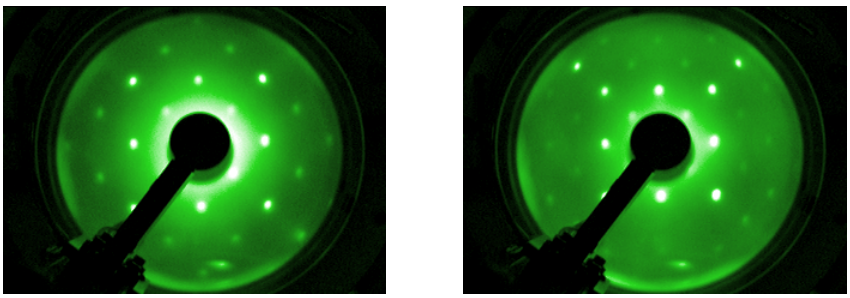

(c) E=151 eV (d) E=218 eV

Figure 3.9: LEED patterns ok sample A336 taken at differen energies.

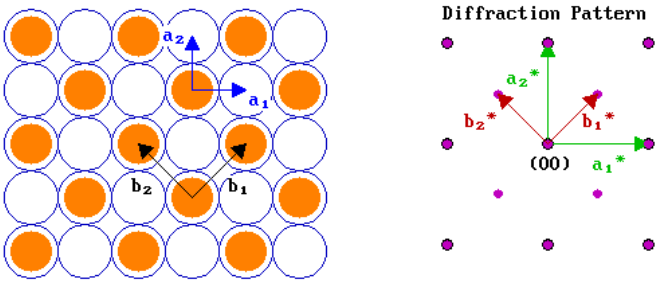

Figure 3.10: Real space EuO fcc(100) surface crystal lattice and its corresponding reciprocal lattice diffracion pattern.

Now one may question which one of the two is the correct vision of the problem. The answer is that they are both, acting simultaneously to reach the final patter. In fact, in the first case one would expect a (a_1^*,a_2^*) diffraction pattern with larger spacing. On the contrary in the second, one would expect a (b_1^*,b_2^*) pattern tilted of 45°with respect to the former, and with all the spots with the same intensity. What we see indeed is a (b_1^*,b_2^*) like pattern, but with half of the spots, i.e. the ones corresponding to the (a_1^*,a_2^*) like pattern, higher in intensity.

To explain this concept one has to consider that the real primitive cell of EuO is indicated by the (b_1^*,b_2^*) vectors. Nevertheless the base is composed by two different atoms, with different scattering cross section, thus giving rise to non uniformity in the spots intensity. In the limit that all the atoms are the same then half of the spots will disappear, whereas in the limit that only one specimen is present all the spots will gain the same intensity. Therefore in our case, where Europium (mass number 68) and Oxygen (mass number 8) are composing the base of the total lattice, and intermediate situation between the two limiting case is what we expect and actually see.

In conclusion we can argue that the LEED patters indicates that we are growing well ordered stochiometric EuO with a good surface structure and almost defect-free. Depending on the level of doping or vacancies then, the departure from stoichiometry can result in an increased broadening of the spots. However all the sample shows good LEED patterns, meaning that a basic good crystalline structure is manteined, even in presence of slightly non stoichiometric compounds.

3.3 XPS

Photoemission electron spectroscopy (PES) is the most powerful experimental method to acquire informations on electronic states in solids[35]. In surface physics it can provide valuable informations about the electronic structure and chemical composition of the film.

In X-ray photoemission spectroscopy (XPS) mono-energetic X-rays are generated and focused into a beam that hits the sample with a penetration depth of $1 \div 10$ μm. The incident photons can be adsorbed by core or valence electrons, if the energy of the beam is in the range of hard or soft X-rays, respectively, thus exciting them to higher unoccupied states. Those electrons which have gained enough energy can escape the crystal into the vacuum and their kinetic energy is measured by an electron energy analyzer. Thus out of the kinetic energy one can determine the binding energy of the excited electrons, and therefore reconstruct the electronic structure of the investigated material. Nevertheless the probing depth of XPS technique is determined by the inelastic mean free path of the photoelectrons, which is dependent on their energy, as inferred from Figure 3.11. For typical soft energies the electron escape depth is limited to about $5 \div 20$ Å, so that XPS can be considered a quasi-surface sensitive technique.

By varying energy, angle and polarization of the incident photons and observing kinetic energy and angle of emerging electrons XPS provides means to probe all occupied states of solids and characterize their properties. In our experiments however we will focus on soft X-ray photoemission for the study of valence band structure of Europium Oxide thin films.

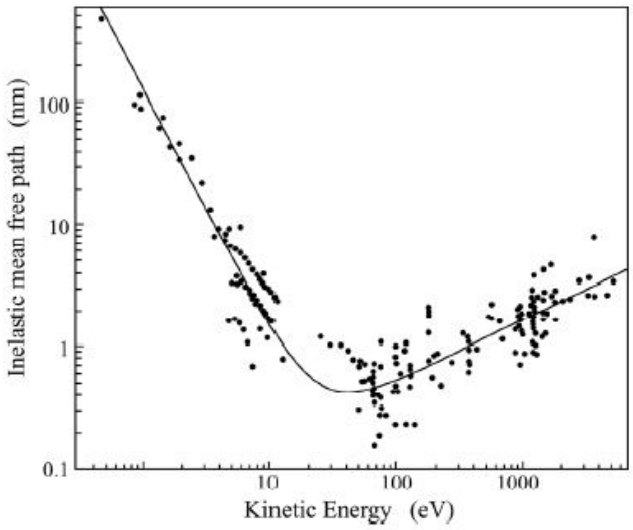

Figure 3.11: Mean free path of electrons in solids as function of their energy.

Physical Principle and Spectra

X-ray photoemission spectroscopy is based on the application of the *photoelectric effect*, initially observed by Hertz and later explained by Einstein as a manifestation of the quantum nature of light. When light is incident on a sample an electron can adsorb a photon and escape from the material with a maximum kinetic energy $E_{kin} = h\nu - \phi$, where ν is the photon frequency and ϕ the material work function[2].

Since the electrons in solids are held on the crystal structure, the energy of the emitted photoelectrons depends also on the binding energy E_B, that is higher for inner shells electrons, and lower for outer ones. The final kinetic energy is thus given by

$$E_{kin} = h\nu - E_B - \phi \tag{3.8}$$

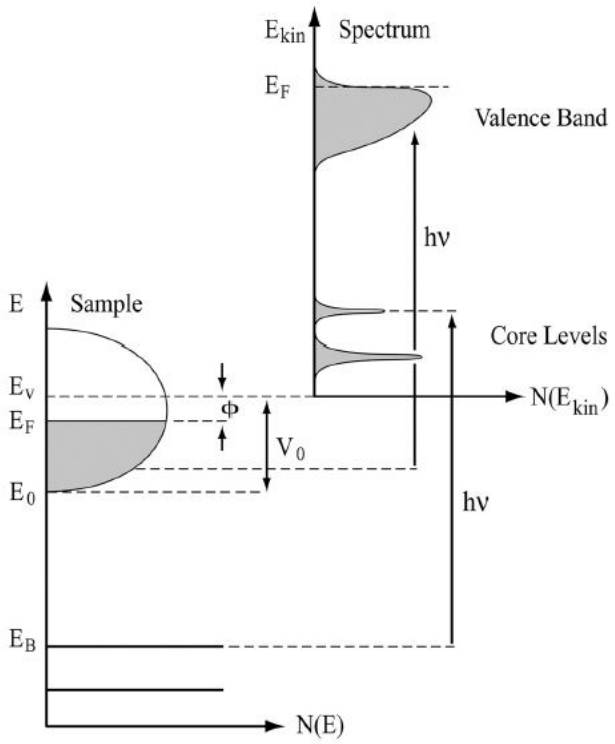

Figure 3.12: Relation between the spectrum measured by XPS (on the top right side) and the materials occupied density of states (on the bottom left side): one can see sharp core levels and the broad valence band filled up to the Fermi level, which is separated from the vacuum level by ϕ. [36]

[2]the work function is a measure of the potential barrier at the surface that prevents the valence electrons from escaping, and is typically 5-4 eV in metals

Since the photon energy $h\nu$ is fixed, and the work function as well, the corresponding distribution of the electrons kinetic energies escaping the crystal yelds a quantitative image of the distribution of occupied electronic states, as it is shown in Figure 3.12. However it is necessary to remark that this is valid in the one electron framework where electron-electron interactions are neglected, and it is commonly accepted that XPS photoemission spectra are interpreted as the occupied density of states (DOS).

The XPS spectra comprises sharp peaks which are superimposed to a broaden background feature. The formers come from photoelectrons with negligable energy loss, corresponding to the effective electron structure features of the analyzed material. The latter instead comes from secondary electrons which have suffered energy loss due to inelastically scattering with other particles inside the solid. The photoelectron spectrum is often accompained by Auger electrons peaks, which are emitted after the decay process of other electrons from higher states into core holes created by the X-ray incoming beam. Part of this energy is trasferred to electrons that are thus emitted at Auger energy lines independent from the energy of the x-ray source.

Since the binding energies of the core levels are specific of each element, photoemission spectra can be also used as a chemical characterization technique. The energy shifting in the spectra and the number of countings of each peak can therefore provide informations useful to determine which element is present and its quantity with respect to the others.

Experimental Setup

A typical XPS experimental setup consists of a combination of an *x-ray source*, a *lens system* and an *energy hemispherical analyzer*, as shown in Figure 3.13.

Standard laboratory X-ray sources are the Mg-K_α and Al-K_α emission lines, at 1253.6 eV and 1486.6, respectively. However in the last years, synchrotron sources became available, combining a polarized high photon flux with tunability in a wide spectral range with energies between 10 eV and several keV. In our laboratory in cologne the x-ray source consists of an electron gun, a water cooled Al anode and a Vacuum Generators twin crystal monochromator. The gun generates electrons which are accelerated up to 10 keV onto the Al anode, and wo types of radiation are emitted as a consequence. From the deceleration of the Alternatively the incoming electrons can eject electrons from core orbitals of the target material by ionization. As a consequence characteristic x-ray lines are emitted from the recombination between the generated holes and electrons from higher orbitals. The produced x-ray beam is subsequently monochromatized be two separate adjustable quartz crystals by Bragg reflection into the K_α line at 1486.6 eV. The monocromatized x-ray beam is then focused onto the

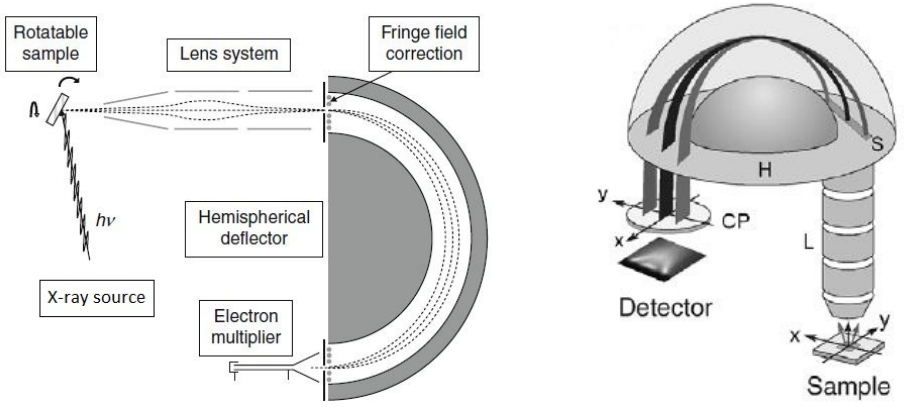

Figure 3.13: XPS experimental setup. (a) Schematic section of the kinetic energy electron analyser system, composed by a lens system and the electron multiplier for detection. (b) 3D representation of the same object.

sample whence photoelectrons are then generated.

Once ejected from the sample the electrons are collected usin a Gamma-data Scienta SES-100 electron energy analyzer, which consists of an electron lens-system, an emispherical electrostatic deflector unit, and a micro-channel plate (MCP) with a phosphor screen as a detector device. The electron lens system serves to focus the photoelectrons onto the entrance analyzer slit, to define the angular aperture and to vary their kinetic energies in order to be matched with a selected energy scanning range.

At the hemispherical analyzer, an electric fiels is estabilished within two concentric hemispheres with radii of 110 mm and 190 mm. This field only allows photoelectrons of a given energy, i.e. the *pass energy* to arrive at the detector slit and onto the MCP itself. To keep the resolution constant during energy scans the analyzer operates at constant pass energy while a lens system accelerate or decelerate electrons to match the kinetic energy to the pass energy. When equipped with a fringe fields at the entrance and exit slits, energy resolutions down to 1meV can be realized. The resolving power, RP, of a hemispherical analyzer is approximated by:

$$RP = \frac{E_{pass}}{\Delta E} \simeq \frac{2R}{s} \tag{3.9}$$

where r is the analyser radius, s the slit width, E_{pass} the pass energy and ΔE the energy resolution of the spectrometer.

The micro channel-plate (MCP) is used to amplify the electrons signal arriving at the exit slit of the hemispherical analyzer. It serves as an electron multiplier with a gain of 10^6 order. The amplified electrons then arrive at the phosphor screen, where the light signal is recorded by means of a CCD camera. The position of the flashes is related to the kinetic energy of the

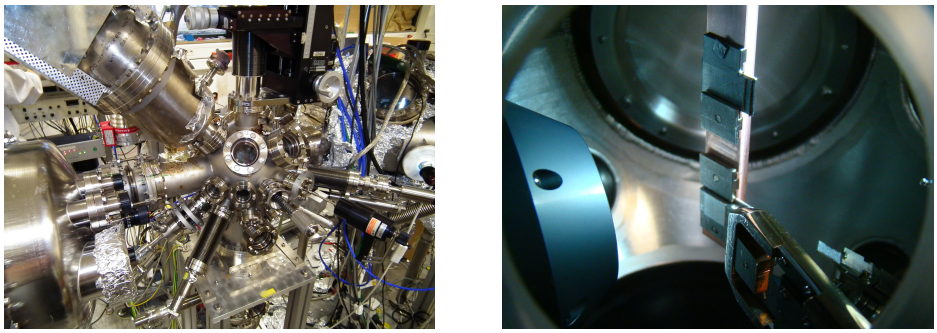

Figure 3.14: Inside view of XPS chamber. On the right a magnification of the manipulator.

photoelectrons, so that by means of a computer the spectra can be recorded controlling the detection unit via the SES software.

EuO characterization

The EuO thin film samples are transferred to the XPS chamber immediately after growth for electronic and chemical characterization. Here they are mounted on the 3-axial manipulator, and x-ray beam is centred and focused on them (see Figure 3.14). The azimuthal position is set at θ=75°for normal emission (NE) measurements. The optimization process is done by setting the analyzer around the energy of a specific peak expected to be high (the Eu 4d at 1354 eV with E_{pass}=200 eV) and maximizing the countings of the calibration function of the SES program.

All the grown samples were characterized in the same way, operating the analyzer in transmission[3] mode, by taking the following set of spectra:

- *very wide scan*: 200 ÷ 1500 eV at 200 eV pass energy and 500 meV step, 2 sweeps.
- *O1s Eu4d*: 900 ÷ 1400 eV at 200 eV pass energy and 200 meV step, 2 sweeps.
- *O 1s peak*: 944 ÷ 960 eV at 200 eV pass energy and 50 meV step, 20 sweeps.
- *Eu 4d peak*: 1310 ÷ 1370 eV at 200 eV pass energy and 50 meV step, 10 sweeps.

[3]in transmission mode the analyzer operates an integration over all the emission angles of electrons.

- *valence band*: 1467 ÷ 1485 eV at 100 eV pass energy and 25 meV step, 20 sweeps.

The very wide scan spectra gives a general overview of the sample and its qualitative chemical composition. Moreover one can see if the sample is charging or not by checking the position of the peaks, whether they ar shifted or not. The same is valid for the O1sEu4d spectra with the difference that the resolution is better and the range is in the range scanning from O1s to Eu4d peak.
The two following spectra are taken in order to calculate th O/Eu rate for quantitative analysis. The energy range is very short and centered around the O 1s and Eu 4d peaks, but the step is set very narrow and several sweeps are collected in order to have the best resolution and enough statistics for a precise calculation, as will be better explained in Chapter 5.
The last spectra is the valence band, taken in the range of the highest kinetic energies, corresponding the lowest binding energies with a very narrow step. These spectra are the most interesting because they show all the important features specific of a EuO, and by its analysis one can discover the presence of contaminations, and infer about the insulating or metallic behaviour.

Europium Oxide typical valence band spectra consist of an $Eu^{2+}4f$ peak at about 2 eV binding energy, corresponding to a $2p^6 \rightarrow 2p^5$ transition, and an $O^{2-}2p$ peak at 4÷7 eV, corresponding to a $4f^7 \rightarrow 4f^6$ transition. If non stoichiometric growth occurs and Eu_2O_3 oxides have been created, the consequence is an unwanted change in the electronic configuration and subsequently in the magnetic and transport properties of the film. In Eu_2O_3 in particular, Eu^{3+} ions are formed which present a $4f^6$ electronic configuration. In the XPS spectra the formation of this compound results in a weaker intensity of the $Eu^{2+}4f$ peak and a multiplet structure peak appears at energies around 6÷12 eV, corresponding to the Eu^{3+} $4f^6 \rightarrow 4f^5$ transition. In case of Eu-rich EuO instead, the formation of oxygen deficiency will result in an excess of Eu atoms with respect to the oxygen, so that films grown under this condition display a small spectral weight at the Fermi level, indicated as *Fermi edge*, indicating a metal character.

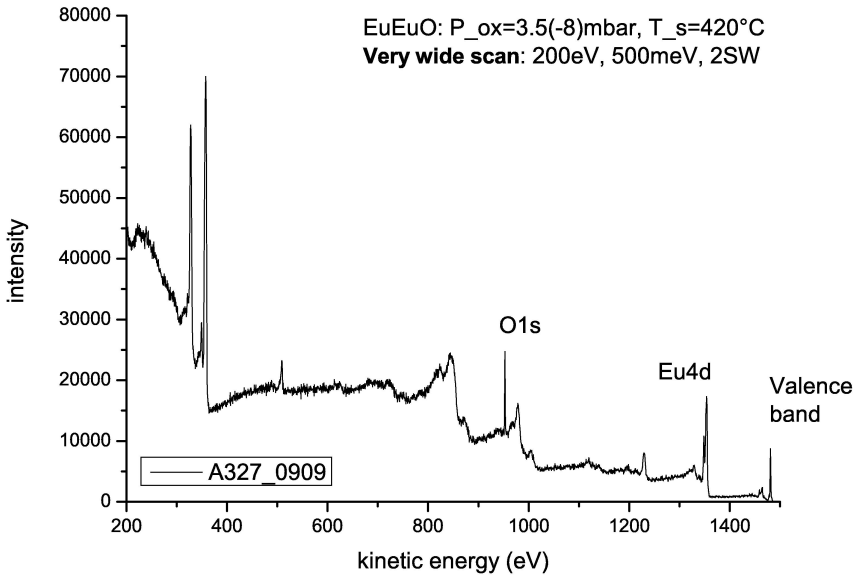

Figure 3.15: *Very wide scan* of sample A327. This is the typical spectra of stoichiometric EuO out of which one can infer about the presence of contamination or the charging of the sample if the specra is shifted to lower energy.

3.4 Transport Measurements

In order to relate EuO growth conditions to its transport properties , it was necessary to develop a solution to measure resistivity of the grown films.

The transport measurements were performed *in-situ* in order to prevent the surface from further oxidation. Therefore a system for electrical DC transport has been developed in the MOKE chamber. It consist of two aluminum tips equipped with copper contacts made of wires with diameter of 0.2 mm and covered with a polyamide insulatin layer. The tips are mounted on a push-pull mechanism driven by a screw which allows the contacts to lay down on the chromium islands on the sample. The chromium island of at least 50 nm thickness were previously grown on the substrate in a separate UHV chamber by means of a copper mask, before thin film deposition. Between the two islands a gap of 0.04 mm is left, by adding a thin wire to the mask during Cr deposition. It is in this gap the resistivity (or conductivity) of the films is actually measured.

The two wires are then connected to the outside of the chamber through the manipulator of MOKE chamber, which is provided with 4 BNC connections on top of it. Here is where BNC cambles are plugged in order to

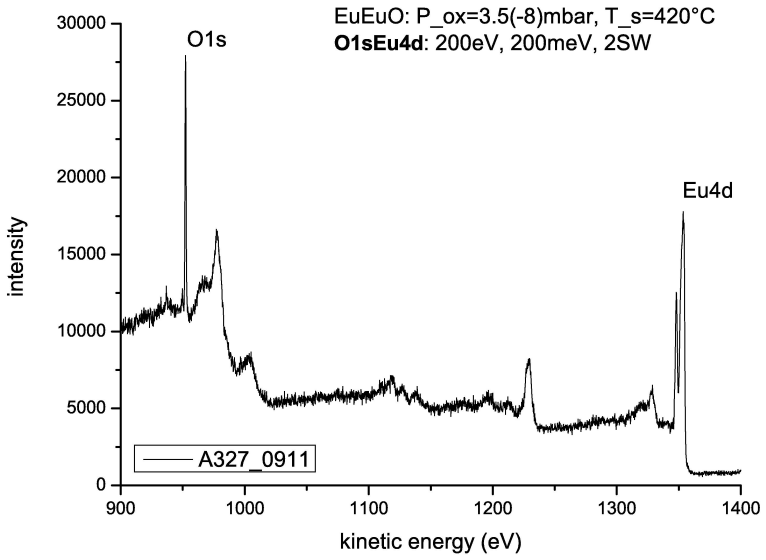

Figure 3.16: *O1s Eu4d* spectra of sample A327.

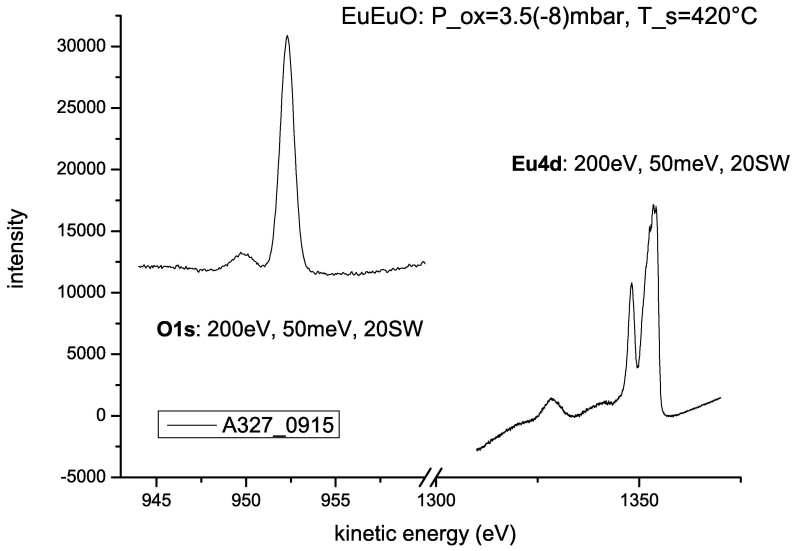

Figure 3.17: *O1s peak* and *Eu4d peak* of sample A327. Out of the integral of the area of these peaks a is calculated the ratio between Eu and Oxygen in the film thus revealing the oxygen vacancy concentration.

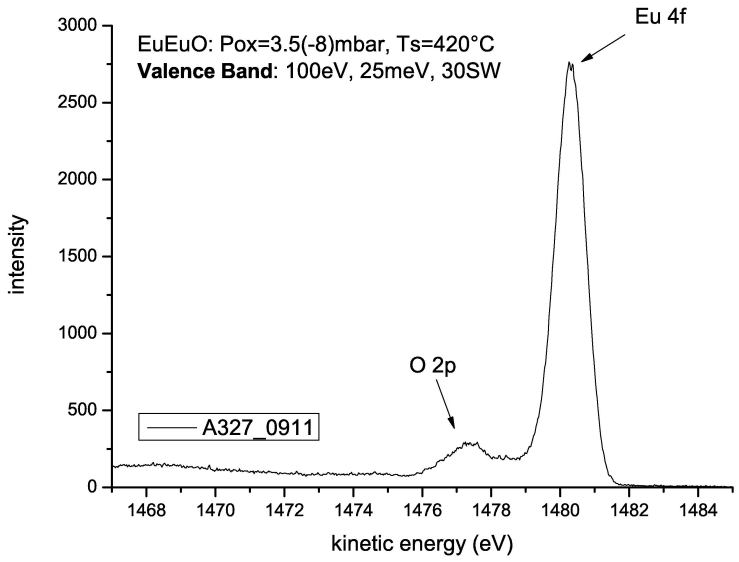

Figure 3.18: *Valence Band* spectra of sample A327. Stoichiometric EuO: no Fermi edge is observed.

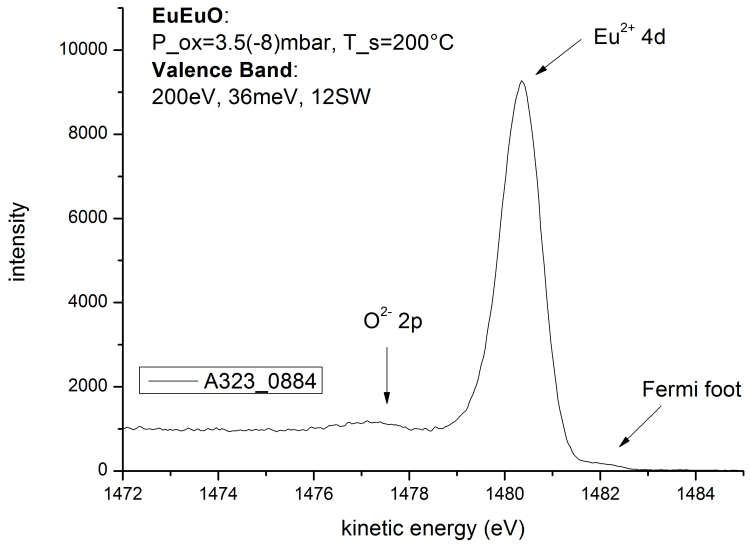

Figure 3.19: *Valence Band* spectra of sample A323. Eu-rich EuO: the presence of Fermi edge indicates the half metal character of the film.

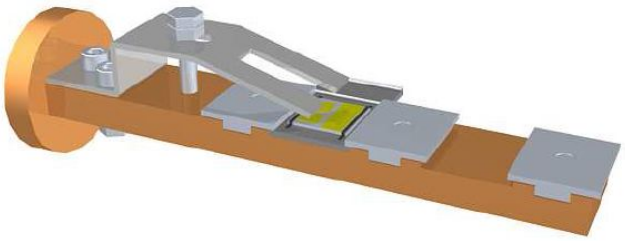

Figure 3.20: 3D model of the push-pull mechanism for transport measurements.

connect the system to the measurements setup. The quantity that is measured is resistance R (Ohm), from which is possible to get back to resistivity by the following formulas:

$$R = \rho\frac{l}{A} \qquad \rho = R\frac{A}{l} \qquad \sigma = \frac{1}{\rho} \tag{3.10}$$

where l is the distance in between the islands, A the correspective area of the contacts, given by

$$A = 2 \text{ mm} \times \textit{film thickness}$$

ρ is the resistivity and σ the correspective conductivity.

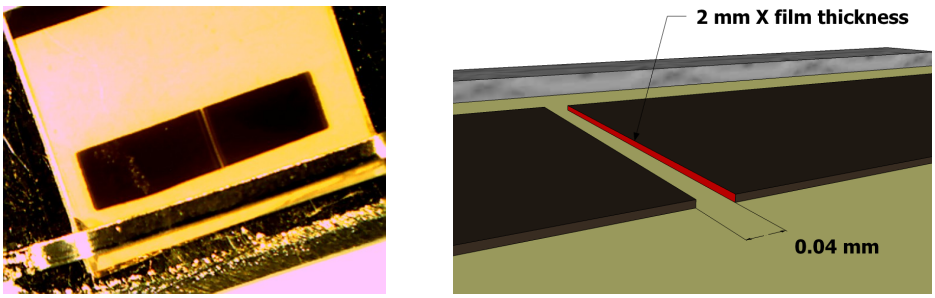

Figure 3.21: Top view and 3D model of the islands for resistivity measurements.

The aim of this type of trasport measurements is to verify the existance of a Metal-Insulator transition (MIT) in the grown EuO films depending on their stoichiometry and composition. Therefore the resistivity is measured as function of temperature R(T), in the range between ∼5 kelvin and room temperature. To lower temperature liquid helium is run into the

manupulator channel, thus gradually cooling down the manipulator and the sample itself to the He liquid temperature. To warm up it again, the helium flow is stopped and temerature increases slowly till room temperature again. Temperature is measured by a silicon diode located on the manipulator about 6 cm far from the sample, connected throug specific electronics to the computer. For this reason one of the main issues is to provide an optimal thermal conductivity between manipulator, sampleholder and sample while at the same time reducing thermal losses through the contacts during the measurements. A very good solution for the first issue was found to insert a 0.5 mm thick gold foil to improve between the substrate and the stainless steel plate, which is fixed to the sampleholder by two lateral clamps. To reduce thermal losses instead those wires reaching the samples were attached all along the manipulator with Torrseal glue to get them at the same temperature of the system.

Two different measurements are recorded of the transport properties of each film, the first while cooling down, and the second while warming up the sample. This is done in order to have a double check or a backup measurements in case something goes wrong with one of them.

Moreover the resistivity of the films can differ of several orders of magnitude depending on the growth conditions, from the MΩ range for stoichiometric EuO, till hundreds of Ohm for Eu-rich EuO thin films. Therefore two different setups were employed in order to perform accurately both high-resistance and low-resistance measurements.

High resistance setup

For resistance values of the sample exceeding 100 kΩ a 2-point measurement setup is employed. In this setup a constant voltage of 9 V is applied to the sample by means of a grounded battery box in between the two contacts and the current flowing through the gap is measured. The current measurement is performed employing a Keithley 6512 electrometer connected to the sample contacts through a special circuit as shown in the scheme of Figure 3.22. Therefore the resistance value $R(T)$ can be deduced by the following formula:

$$R = \frac{V}{I} \qquad R(T) = \frac{9\ \mathrm{V}}{I_x(T)} \tag{3.11}$$

where 9 V is the applied voltage through the battry box and $I(T)$ is the measured current as function of temperature.

Here, in order to perform low noise and accurate high resistance measurements a *constant voltage* configuration is used. In fact high resistivities are often function of the voltage so that this configuration is preferred to the constant current one. The voltage is provided by a low noise battery

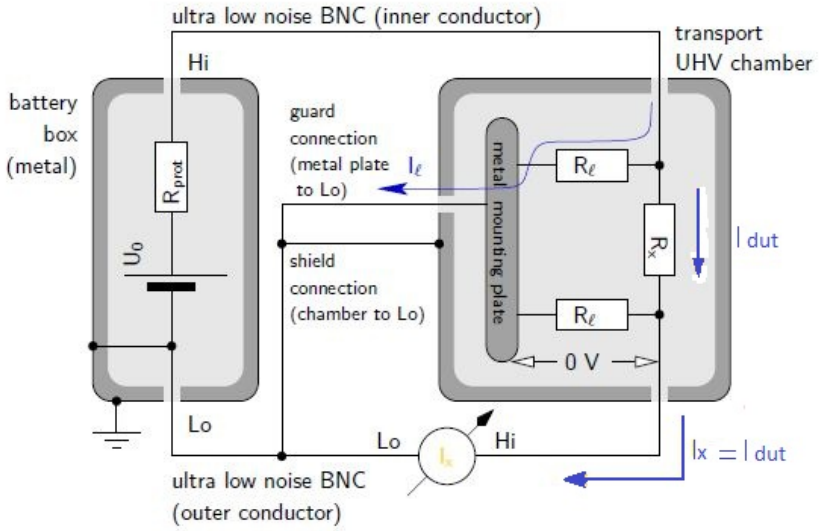

Figure 3.22: High resistance setup connection scheme.

box connected in series with the sample and the picoammeter. The latter is interfaced to a computer where a LabView program deals with the simultaneus acquisition of current and temperature. All the sistem is shielded against electrostatical fields by consistently using BNC connections and and using the steel chamber as a grounding itself. Moreover a guarding connection is realized to prevent from measuring any leakage current going through the sample.

Low resistance setup

For samples with resistance in the order of few kΩ and below a 4 points setup is preferred. In the low resistance measurements a *constant current* of 1 μA is run into the sample in between the two Cr islands and the correspective voltage V_x is then measured. In this configuration R(T) is determined as following

$$R(T) = \frac{V}{I} = \frac{V_x(T)}{1\mu A} \tag{3.12}$$

The current flow is generated a constant current source and set at 1 μA, measured by a Keithley 2400 for double check, and run throgh the first pair of contacts till to the islands on the film. Here the voltage drop $V_x(T)$ between the two islands is measured by means of a Keithley 2000 connected to the second couple of contacts through ultra low noise BNC cables. In this way no voltage drop due to the flowing current on the copper wires is

measured, but only the right value in between the two islands.

Temperature is measured in the same way as for high-resistance setup and the both R and T values are recorded by means of a computer with a different LabView program created for this setup.

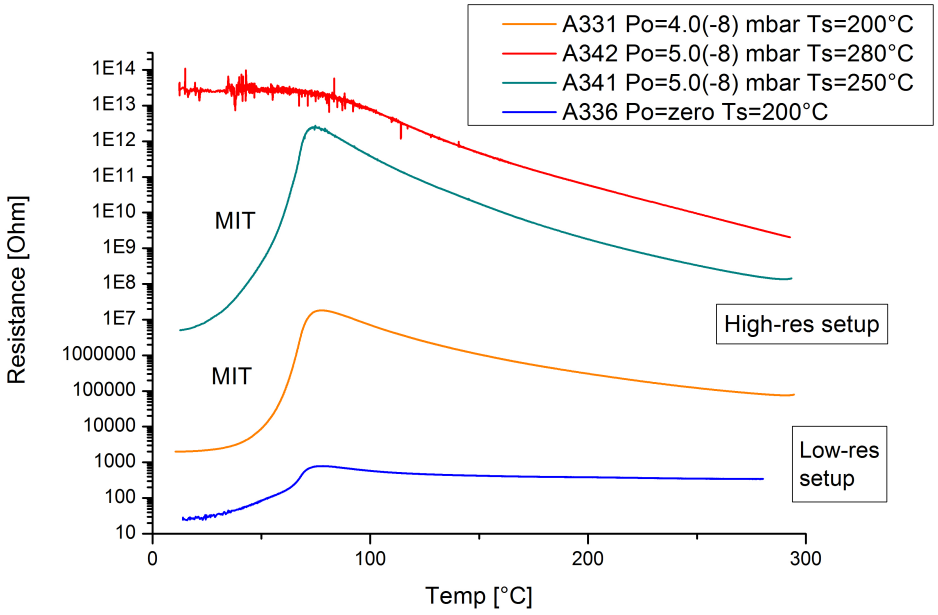

Figure 3.23: Transport measurements of various samples showing different resistance curves. The measurements are performed with two different setups depending on the resistance value, due to the strong dependence of the latter from stoichiometry.

Chapter 4

Ex-situ Characterization

In this section Superconducting Quantum Interference Device (SQUID) is described. This is an *ex-situ* technique for Magnetization characterization of the sample which cannot be performed in the same enviroment where the films are grown. It is indeed necessary to take the samples out of the UHV enviroment and insert them into a specific device, reason why it is required a proper capping of the films to prevent them form contaminations.

4.1 SQUID

Superconductin Quantum Interference Device is the most powerfull and sensitive instrument for characterizing the magnetic moment m of a sample over a broad range of temperatures and applied magnetic field. It makes use of the properties of electron-pair wave coherence and Josephson effect in superconductors in order to detect very small magnetic fields.

A SQUID magnetometer is formed by several componets, whose the maine ones are the following:

- a *superconducting magnet*. It consist of a superconducting solenoid which is kept at liquid helium temperature to operate in the superconducting regime. It produces a uniform magnetic field H used to magnetize the samples for calibration and field dependent measurements.

- the *detection coils*. Three counterwound coils made up out of a single superconducting wire serve as detector of the magnetic moment. The measurement is performed by moving the sample along the symmetry axis of the coils with an oscillating movement. This will induce a variation in the electric current flowing in the detection coils which is proportional to the magnetization of the sample. The Detection coils are configured as second-order gradiometer, which eliminates spurious

signals caused by the fluctiation of the field and also reduces the noise from magnetic objects in the surroundings.

- the *SQUID* itself. This is the key component of the device, which permits to convert the current fluctuation induced in the coils into voltage in an extremely sensitive manner.

- a *superconducting magnetic shield* which serves as protection for the SQUID sensor from external magnetic field nearby the location of the magnetometer and from the large magnetic fiel produced by the superconducting magnet itself.

Cooper Pairs and Josephson Junction

A SQUID magnetometer is able to detect in principle variation of magnetic field till to a quantum of magnetic flux, i.e. the *fluxon* whose value is $\Phi_0 = 2.07 \times 10^{-15}$Wb. This is possilble by taking advantage of the so called *Josephson Effect* occurring in superconducting tunnel junctions operating below the critical temperature T_C.

In superconductors, current is carried by the so called **Cooper Pairs**, in which phonons mediate a weak non-repulsive interaction between two electrons which can flow through the supercunducting material without any applied potential. Lattice deformations due to the first electron cause a local increase of positive charge which screens the electron-electron Coulomb repulsion[31]. The two electrons result then coupled and, since the motion of lattice ions is very slow, their wave-functions result coherent over quite long distances. Moreover in a uniform current density all the elctron pairs phases are coherent and they can be described by a single wavefunction

$$\Psi_p = \Psi e^{i(p \cdot r)/\hbar} \tag{4.1}$$

where r is the centre of mass position of the pair and p its net momentum which is related to the wavelength by the relation

$$\lambda = \frac{h}{p} = \frac{h}{2mv} = \frac{h}{2m}\frac{n_s e}{J_s}$$

So in a monodimensional case, if resistanceless current flows between two points X and Y in a superconductor there will be a phase difference $\Delta\varphi$ between the two points that is constant in time and depends on the current density J_s as follows

$$[(\Delta\varphi)]_{current} = \frac{4\pi m}{h n_s e}\int J_s \cdot \mathrm{d}l \tag{4.2}$$

Moreover, when a charged particle is immersed in a magnetic field, a further term will influence the particle momentum, which is given bby the product of

the charge particle and the vector potential A of the field. As a consequence also the phase difference between two points is affected and the further contribution is

$$[(\Delta\varphi)]_{magnfield} = \frac{4\pi e}{h}\int A \cdot \mathrm{d}l \tag{4.3}$$

If we apply these considerations to the case of a superconducting ring with area S in presence of a magnetic field B perpendicular to the plane of the ring it is straightforward to derive the phase change along the closed path:

$$[(\Delta\varphi)]_{current} = \frac{4\pi m}{hn_s e}\int J_s \cdot \mathrm{d}l + \frac{4\pi e}{h}\iint_S B \cdot \mathrm{d}l \tag{4.4}$$

In this framework the phase $\Delta\varphi$ is single valued and must be equal to $w\pi n$ with n integer, so rewriting the refphasediff one obtains

$$\frac{m}{n_s e^2}\int J_s \cdot \mathrm{d}l + \iint_S B \cdot \mathrm{d}l = n\frac{h}{2e} = n\Phi_0 \tag{4.5}$$

A **Josephson junction** consist of two superconducting region separated by a thin insulating layer. If the regions are close enough the Cooper pairs wavefunctions will become coupled and the electrons will be able to tunnel across the insulator gap even in absence of any applied voltage. This effect is known as Josephson tunneling. The supercurrent i_s that flows across the gap is related to the phase difference between the regions as described by the *first Josephson equation*

$$i_s = i_c \,\mathrm{sin}\Delta\varphi \tag{4.6}$$

where i_c is the critical current, i.e. the maximum current which can the Josephson junction can support without developing any voltage across it. Above this value the junction will behave as a normal tunnel junction with a Ohmic resistor-like $I(V)$ characteristic.

The *second Josephson equation* represents the variation of the phase difference $\Delta\varphi$ by the application of a finite voltage V across the junction

$$\frac{d\varphi}{dt} = \frac{2e}{\hbar}V = \frac{2\pi}{\Phi_0}V \tag{4.7}$$

In a Superconducting Quantum Interference Device, two Josephson junctions are coupled togheter as represented in Figure 4.1. A highly coherent supercurrent is divided so that it flows along the two paths and the total wavefunction of the superconducting electron pairs of region II experiences a phase shift compared to that in region I. In a magnetic field **B**, however, also vector potential also affects the phase shift and since the latter has to be identical in both the regions one obtains

$$\delta_b - \delta_a = \frac{2e}{\hbar}\int A \cdot \mathrm{d}l = \frac{2e}{\hbar}\int B \cdot \mathrm{d}S \tag{4.8}$$

The total phase difference around the ring can therefore be controlled by varying the magnetic flux. The phenomenon is known as *supercurrent interference* and it becomes evident if the total current I is considered due to the sum of the currents I_a and I_b in the presence of a magnetic field, which are given by

$$I_a = I_c \sin\delta_a \qquad I_b = I_c \sin\delta_b \tag{4.9}$$

For the total current we then find

$$I = 2I_c \sin\delta_0 \cos\left(\frac{e}{\hbar}\int B \cdot \mathrm{d}S\right) \tag{4.10}$$

The supercurrent through two parallel Josephson tunnel junctions therefore varies as the cosine of the magnetic flux through the loop, and maxima in the current occur whenever a further magnetic quantum flux is enclosed in the ring.

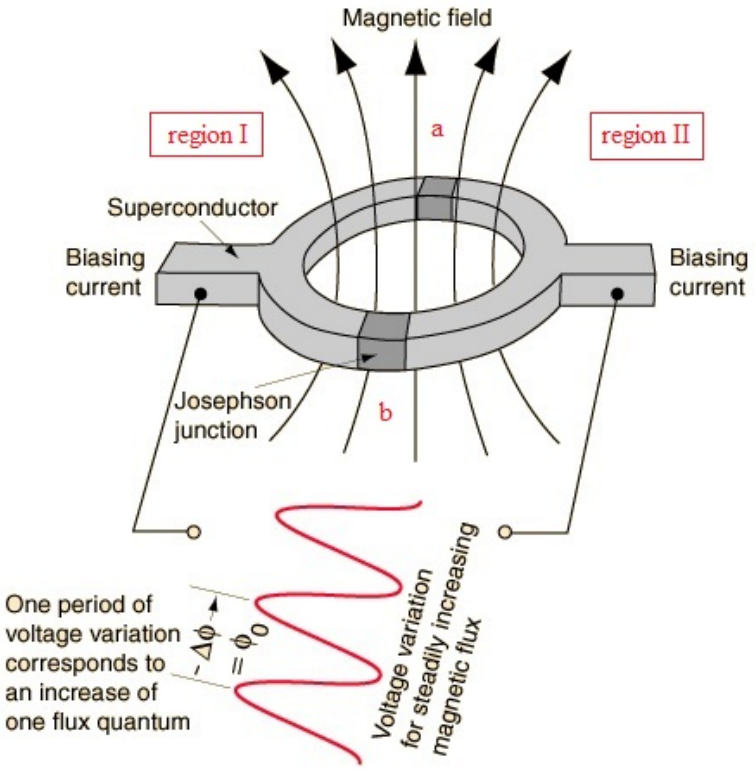

Figure 4.1: SQUID device operation schematics. Two superconducting metals are connected formin a ring and separate by two insulatin layers. The magnetic flux within the ring induces variations in the supercurrents thus allowing its measurement.

EuO characterization

Right after Aluminum capping of EuO thin films, the samples are extracted from the UHV enviroment and prepared for *ex-situ* magnetic characterization. In order to insert them into the SQUID, the films are cutted into smaller pieces whose area is measured by means of a specific software able to calculate it out of a picture of the pieces. The pictures are taken with an optic microscope connected to a computer camera and the program compares themanually selected area with a reference given one.

Our SQUID magnetometer is a Magnetic Property measurement System (MPMS)-XL7 from Quantum Design. The system consist of two parts:

- the first comprising the probe, dewar and SQUID assembly where the measurement is performed
- the electronic control system connected to a PC for settings and data acquisition

The probe allows to perform measurements between 1.9 and 400 K with an accuracy of $\pm$ 0.01K under an applied field up to 7$\pm$0.06 Tesla. Whereas the dewar cosist of an inner liquid helium reservoir and an outer liquid nitrogen jacket to better insulate the inner system.

Samples are mounted within a clear plastic straw that has a minimal magnetic susceptibility, as for the Al-capping. The straw is connected to the end of a rod which is inserted into the dewar and to a motor which serves to place the sample whithin the centre of the SQUID pick-up coils.

All films are measured using the *Reciprocating Sample Option* (RSO) with *center* scans method. The RSO measurements are performed using a servo motor which rapidly oscillates the sample while a shaft encoder records the position of the sample synchronous with the SQUID signal. The data received is then fitted to an ideal dipole moment response, reason why the samples has to be as small as possible. In center scans method large oscillations (3 cm) around the center point of the pick-up coils are operated, so that a large amplitude signal can illustrate the entire SQUID response curve. The sensitivity of an RSO masurments can be very high, in the order of about 5×10^{-8} EMU and its accuracy strongly depends on how well the sample is centered within the coils. Autotracking and an iterative regression algorithm ensure that the sample remeins centered also when temperature changes altering the geometry of the holding rod. The only drawback of RSO mode are the longer operative times and magnetic field inhomogenities. The raw data are collected in the form of sample position-dependent voltage from SQUID sensor using a MPMS MultiVu software and subsequently fitted through the iterative regression algorithm to extract the value of the magnetic moment.

The value of the magnetic moment measured on EuO thin films is affected by the substrate contribution. YSZ is indeed diamagnetic, meaning

that no effect is expected at zero field and it gives a linear contribution under applied fields that can be clearly distinguished in the sample saturating region.
Two set of measurements are taken for all the analyzed samples:

Temperature dependent magnetization measurements during which the magnetic field is kept constant at three different intesities: 10 G, 100 G and 1000 G. Since zero-field measurements are almost impossible due to the residual magnetization, the 10 G measurement is used to impose a direction to the field. However its contribution is almost negligable thus leading to almost field unaffected measurements. The temperature of the sample is then varied between 300 K and 2 K across te Curie temperature and $M(T)$ curves are recorded.

Hysteresis measurements where conversely temperature is kept constant below T_C and the intensity of external field is varied from about zero to its maximum value so that field dependent curves, $M(H)$, are recorded.

The output of the measurement system is the magnetization M expressed in *emu*. The value of the effective magnetic moment expressed in magneton bohr $\mu_B$is obtained through the following relation:

$$\mu_{eff} = M[\text{emu}] \cdot \frac{V_{\text{unit cell}}}{V_{\text{sample}}} \frac{1}{4\mu_B} \tag{4.11}$$

with

$$V_{\text{unit cell}} = a_{EuO}^3 \qquad V_{\text{sample}} = A \cdot t$$

where a is the lattice parameter of EuO, A the sample surface area and t its thickness. The number 4 arises from the first neighbor in fcc structure and the value of a magneton Bohr is $\mu_B = 9.274 \times 10^{-21}$.

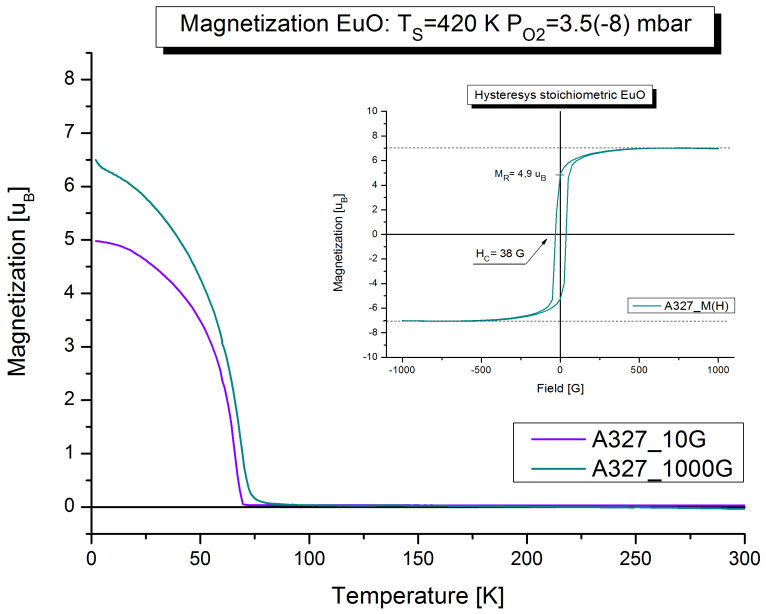

Figure 4.2: Temperature dependent magnetization $M(T)$ and hysteresis $M(H)$ of sample A327: stoichiometric EuO.

Chapter 5

Eu-rich EuO Thin Films: Role of oxygen Vacancies

In this Chapter, the main results of the work carried out in Cologne during the master Thesis period will be presented and discussed.

This work focuses on the role of oxygen vacancies in the occurrence of the metal-insulator transition in EuO thin films. In particular the amount of oxygen vacancies is determined by using XPS characterization for various films grown under different conditions. The amount of oxygen vacancies is then related to the transport propeties in order to find the critical level leading to MIT.

In order to perform such analysis it is necessary to prepare samples with different stoichiomety by varying their growth conditions narrowly. Contemporary specific analysis of transport and magnetic propertis together with chemical composition of each sample has to be performed as well in order to fully characterize them and infer about the possible mechanism involved.

The structure of the chapter consist of an introduction section which will describe in detail how is possible to tune EuO properties by changing the growth conditions, the procedure used to perform the experiments as well as the models for data analysis. It follows a complete description of the results obtained and a main conclusion.

5.1 Introduction: Tuning of EuO properties

Soon after the discovery of ferromagnetism in Europium chalcenogides[4], it was reported tha these compounds exhibited spectacular transport properties with huge Metal-Insulator transition (MIT) and Colossa Magnetoresistance (CMR) effects around the Curie temperature[6].

The metal insulator transition is not observed in stoichiometric EuO but only in Eu-rich EuO. Many studies indeed reports about MIT, however this spectacular change in resistance is that can only occurr in samples with increased conductivity. This can be done by doping of EuO with rare earths such as Gd, La, or simply by leaving oxygen vacancies as it is in Eu-rich EuO thin films. In the latter case it is the intrinsic excess of Eu atoms with respect to the oxygen that provides the required doping level to make the transition to metal state below T_C to happen[14][15]. This strong doping dependance of the MIT results in a general acceptance of the notion that it is mainly due to the delocalization of trapped electrons at oxygen vacancies as result of changes in the electronic structure coupled to the magnetic phase transition. What has never been investigated is the rate of the oxygen vacancies with respect to Europium relatively to the preparation condition and the minimum amount of doping level that is needed to the film to show MIT.

Nevertheless in the recent EuO research that control of stoichiometry remains still a serious issue. Many works indeed reported the presence of Eu^{3+} ions in their films or that the magnetic moment per unit formula was not close to the expectet value of $7\mu_B$ for a $4f^7$ system like EuO. Also layer-by-layeris has never been mentioned although epitaxy has been often reported and it is not clear how precise the amount of oxygen and europium were supplied in these works.

In Tjeng *et al.* group this process has been widely investigated and Sutarto *et al.*[51] found out an optimal recipe to grow epitaxially on YSZ(100) perfect stoichiometric Europium Monoxide free of contaminants. This recipe takes advantage of the so called *distillation technique* which allows a less precise control of supply rates of oxygen and europium thanks to an auto-limited growth mode induced by varying the substrate temperature.

In this work we start from this previous result and we gradually depart from the original receipe in order to investigate the Metal Insulator Transition, and the conditions that make it possible to occurr.

Making use of the Eu-distillation-assisted MBE we are able to achieve full control of the stoichiometry and slightly varying the oxygen pressure P_{O2} and substrate temperature T_S we can modify the Europium to oxygen rate of the growing film. In this way we are able to tune its transport and magnetic properties, by moving away from the stoichiometric EuO condition in the direction of more and more Eu-rich EuO thin films.

By departure from the distillation condition one can obtain very different compounds depending on the direction in the variation. Sutarto receipe to grow pure stoichiometric EuO is summarized in Table 5.1

Distillation Technique		
Substrate temperature	Ts	400 ℃
oxygen pressure	P_{O_2}	4.0×10^{-8} mbar
Europium flux	Φ_{Eu}	8.1 Å/min

Table 5.1: Parameters of the distillation technique used by Sutarto *et al.*[50].

The distillation technique represents our starting point and it is based on two main aspects. A high substrate temperature, T_S=400℃ that makes re-evaporate all excess Eu adatoms that impinge on the surface and do encounter an oxygen atom to react with. A pressure of oxygen in the chamber sufficiently low, i.e. $P_{O2} < 8 \div 10 \times 10^{-8}$ mbar, in order to keep the oxygen flux rate value lower than the Eu one. The combination of these two factors permits to prepare high quality EuO thin films free of higher oxide states contaminants.

In the present work we will keep constat the Europium flux rate to $\Phi_{Eu} = 8.1 \div 8.2$ Å/min, but we will systematically vary the temperature of the substrate and oxygen pressure in order to explore a wider region of Eu-rich EuO growth conditions. This will allow us to determine the *critical condition* for MIT to occurr and reveal the oxygen vacancy level x in the chemical composition Eu_1O_{1-x} of the film.
The process is organised into three steps:

- first lowering the substrate temperature to a value such that re-evaporation of excess Eu is significantly reduced. $T_S = 200$ ℃.
- then varying the oxygen pressure in the range between $3.5 < P_{O2} < 7 \times 10^{-8}$ mbar, to find the critical pressure above which MIT is not occurring anymore. A value below this limit is choosen for the next step.
- finally rising up again the substrate temperature to get very close to the limiting condition again.

What is already well known from previous studies[50] is schematically represented in Figure 5.1. If oxygen pressure is increased above $10 \div 12 \times 10^{-8}$ mbar, , with a Eu flux rate of 8.1 Å/min, it is very likely the formation of higher oxidation states in the film. This value represents the critical oxygen pressure which delimits the region of growth free of contaminations. On the other side, when both oxygen pressure and substrate temperature are low

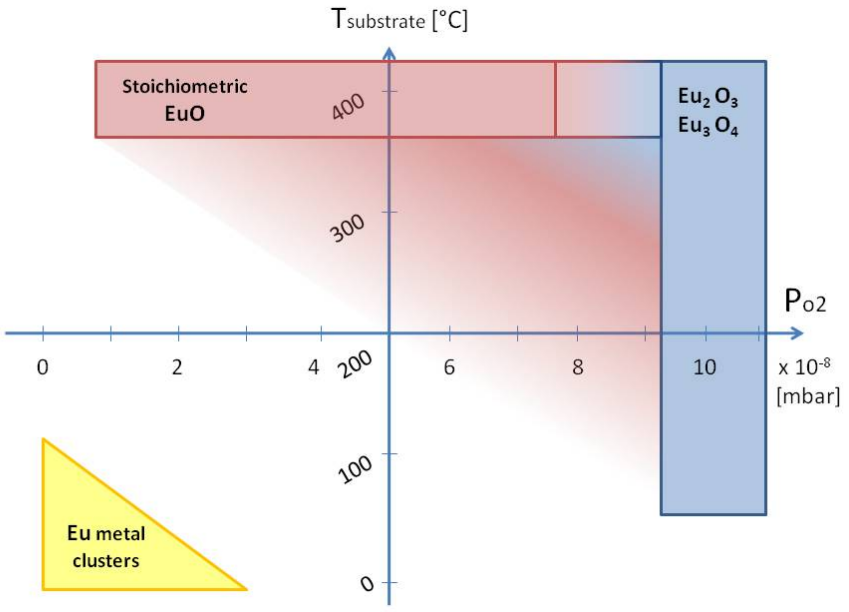

Figure 5.1: Schematic representation of EuO growth conditions.

(bottom left in Figure 5.1) the formation of Eu clusters is unavoidable thus influencing significantly spectroscopic, transport and magnetic properties. As a consequence to grow pure Europium Oxide with 1 to 1 stoichiometry and free of contaminants oxide compounds it is necessary to keep the temperature of the substrate quite high and oxygen pressure below the critical value (red region in the figure).

In the area between these regions Eu-rich EuO thin films are forming, with different stoichiometry depending on the specific values of T_C and P_02. A detailed analysis of this region has been carried out in this work and is presented in the following sections.

5.2 Data Analysis

In this section the methods used for the analysis of specific set of data are presented. In particular how the integration of the XPS spectra peaks of oxygen and europium was carried out by means of an ad-hoc MATLAB program, in order to check the chemical composition of the films, andto determine the absolute value of the density of the oxygen vacancies. In addition is given a remark about how the thickness of the sample is determined.

5.2.1 Stoichiometry analysis with MATLAB

In order to perform a systematic stoichiometric analysis of each sample *In-situ* XPS analysis was employed. It consist basically in the comparison of the intensity of specific peaks in the XPS spectra for each EuO thin film, whose integrated area is supposed to be proportional to the amount of the specific element in the film. However, the intensity of a peak in an XPS spectra is determined not only by the electrons generated form the corresponding excitation, but also by the contribution of the inelastically scattered secondary electrons which give rise to the background feature of the spectra.

For Europium Oxide the choosen peaks for the analysis are the Eu 4d centered at 128 eV binding energy, and the O 1s centered at much higher biding energy E_B=530 eV. Therefore specific high resolution spectra of the region around the peaks are taken and subsequently analyzed thanks to a MATLAB program designed for the scope.

The program takes into account a model for removing the background of the spectra and calculates the area of the peak by integral calculation. The program consists of two MATLAB M-file which defines functions of the form:

```
function[v] = INT1s (d, step, sweeps, m)

function[v] = INT4d (d, step, sweeps, m)
```

where d is the set of data that has to be imported. It consist of a 2 row matrix which contains the *Counts VS Energy* data of the XPS spectra. Three more variables have to be given manually to the function: the *step size* of the energy scan set with the SES program, that in the case of the O1s and Eu4d peaks corresponds to 25 meV, the *number of sweeps* taken for the specific spectra, and the number m of iterations that the program has to perform.

The program code is reported in Appendix A, and its operations are briefly described as following. The function applies to the XPS spectra an iterative algorithm whose first two steps are represented in Figure 5.2.It is

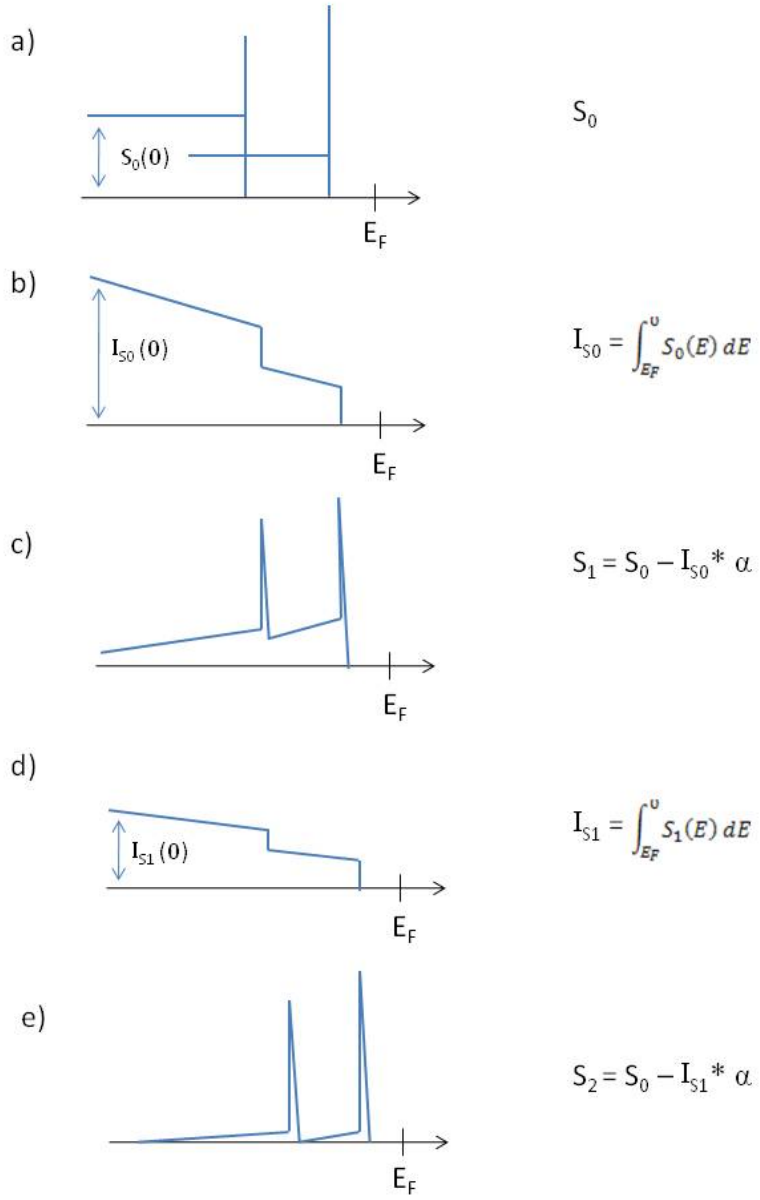

Figure 5.2: Schematic of the model for background fitting implemented in the algorithm of the MATLAB program.

based on the basic assuption that each peak in the spectra gives rise to a contribution to the background which is constant for each energy below the peak value. All the contribution sums up to generate the background feature. The original spectra S_0 is integrated from right (higher energies) to

left (lower energies) and a new integral function I_{S_0} is defined. A coefficient α is determined by imposing $\alpha \cdot I_{S_0}(0) = S_0(0)$ which results in

$$\alpha = \frac{S_0(0)}{I_S(0)} \tag{5.1}$$

The integrated function scaled by the α factor is subtracted to the original spectra and a new spectra is obtained:

$$S_{n+1}(E) = S_0(E) - \alpha \int_{E_F}^{0} S_n(E)\mathrm{d}E \qquad n = 0, 1, 2, ... \tag{5.2}$$

The process can be therefore iterated several times getting each time a better spectra. Once the itration is finished the function caluclates the value of the area below the peak, considering the step size and the number of sweeps, and gives it out as its output v. By simply calculating the ratio of the two output for O1s and Eu4d peaks

$$r = \frac{\text{Area O1s}}{\text{Area Eu4d}} \tag{5.3}$$

we are able to determine the oxygen vacancy level, by scaling this value with a reference value taken from a pure stoichiometric sample. We used sample A327[1] for this scope, whose O1s to Eu4d ratio is about 0.25. We expect therefore that an Eu-rich sample has a ratio below this value. By calculating and rescaling the ratio between this value and the Eu-rich film ones we can therefore determine the effective oxygen vacancy rate.

However the background model assumed is not the real case, where the background feature generates form multiple peaks and more complex mechanism of scattering. Nevertheless by first approximation and for limited energy region it can work very well and results very usefull in removing the first part of background generated from a single peak.

5.2.2 Thickness of the film

In order to calculate the magnetic moment per unit area of the samples out of SQUID measurements it is necessary to know exactly the volume of the EuO film measured. Nevertheless, although the area is calculated quite easily, knowing the thickness of the films remains still a crucial issue.

Since it was not possible to perform X-Ray Reflectivity (XRR) measurements of the samples, it is necesary to find another way to to get an estimation of the thickness of the samples. It is indeed possible to extrapolate the final thickness by considerations on the growth rate of the layers and the duration of the process itself.

[1] stoichiometric Eu_1O_1, grown at T_S=400℃ and $P_{O2} = 3.5 \times 10^{-8}$ mbar

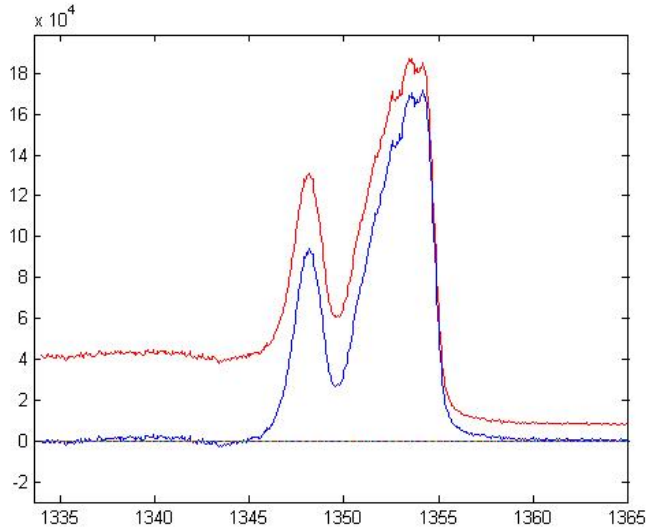

Figure 5.3: Matlab plot of the Eu4d peak spectra before(red) and after(blue) the iterated fitting of the background.

Growth rate It indicates the speed of growth of the film and it is usually expressed as the time needed to grow 1 mololayer (ML) of the film. One monolayer of EuO corresponds to half the lattice parameter of the unit cell, $1ML = 2.5635$ Å.

Duration of growth All the sample were grown for 90 minutes each, with the only difference that some of them with one extra minute of europium flux in order to compensate the residual oxygen left in the chamber.

However determining the growth rate is not easy. One way is out of RHEED oscillations, whose period corresponds exactly to the time needed to the growing layer to be completed. All the samples we have oscillations shows a period between $23 \div 24$ and $26 \div 27$ seconds for the initial stages of growth. This result is in agreement with what Sutarto found in his work[51] on the Initial Stages of EuO growth: for the first 5-6 monolayers YSZ (100) substrate acts as oxygen source for the film and the growth rate is of 25 seconds/ML. In this regime the growth rate results determined from the Eu flux-rate.

Concerning the following stages of the growth, i.e. when oxygen is supplied to the growth chamber the rate for sustained growth under distillation condition is therefore proportional to the oxygen pressure. We need therefore to compare the results obtained by Sutarto of samples with similar growth conditions to ours. Figure 5.4 shows some of these results and the

P_{O_2} limited growth trend where the thickness is proportional to the product of oxygen pressure per deposition time.

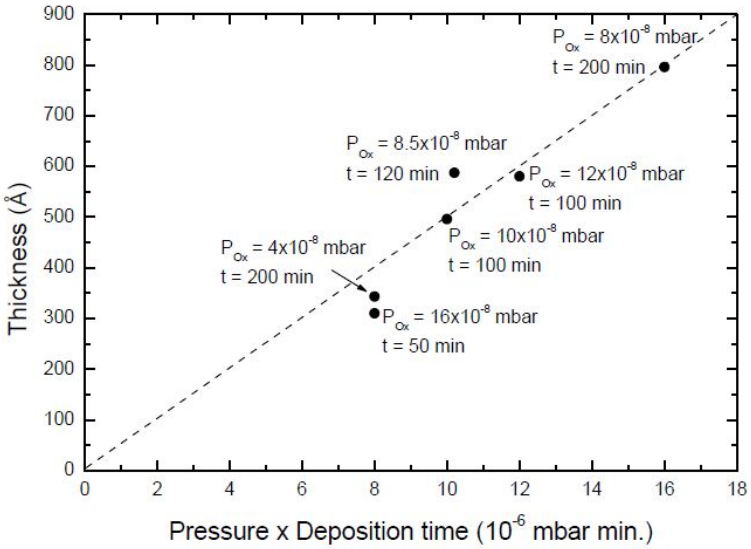

Figure 5.4: EuO film thickness, as determined from XRR measurements, versus the product of oxygen pressure and total deposition time.[50]

However Eu-rich EuO thin films are not obtained under distillation condition, and the oxygen limited growth assumption is not valid anymore. The growth rate therefore is expected to be higher for Eu-rich samples at the same oxygen pressure but with lower substrate temperature. Since the limiting case where $\Phi_{Eu} \simeq \Phi_O$ at 10×10^{-8} mbar show a growth rate of about 2 ML/min, and the lower case at 4×10^{-8} mbar shows about 0.7 ML/min, we expect to find a growth rate for our samples in between these values, but closer to the first for T_S=200℃.

With a growth rate of about 2 ML/min for 90 minutes we expect thickness of about 40 - 50 nm for Eu-rich samples.

5.3 Results: Effect of Oxygen pressure P_{O2} on the Properties of EuO Thin Films

The first result we report in this work is the set of oxygen pressure dependent measurements. They are taken by setting the substrate temperature and Eu flux rate to the constant value T_S=200 ℃ and Φ_{Eu}=8.1 Å/min and varying P_{O2} in the range between 3.5 and 7.0 mbar as depicted in Table 5.2.

Sample	$\mathbf{T}_S$	$\mathbf{P}_{O2}$	**MIT**	**O_2 vacancy**
A334	200 ℃	7.0 (-8)	–	–
A333	200 ℃	6.0 (-8)	–	–
A338	200 ℃	5.5 (-8)	MIT	19.1 %
A332	200 ℃	5.0 (-8)	MIT	31.6 %
A331	200 ℃	4.0 (-8)	MIT	58.5 %
A330	200 ℃	3.5 (-8)	MIT	64.3 %
A336	200 ℃	0.0	MIT	77.1 %

Table 5.2: Set of sample of P_{O2} dependent measurements.

The choice of starting with a pressure adjustment comes from the fact that the previous T_S dependent measurements (see List of Samples) were not flexible enough in order to get close to a critical value. Pressure indeed was set to 3.5 $\times 10^{-8}$ mbar, and temperature varied in the range from 420 ℃ down to 200 ℃ . Such a low P_{O2} value led all the sample to show Metal Insulator Transition, except from the very stoichiometric ones at 350 ℃ and 420 ℃ which were too insulating for transport measurements and charging up during XPS characterization. This results in energy shifting of the spectra thus compromising the reliability of the measurement.

Hence we need to find first a Critical Pressure level below which MIT occurr, but still enough conducting to ensure XPS characterization and reliable transport measurements. To do this T_S is set to 200 ℃ , a quite low value which ensures us to be far from distillation condition, and thus MIT to occur at least for a low oxygen pressures range. Except from the first, P_{O2} is then increased by step of 1×10^{-8} mbar till to overtake the critical pressure level. Two more samples were grown later A336 at zero and A338 at 5.5×10^{-8} mbar oxygen pressure. On each sample XPS and transport measurements are performed immediately after growth in order to be able at to know the chemical composition and the related transport behaviour of the specific grown compound.

Results of transport measurements of the current set of samples are shown in Figure 5.10, while oxygen vacancy concentration level is listed in Table 5.2.

RHEED and LEED

The RHEED and LEED pattern of two of the samples of the current set are shown in Figure 5.5 and 5.6. They are both grown with the same conditions, i.e. T_s=200℃ , Φ_{Eu}=8.1 Å/min for 90 minutes, except from oxygen pressure, which was set to 5.0×10^{-8} mbar for A332 and to 7.0×10^{-8} for A334. Sample A332 shows MIT while sample A334 does not.

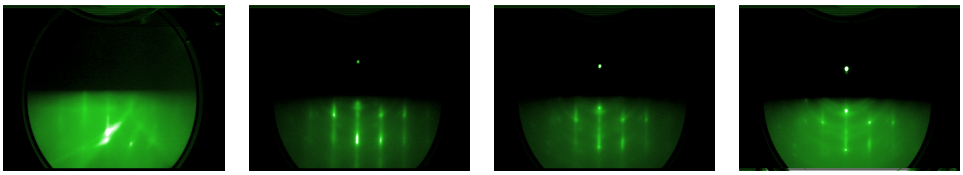

(a) A332 substrate (b) A332 at 24 min (c) A332 at 41 min (d) A332 at 83 min

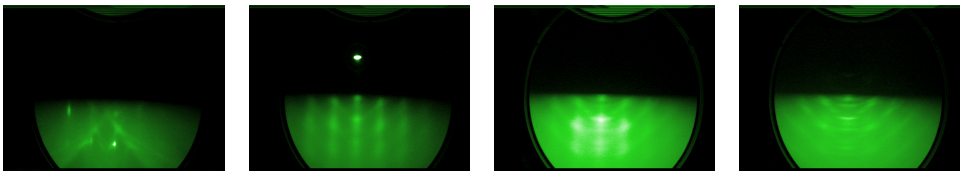

(e) A334 substrate (f) A334 at 28 min (g) A334at 51 min (h) A334 at 83 min

Figure 5.5: RHEED patterns of A332 (a-d) and A334 (e-h) samples grown at $P_{O2} = 5.0 \times 10^{-8}$ and $P_{O2} = 7.0 \times 10^{-8}$, respectively.

As we can see for sample A332 the RHEED pattern does change in time during growth. in the first 20 min a sharp RHEED pattern is observed. The distance between the streaks of EuO is identycal to the pure YSZ substrate, meaning that epitaxial single-crystal growth is sucesfully obtained. The occurrence of the spots indicate that 3D islands started to nucleate on the surface. After 80min the surface quality of the film changes, but streaks are still clear visible.

On the contrary for sample A334, which in transport measurements does not shows MIT, also the RHEED pattern is quite different. Indeed soon after the initial stages of growth the streaks become modulated and the spots are broaden. Moreover in the second half of the growth we clearly observe the appearance of concentric rings features, typical of polycrystalline films.

Also LEED photographs of sample A332 report good single crystallinity, consistent with the RHEED results. All the images show indeed sharp pattern for all the energy in the scanned range, typical of a perfect (100) surface of an fcc EuO single crystal. For sample A334 instead it was not possible to record any LEED image, since the non-crystallinity of the surface led to only blurry background intensity with no spots at any energy.

These results are consistent with RHEED ones and we can desume that below the critical oxygen pressure growth proceeds epitaxial giving rise to

good single crystalline samples which shows MIT, whereas above the same value we clearly observe departure from single crystallinity and expitaxy.

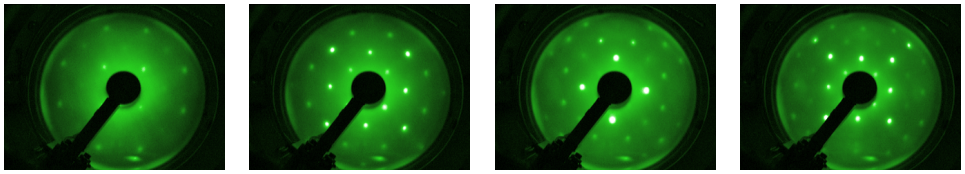

(a) A332 at 135 eV (b) A332 at 152 eV (c) A332 at 206 eV (d) A332 at 220 eV

Figure 5.6: LEED pattern of A332 sample at different electron energies.

XPS characterization

In order to analyze the chemical composition we also carried out photoemission experiments on those films. The main purpouse is to calculate the stoichiometry of the films by calculating the ratio of O1s to Eu4d peaks intensities. However XPS analysis results very useful to discover the presence of contaminats speicemen in the films, such as higher oxidation states, as well.

In Figure 5.7 are plotted the XPS valence band spectra of the complete set of pressure dependent measurements, while in Figure 5.8 two samples are shown and compared in detail: A332 and A334, grown at 5.0×10^{-8} mbar for A332 and to 7.0×10^{-8} oxygen pressures, respectively, the former belonging to the MIT region and the latter not.

As one can easily note, a general trend is clear the incrising hight of the *O2p* peak with increasing pressure from 0 to 5.5×10^{-8} mbar, while Eu4d stays roughly the same hight. Only exceeding this treshold value another effect is observed, i.e. the formation of Eu^{3+} contaminants together with the reduction of $Eu^{2+}4f$ peak intensity.

Looking in details in Figure 5.8, the same valence band spectra of the two regions look quite different. In sample A332 indeed the spectra is dominated by the intense Eu^{2+} peak originating from the high localized *4f* states and by a weaker feature given by the O^{2-} *2p* states. The former is centered at 1479 eV, corresponding to a binding energy of 2 eV, while the latter at 1476 eV, correspondint to E_B=5 eV. Moreover a small Fermi edge is present at the limit of the valence band, idicating the presence of free electrons in the sample. This metallic character is indeed related to the presence Eu metal excess or, vice versa, to the oxygen vacancy left in the film.

Sample A334 instead shows, besides from the two peaks mentioned before, a quite intense third peak at lower energies as well. This peak, centerd

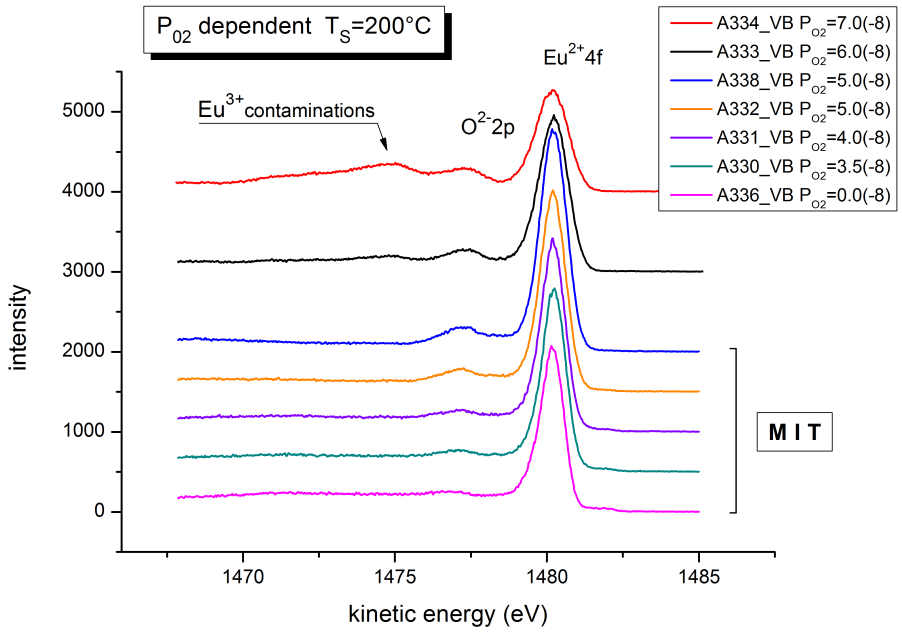

Figure 5.7: XPS valence band spectra of pressure dependend set of samples.

around 7 eV biding energy, is given by the Eu^{3+} $4f^6 \rightarrow 4f^5$ transition and therefore related to the presence of Eu_2O_3 oxidation states in the film. Interesting to note is also the higher intensity of the *O2p* peak, indicating the presence of a larger amount of oxygen. This is consistent with the fact that higher oxygen pressures favour the formation of higher Eu oxidation states, which forms more easily, and with the disappearence of single crystalline epitaxial growth due to the different lattice constant, as shown before in RHEED patterns as well. Moreover no Fermi edge is observed in this case, confirming the insulating character of the sample.

As already discussed istead the intensity of O1s and Eu4d peaks were analyzed and out of their ratio is calculated the stoichiometry of the film, i.e. the oxygen vacancy level. The values reported in Table 5.2 are plotted in Figure 5.9. As one can clearly see oxygen vacancy level is inversely proportional to oxygen pressure, with a clear decreasing trend which is faster at higher pressures. Important to remark is that for sample A333 and A334, grown above the critical O_2 pressure, no oxygen deficiency level is reported. This is related to the fact that for those samples the amount of oxygen is overflowing the limit for stoichiometric EuO growth, thus resulting in the opposite situation with oxygen excess in the sample and the formation of higher oxidation states as seen also in valence band spectra.

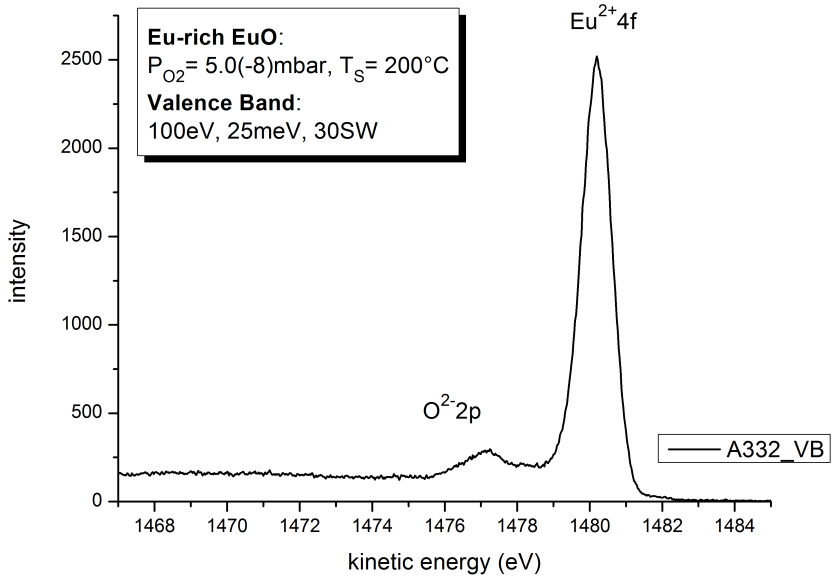

(a) A332

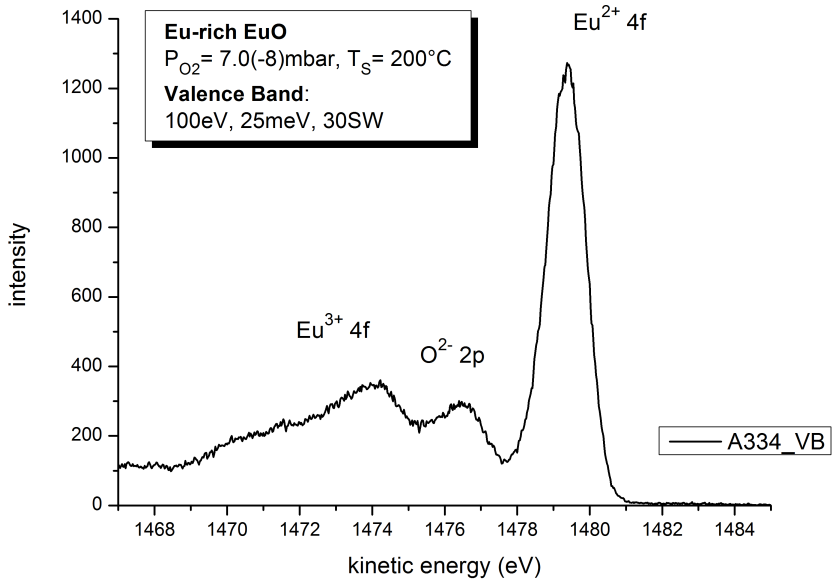

(b) A334

Figure 5.8: XPS valence band spectra of A332 and A334 samples.

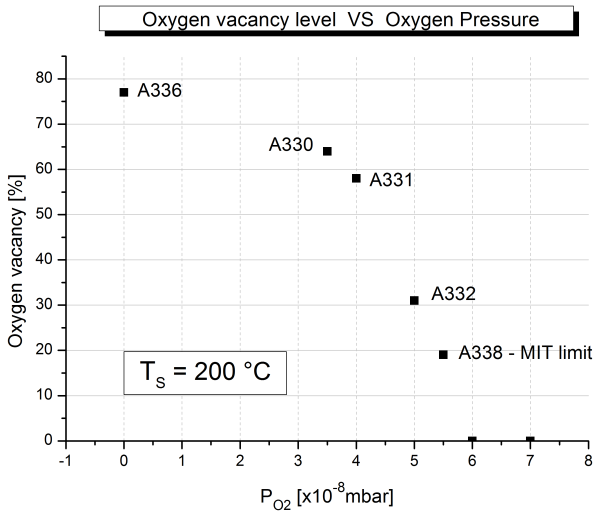

Figure 5.9: Oxygen vacancy level versus P_{O2}.

Transport properties

In order to analyze the conductivity of the samples, temperature dependent electrical DC transport measurements were performed on all the samples of the set. This permits to clearly see which samples show Metal Insulator Transition, allowing to find the right critical oxygen pressure P_{O2crit} above which, for films grown at T_C=200℃ substrate temperature, MIT does not occur anymore.

The transport measurements of pressure dependent set of samples are depicted in Figure 5.10. As can be seen, all samples show a clear semiconductor-like behaviour at high temperatures: the resistance value increases while lowering the temperature due to the reduction of thermal mobility of free electrons. However only those films grown with at oxygen pressure in the range from 0.0 to 5.5×10^{-8} mbar show a marked drop in resistance (MIT) thereabout the Curie temperature T_C. For those ones grown at higer oxygen pressures, i.e. sample A333 and A334, resistance stays at very high values (up to $10^{13} \div 10^{14}\Omega$) for all the temperature range, without any transition to metal-like behaviour at low temperatures.

What is remarkable is that the resistance value at a specific temperature is very different for each sample depending on the oxygen pressure showing a decreasing trend while lowering the oxygen pressure at which the film has been grown. Only in the case of samples A330 and A331 the trend is not respected, and sample grown at higher P_{O2} shows a slightly lower resistance

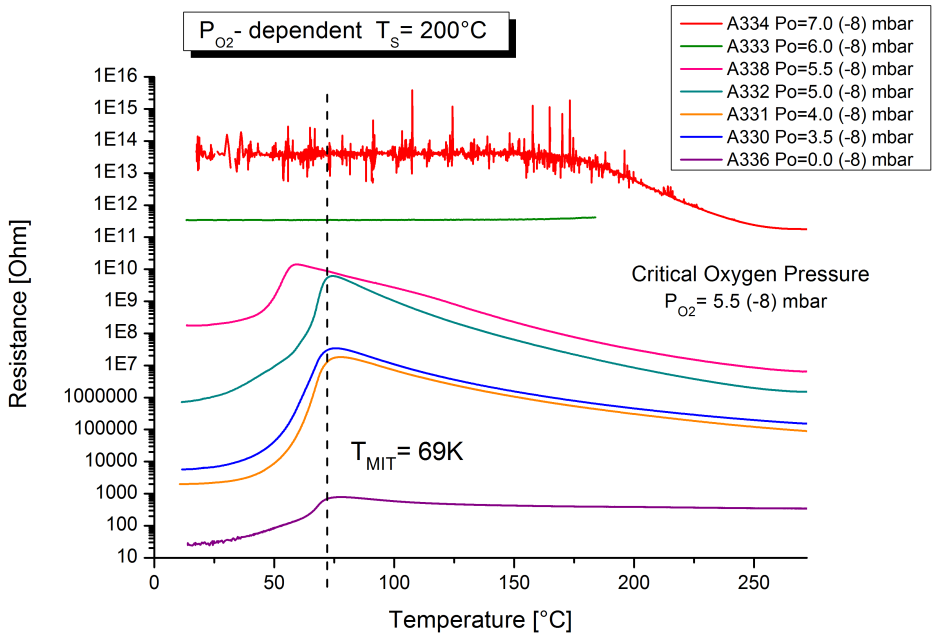

Figure 5.10: Transport measurements of pressure dependend set of samples.

value. However the two values are very close and this effect may be due to variations of Europium flux rate or to the instability of the oxygen supply from the leak valve.

Moreover, all the samples show Metal-insulator transition at about 69 K, which corresporrespond to the Curie temperature and seem to be unaffected from the stoichiometry of the films an thus from the amount of oxygen vacancies. Only in the case of sample A338, grown at 5.5×10^{-8} mbar, we report MIT transition at lower temperature, T_{MIT}=55 K. However since it looks like that also a departure from semiconductor behaviour in the range from T=130 K till to T_MIT is present, we can infer that a leakage current in the sample may be responsible of this deviation.

For sample A333 instead we encountered problems in measuring its temperature dependent resistance but we still report it in Figure 5.10 because the values we were able to measure are in agreement with the general trend described before, with a high resistance at low temperature with no MIT and a lower value at room temperature of R(300K)=$8.7\times10^{9}\Omega$.

From this consideration we can therfore deduce that:

- samples grown at $T_S > 5.5\times10^{-8}$ mbar show an insulating/semiconducting behaviour with no MIT, while samples grown at $T_S \leq 5.5\times10^{-8}$ mbar show metal insulator transition at T$\simeq$69 K, which is independent on

the O_2 vacancy level.

- resistance value of each sample is directly proportional to P_{O2} and in other words inversely proportional from the oxygen vacancy concentration.
- the film grown at the highest oxygen pressure, i.e. $P_{O2} = 5.5 \times 10^{-8}$ and T_S=200℃, but still showing MIT is sample A338, whose oxygen vacancy level is 19.1 %. This can be considered a first approximation to the concentration of oxygen vacany needed for EuO to show metal insulator transition.

Magnetic properties

All the EuO films were characterized by SQUID in order to see the influence of oxygen vacancies on the magnetic properties.

The magnetic moments in dependance of the temperature $M(T)$ for the pressure dependent EuO/Eu-rich samples are presented in Figure 5.11. Both figures show the magnetic moment versus temperature but the first with an applied field of 10 G, while the second with a higher one of 1000 G. With known thickness[2] we are able to find the correct magnetization per formula unit (expressed in μ_B) out of SQUID measurements.

As we can see from 10G field measurements the highest magnetization value at about 4K is right about $7\mu_B$ per unit formula, as expected for a $4f^7$ system. All the films moreover have a Curie temperature of 69 K, the same value of EuO bulk compounds. The samples are listed in the legend form the one at lowest P_{O2} to the one at highest, but the trend of the maximum magnetization value is not linear. We do see indeed an increasing trend till to a maximum value obtained for sample A338, grown at 5.5×10^{-8}mbar, after which an abrupt decrease in magnetization value for sample A333 and A334. We know from XPS analysis that those samples grown at higher oxygen pressure present higher oxidation states compounds, such as Eu^{3+} which are non-magnetic, thus destroying the ferromagnetic coupling of Eu^{2+} ions below T_C. The increasing trend of the first five Eu-rich samples suggest us that the more doped is the film, and at the same time less stoichiometric, also the magnetic coupling via double exchange is reduced, thus reducing the magnetic moment per formula unit. Only in the case of sample A332 this trend is not respected, but it could arise from errors in SQUID measurement or more likely in a bigger deviation of the thickness thus leading to an incorrect calculation of the volume of the

[2] we assumed a thickness of 46 nm for each sample. Small variations could be possible but this avarage value is good for comparison between the samples.

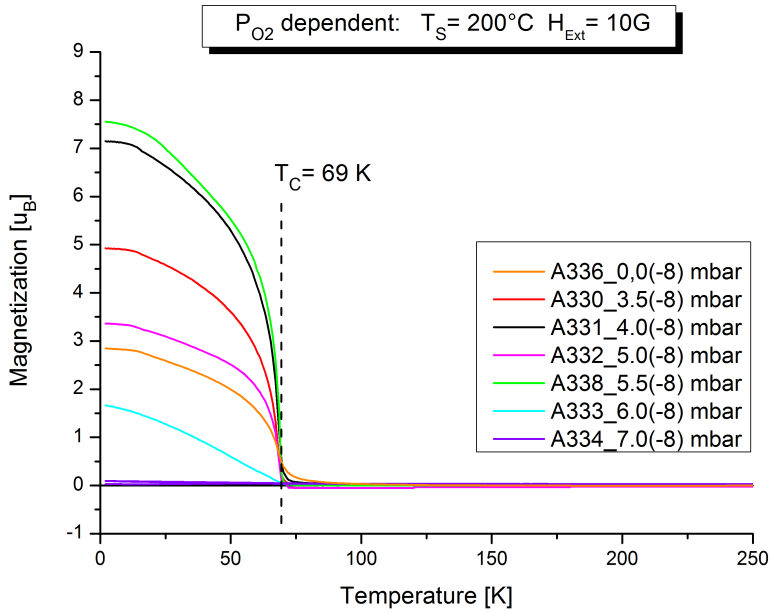

(a) 10G

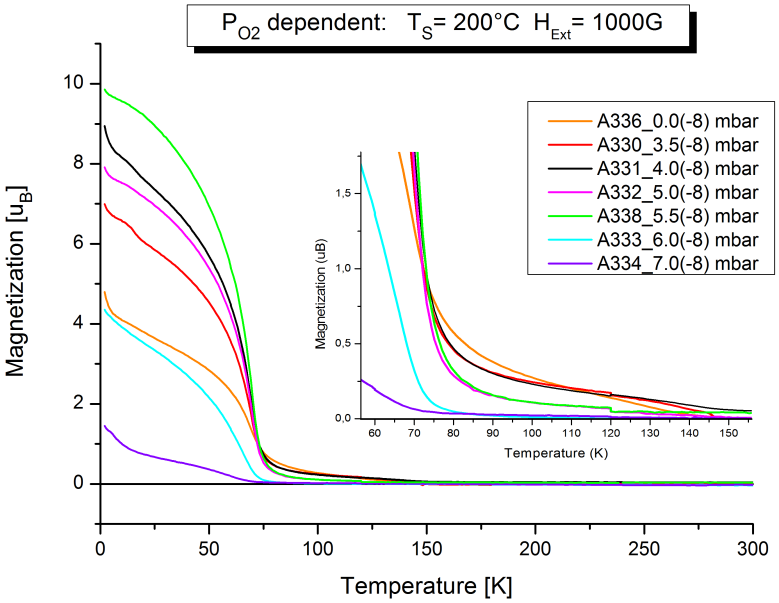

(b) 1000G

Figure 5.11: Magnetization per formula unit of EuO films grown under various oxygen pressures P_{O2}.

sample. However in Eu-rich samples magnetization never vanishes, as for the case of $P_{O2} \geq 6.0 \times 10^{-8}$ mbar, which denotes the strong relation between the occurring of metal-insulator transition and the ferromagnetic transision of EuO below T_C.

In the case of 1000G field measurements instead one can easly see that the magnetic moment per formula unit overtakes the ideal value of $7\mu_B$ per formula unit. However in this case the high applied external field induces further contribution from the paramagnetic substrate and aluminum capping layer. What is interesting to see here is t sample A332 take a better position in the linear trend discussed above, and above all the second magnetization feature shown by Eu-rich samples. This small residual magnetization of about 0.1–0.3 μ_B stays indeed from 70 K to 150 K and is more pronounced the lower the oxigne pressure is (see sample A336). This behaviour could be ascribed not to Europium Oxides but more likely to Europium metal clusters which can form when T_S and P_{O2} are significantly low. The same behaviour was indeed observedand investigated by Tjeng's group which reported[32] that the second magnetization feature is not to be related to the EuO crystals but rather to Europium metal clusters magnetically aligning in strong fields.

The hysteresis curves, $M(H)$ (magnetic moment versus appliyed field), of four representative samples are plotted in Figure 5.12. All films show ferromagnetic behaviour and the curves provide information about when the saturation for different EuO samples is reached.

Sample A336 and A331 are chosen out of Eu-rich samples grown below P_{crit} and shows MIT, whlie A333 and A334 have been grown at higher oxygen pressures and show the presence of non magnetic contamints like Eu_2O_3 and Eu_3O_4 and no MIT.

The high doped Eu-rich samples (a-b) get easily to saturation which has a higher value the closest they are grown to the critical pressure, i.e the more stoichiometric the film is. They also show a very low coercive field H_C of about 30-50 Oersted, and a quite high residual magnetization M_R (4.5 μ_B for A331). The hysteresis area is very small. For samples grown at pressures above P_{crit} we note a progressive lowering of the magnetization value and staturation is reached only for much higher values of the external field. However the residual magnetization in those samples is very low, e.g. 0.8 μ_B in sample A334, whlie on the contrary the cohercive field is considerably high (H_C=355 Oe).

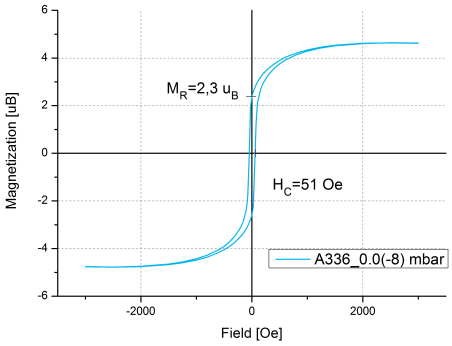

(a) A336 at $P_{O2} = 0.0 \times 10^{-8}$mbar

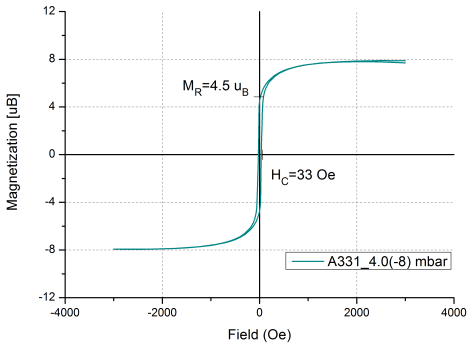

(b) A331 at $P_{O2} = 4.0 \times 10^{-8}$mbar

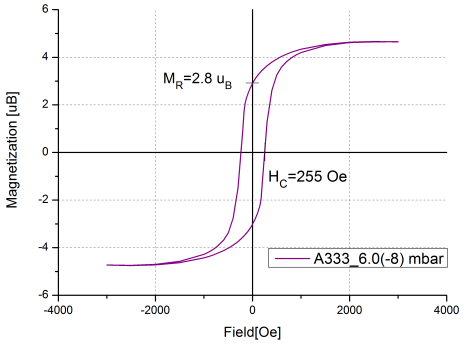

(c) A333 at $P_{O2} = 6.0 \times 10^{-8}$mbar

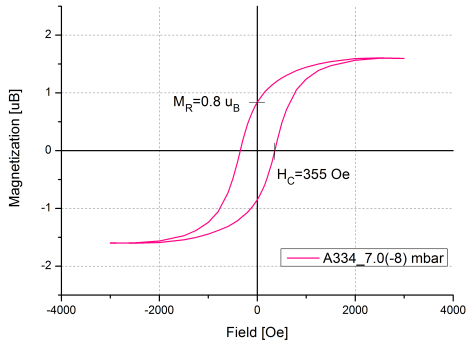

(d) A334 at $P_{O2} = 7.0 \times 10^{-8}$mbar

Figure 5.12: Hysteresis curves of sample A336, A331, A333 and A334.

5.4 Results: Effects of Substrate Temperature T_S on the Properties of EuO Thin Films

As a direct continuation of P_{O2} dependent measurements we report as second result the set of substrate temperature dependent measurements. The latter are take as starting point the result of the former, in order to obtain a more accurate estimation of the limiting condition ti MIT to occurr. They are performed by setting Europium flux rate and, in this case, oxygen pressure to a constant value and than slygthly increasing substrate temperature T_S. The oxygen pressure is choosen very close to the limit but below the critical value, i.e. $P_{O2} = 5.0 \times 10^{-8}$mbar, so that MIT can still occurrr. Europium flux rate is, as usual, set to Φ_{Eu}=8.1 Å/min, while substrate temperature is increased from 200℃ to 300℃ in small steps as listed in Table 5.3.

Sample	T_S	P_{O2}	MIT	O_2 vacancy
A340	300 ℃	5.0 (-8)	–	2 %
A342	280 ℃	5.0 (-8)	–	8.2 %
A343	270 ℃	5.0 (-8)	–	19.2 %
A348	260 ℃	5.0 (-8)	MIT	22.9 %
A344	260 ℃	5.0 (-8)	MIT	24.3 %
A341	250 ℃	5.0 (-8)	MIT	39.2 %
A332	200 ℃	5.0 (-8)	MIT	31.6 %

Table 5.3: Set of sample of T_S dependent measurements.

In this situation we are definitely exploring a more limited region of growth conditions. All the films indeed are clearly Eu-rich EuO, since oxygen vacancy are present in all of them. This was not the case of the previous set of sample, where right above the critical oxygen pressure departure from stoichiometry resulted in the presence of oxygen excess in the films. We can thus be able to infer more precisely about which is the oxygen deficiency level required for Metal Insulator transition to occur in Eu-rich EuO thin films.

RHEED and LEED

For crystalline structural characterization of the films three samples have been selected out of the presented list and their RHEED and LEED patterns are presented and discussed below. The chosen sample are A341, A343 and A340, grown at T_S=250℃, T_S=270℃and T_S=300℃, respectively, while europium flux rate and oxygen pressure are fixed. The represent roughly

all the temperature range, but only sample A341 grown at 250℃substrate temperture shows MIT.

The RHEED patterns at various stages of growth of the previously mentioned sample are displayed in Figure 5.13.

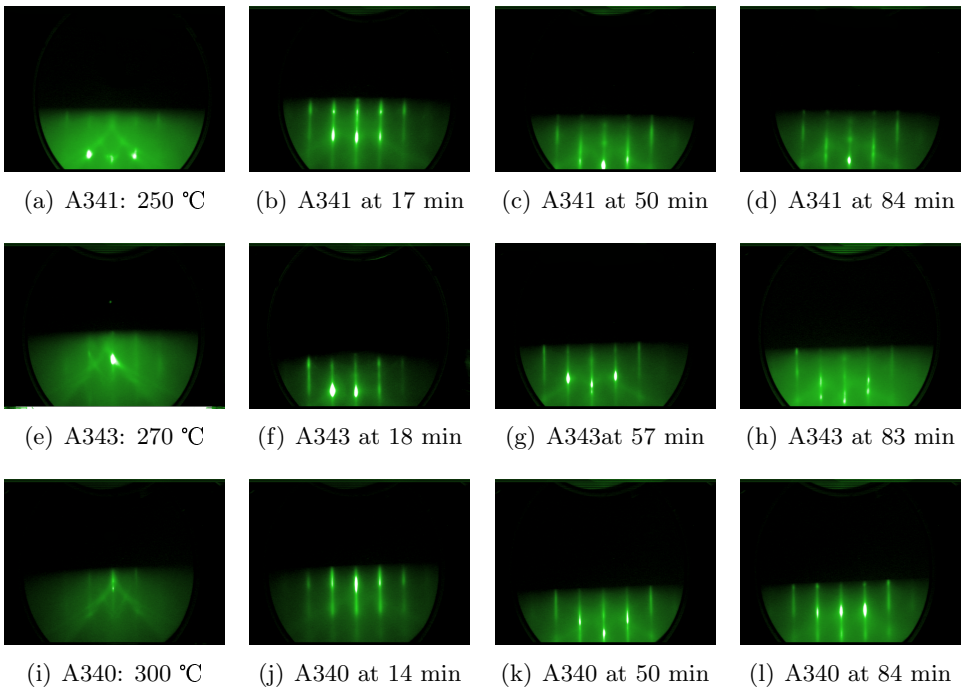

(a) A341: 250 ℃ (b) A341 at 17 min (c) A341 at 50 min (d) A341 at 84 min

(e) A343: 270 ℃ (f) A343 at 18 min (g) A343at 57 min (h) A343 at 83 min

(i) A340: 300 ℃ (j) A340 at 14 min (k) A340 at 50 min (l) A340 at 84 min

Figure 5.13: RHEED patterns of A341 (a-d), A343 (e-h) and A340 (i-l) samples grown at T_S=250℃, T_S=270℃and T_S=300℃, respectively.

As expected from the perfect lattice match between EuO and the substrate, all the films are appears to grow epitaxially even if substrate temperature is far from distillation condition. What is remarkable is that all of them show also quite sharp streaky patterns which means that flat surfaces are growing in layer-by-layer[3] mode. All of the films moreover reveal temporary formation of three dimensional structures at 14-18 minutes, which remains not very prominent for sample 341, and almost disappear for sample 340. The latter indeed has been grown at quite high temperature, T_S=300℃, which is closer to to distillation condition and thus more Eu adatoms are re-evaporated from the surface untill they find an oxygen atom. This results in a more stoichiometric film in agreement with the chemical characterization which displays only 2 % of oxygen deficiency for this film. In the other two samples instead, grown at a lower T_S, Eu atoms are not re-evaporated as easily and thus is possible the fromation of new layers even if the first has not been completed yet. However, all the films show good single crystalline

[3]this can be prooven only by the occurence of RHEED oscillations.

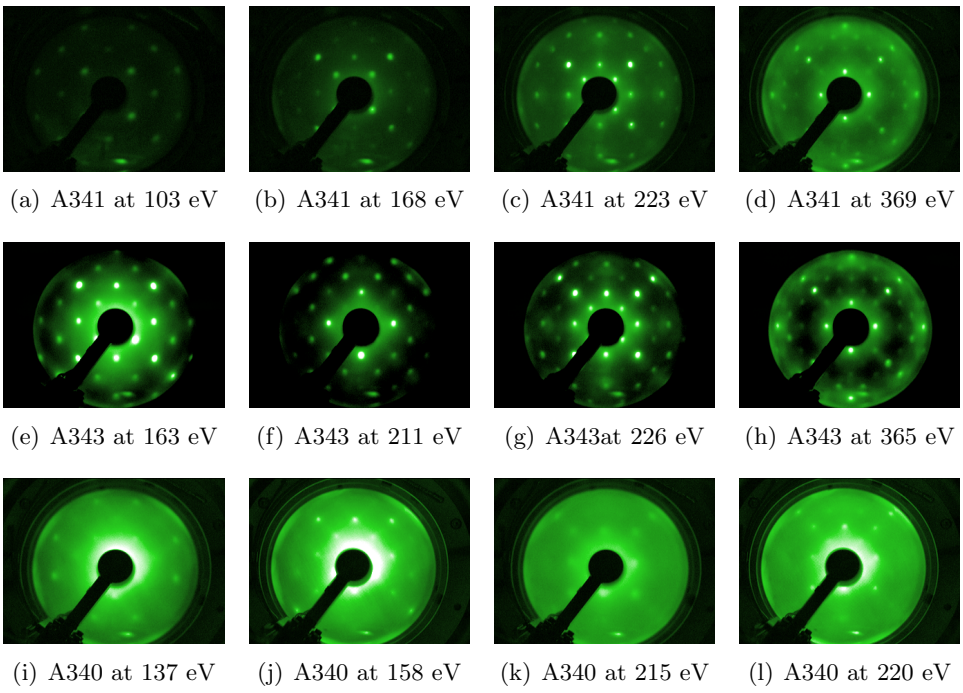

(a) A341 at 103 eV (b) A341 at 168 eV (c) A341 at 223 eV (d) A341 at 369 eV

(e) A343 at 163 eV (f) A343 at 211 eV (g) A343at 226 eV (h) A343 at 365 eV

(i) A340 at 137 eV (j) A340 at 158 eV (k) A340 at 215 eV (l) A340 at 220 eV

Figure 5.14: LEED patterns of A341 (a-d), A343 (e-h) and A340 (i-l) samples grown at T_S=250℃, T_S=270℃and T_S=300℃, respectively.

structure, with no polycristalline formation unlike the previous case for film grown at oxygen pressures above the critical value.

The main features outlined from RHEED images are confirmed also by the LEED patterns of the same three samples, which are displayed in Figure 5.14.

As can bee senn at a first look, sample A340 looks brighter with less marked spots due to the high brackgrount intensity, while the other two instead show a better contrast and sharper spots at every beam energy range. This can be related to the more insulating character of the sample A340, which induces charging on the surface thus increasing the diffusive background intensity.

Nevertheless, as confirmed by both LEED and RHEED patterns, is remarkable that the same crystalline structure is observed in all the samples, independently on the oxygen vacancy concentration. This suggest us that in Eu-rich films the doping mechanism occur more likely thanks to interstitial oxygen vacancies formation than to substitutional Europium excess, which would affect also the reciprocal lattice pattern structure.

XPS characterization

As for the previous case, chemical composition is analyzed by X-ray Photoemission Spectroscopy. Stoichiometry calculation is performed out of O1s to Eu4d rate and results are shown in Table 5.3, while here below we will present the valence band spectra of the current T_S dependent set of measurements.

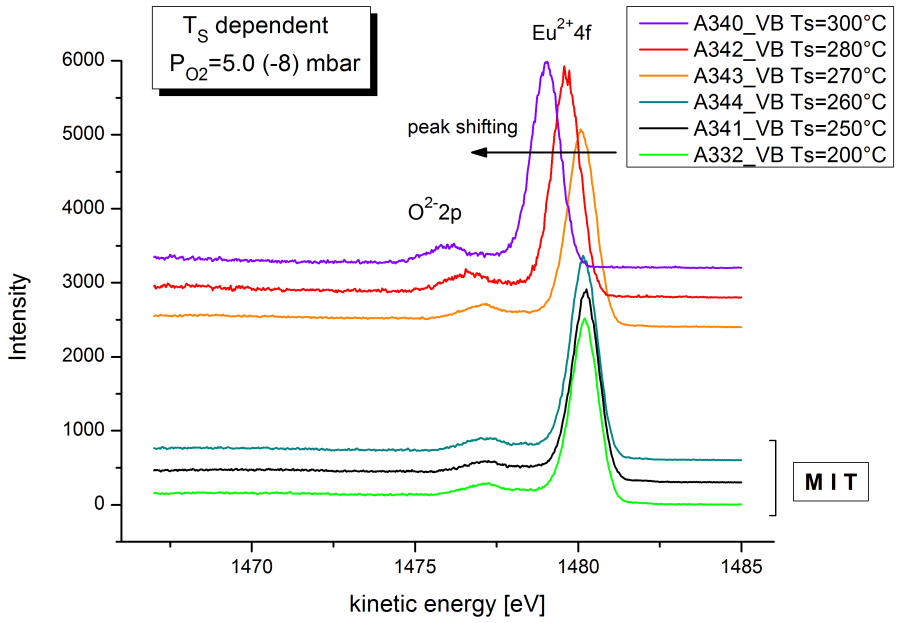

Figure 5.15: XPS valence band spectra of substrate temperature dependent set of samples.

Results are shown in Figure 5.15. They are divided into two subgroups for graphical representation issues and to highlight the differeces between films which shows MIT (bottom ones) and those which does not (top ones).

It can be clearly seen that in the former case (MIT), the three samples show quite identical valence band features typical for EuO films: $Eu^{2+}4f$ high intensity peak corresponding to the $4f^7 \rightarrow 4f^6$ transition centered at 1480 eV, and $O^{2-}2p$ lower peak at 1476 eV, whose intensity varies slightly proportionally to the amount of oxygen concentration in the films. Samples grown at lower temperature, with higher oxygen deficiency level, shows indeed a $O2p$ peak with sligthly lower intensity. However the position in energy of the peaks in those samples is independent on the oxygen vacancy concentration, meaning that all of the films present a sufficiently high metallic behaviour which allows them not to charge up during XPS characterization.

In the latter care (no-MIT) instead, it is clearly evident a shift in energy

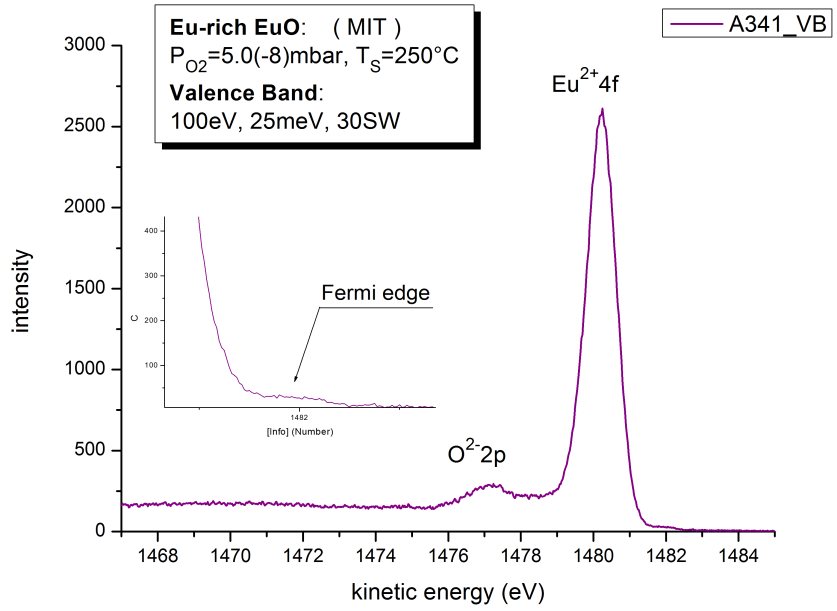

(a) A341 at T_S=250℃

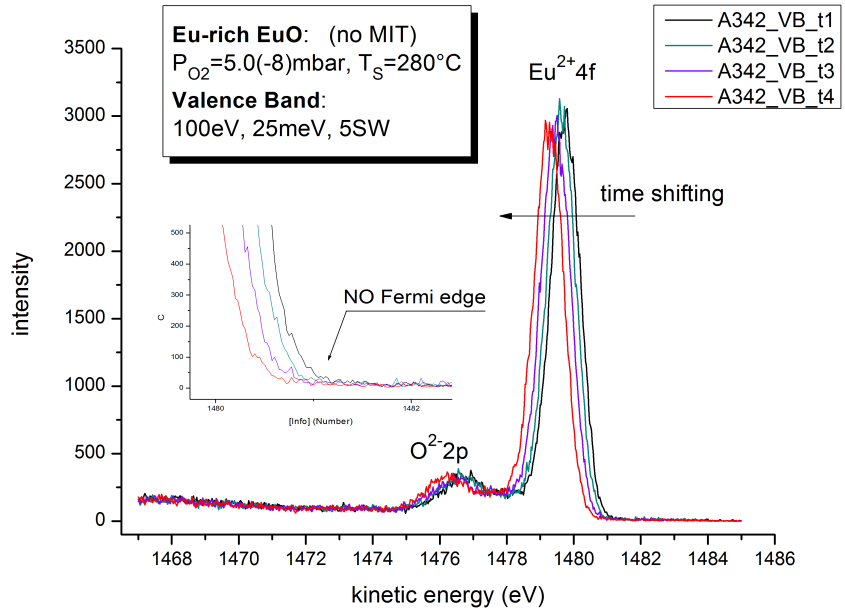

(b) A342 at T_S=280℃

Figure 5.16: XPS valence band spectra of A341and A342 samples.

of the both $Eu4d$ and $O1s$ peaks, while increasing T_S. The shifting is almost unapreciable for sample A343 grown at 270℃ , but it becomes relevant for sample A342 (0.5 eV shifed to the left) and even more for A340 (about 0.9 eV), grown at 280℃ and 300℃, respectively. Even if still in Eu-rich EuO growth regime, these three samples shows already a more insulating charachter although they do not present higher oxidation states in the films. A certain amount of oxygen deficiency is present in the cristalline structure, but it seems not to be a sufficient quantity to get the film conducting enough. The photoemitted electrons are thus replaced slowly, which results in a positive charging of the sample. This increases the workfunction thus shifting the whole spectra to lower energy values.

Two samples, belonging to the different subgroups are analyzed more in details: A341 for the high oxygen vacancy region (MIT) and A342 for the low oxygen vacancy level (no MIT). Their valence band spectra is displayed in Figure 5.16.

In agreement with previous considerations, sample A341 grown at 250 ℃ shows a static valence band spectra, without peaks indicatin contaminations, and displaying a quite marked Fermi edge at the and of the valence band. It can be well seen in the magnification of Figure 5.16(a). This confirms the supposed metallic character of the films grown at T$\leq$ 260℃ for which the doping by oxygen vacancy is able to provide enough free electrons in the top of the valence band to see them by photoemission.

On the contrary, sample A342 grown at 280 ℃ does not show any Fermi edge on top of the valence band, synonimus of its more insulating character. Moreover, the charging of the sample during photoemission results in a time-dependent peak shifting. In Figure 5.16(b) are plotted 4 different spectra (5 sweeps each) of the valence band, taken at different times one next to the other. They are shifted of about 0.4 eV each to lower energy values, index of the positive charging of the sample with time. This involves problems in XPS characterization beacuse it widens the shape of the peaks over many sweeps, compromising the final result.

The results of O1s to Eu4d rate calculations are reported in Table 5.3 and the corresponding oxygen vacancy level is plotted versus substrate temperature in Figure 5.17 shows. Except from A341 sample, an almost linear decreasing trend is appreciable.

Transport properties

The transport measurements for the substrate temperature (T_S) set of measurements are plotted in Figure 5.18. As for the previous P_{O2} dependent case, all of them show the typical semiconductor-like behaviour at high temperature, but only half of them again show metal-insulator transition. More

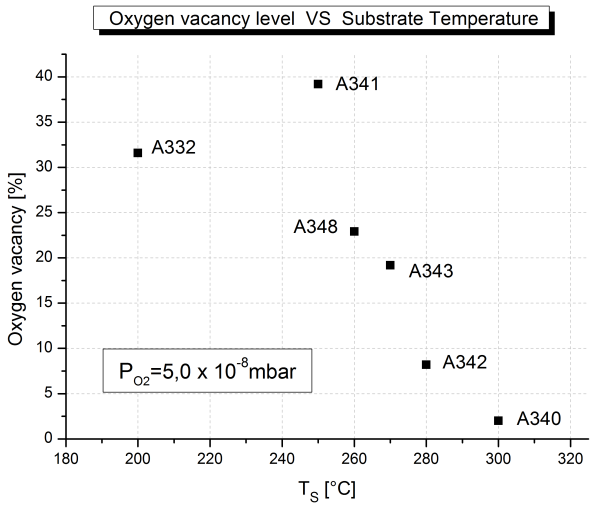

Figure 5.17: Oxygen vacancy versus T_S.

exactly the one grown at $T_S \leq 260$ ℃ .

For those samples the jump in resistance is considerably high, in particular sample A341 which show an change of 6 orders of magnitude at $T_{MIT} \simeq 69$ K. For A332 is about 5 orders while for A348 is not possible to know it exactly because the resistance values exceed the range of the measurements setup, entering the noise region between 60 and 130 K. however we could assume that' if the sahape of the curve resembles the one of A341, it could show a jump in resistance more than 6 orders of magnitude big. What is interesting is that the jump looks larger for sample grown close to the limiting condition for MIT to occur.

For those samples grown at higher substrate temperatures instead, i.e. $T_S \geq 270$℃, MIT does not occur anymore and their resistance value continues to grow while lowering the temperature. As already discussed this is a typical semiconductor-like behaviour according to which increasing the temperature more and more electrons gaing enough energy to populate the conduction band, thus increasing conductivity. In our measurements this trend is reported till when the resistance of the film exceeds the limiting value of $10^{13} \div 10^{14}\Omega$, above which resistance is too high to be measured and a flat noisy line is plotted.

According to our results therefore the limiting condition for metal-insulator transition results to be in between 260 ℃ and 270 ℃ for $P_{O2} = 5.0 \times 10^{-8}$ mbar and $\Phi_{Eu} = 8.1$ Å/min. The corresponding oxygen vacancy concentration calculated from XPS analysis is commprised in between 22.9 We can therefore conclude than an amount about 20 % of oxygen deficiency with respect to the stoichiometric EuO is the required level of doping which allow

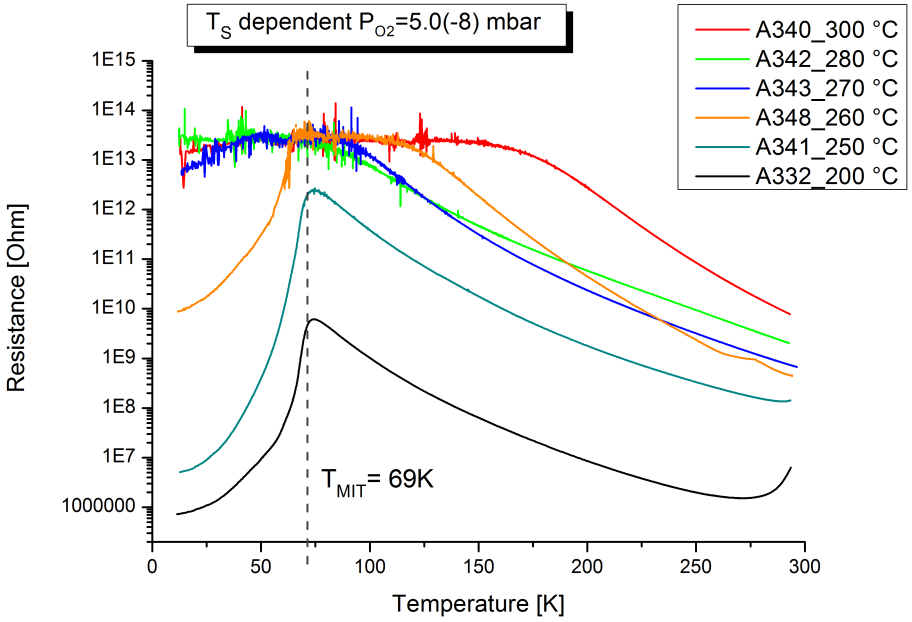

Figure 5.18: Transport measurements of substrate temperature dependent set of samples.

this fascinating phenomena to occurr.

Magnetic properties

In Figure 5.19 are presented the results of $M(T)$ measurements of the substrate temperature dependent Eu-rich samples. As for the previous section those measurements show the magnetic moment per formula unit versus temperature, with an external applied field of 10G in fugure (a) and 1000G in figure (b).

In 10G plots it is clear to see how all the samples grown in between 250℃ and 300℃ show a magnetization colose to the ideal one of 7 μ_B per formula unit at low temperature and a M(T) function resembling very good the *Brillouin law* for a $B_{7/2}$ system. The transition to ferromagnetic ordering is observed around 69 k. Only sample A332 grown at 200℃ presents a smaller value and a slight different shape, indicating that an high oxygen deficiency level contributes to deviate from the typical Heisemberg ferromagnet behaviour of EuO.

Lower doping levels intead seems not affecting too much the ferromagnetic coupling via double and super-exchange mechanism between Eu ions.

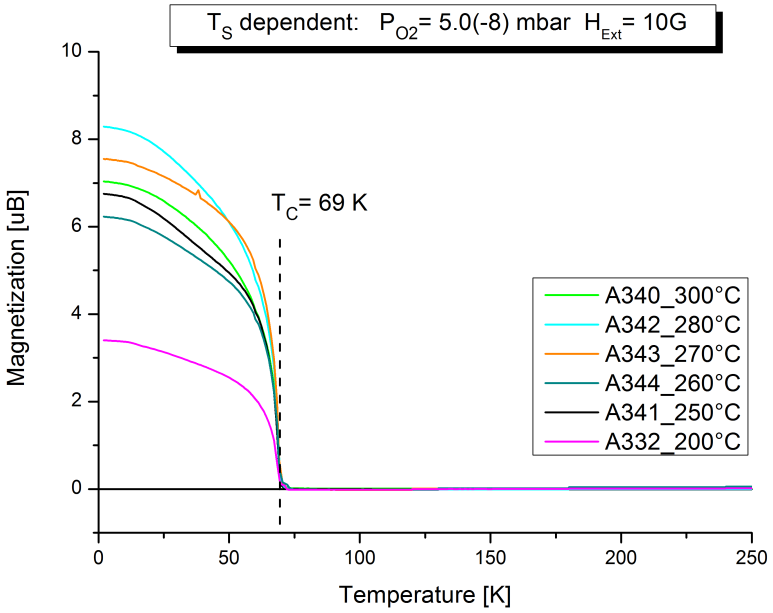

(a) 10G

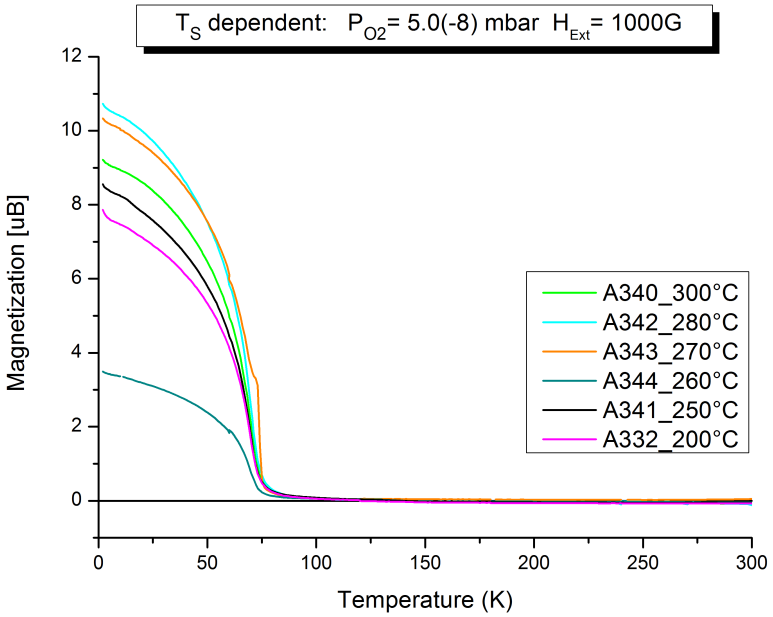

(b) 1000G

Figure 5.19: Magnetization per formula unit of EuO films grown under various oxygen pressures P_{O2}.

Of course the more stoichiometric are the films the higher is the ferromagnetic coupling, which results in a higher measured magnetic moment for the corresponding sample.

It is interesting to see in this case that no big difference is observed in the magnetization curves of samples showing MIT (A332, A341 and A344), and those one which does not (A340, A342 and A343). This clearly confirms our first hypotesis: metal-insulator transition does not arises only for those Eu-rich samples showing good ferromagnetic coupling, but they have to contain an amount of oxygen deficiency sufficently high to activate this mechanism.

Figure 5.20 shows the hysteresys curves $M(H)$ of two samples out from this set, one above and one below the critical oxygen vacancy level for MIT to occurr. What is remarkable is the small difference between the two hysteresis curves and they saturation level for both around 9-10^4 μ_B, with the only difference that in sample A341, richer in Eu, the saturation level is reached for lower values of the applied external fields. Sample A342 (no MIT) instead shows a more gradual rise of the hysteresis curve to saturation, similar to the stoichiometric reference sample A327 of Figure 4.2, but with a definitely lower coercive field (H_C=37 Oe).

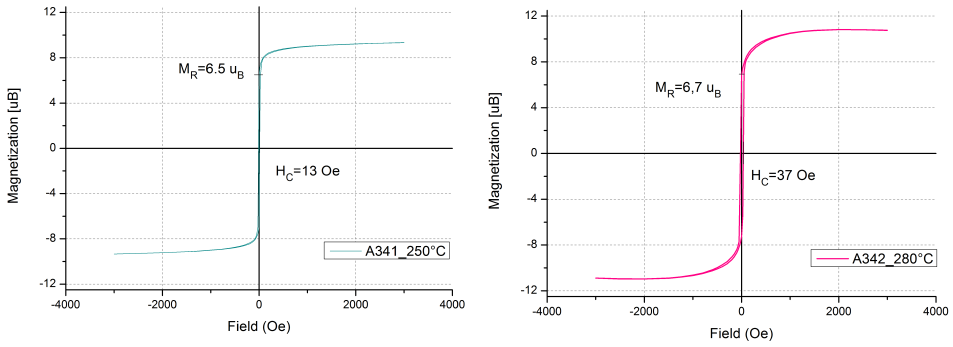

(a) A341: MIT (b) A342: no MIT

Figure 5.20: Hysteresis curves of sample A341 and A342.

[4] such a high value is not likely real and has to be imputable to deviations of the real thickness from the assumed value

Chapter 6

Conclusions

Eu-rich EuO thin films were succesfully grown on YSZ(100) substrates. Samples with different oxygen vacancies concentrations were obtained by departing from the growth conditions of the so called *distillation technique*, in particular by systematically varying oxygen pressure and substrate temperature of the growing films.

The amount of oxygen vacancies was succesfully determined by the analysis of XPS spectra and they were correlated to the observed properties of the different films.

A precise analysis of transport and magnetic properties was well obtained by resistivity and SQUID measurements, respectively, which provided elemental informations to determine the oxygen vacancy limiting concentration for the occurence of metal-insulator transistion in Eu-rich EuO thin films.

RHEED and LEED patterns provided us useful informations about the quality of the crystalline structure of the samples during and after growth. Moreover RHEED oscillations periods were employed to estimate the thickness of the samples.

From the results described in the present work the conclusion are straightforward and we can draw the following picture for Eu-rich EuO samples grown on YSZ(100).

- the O/Eu rate calculated from the XPS spectra was determined to be 0.25 for a stoichiometric EuO film[1] grown under distillation technique. This sample was used as a reference for the calculation of the oxygen vacancy concetration and it was succesfully determined that all Eu-rich samples presented an O/Eu rate below this value.

- From the first set of samples grown at constant T_S=200 ℃ the *critical oxygen pressure* to see MIT in the films was determined to be

[1] the sample is A327 grown at $P_{O2} = 3.5 \times 10{-}8$ mbar and T_C=420℃

$P_{O2} = 5.5 \times 10^{-8}$ mbar. All the samples grown below this value indeed presented typical semiconductor behaviour above T_C and a strong drop in resistance below it. The corresponding amount of oxygen vacancies has been determined to be 20%.

- From the second set of measurements at constant $P_{O2} = 5.0 \times 10^{-8}$ the *critical substrate temperature* for the occurence of MIT in the film was 260 ℃ . Although all the films grown in these conditions were Eu-rich, only those with an oxygen deficiency concentration greater than 19.2%[2] were showing MIT.

- Epitaxial, layer-by-layer growth was succesfully obtained for all the samples grown below the critical oxygen pressure $P_{O2} = 5.5 \times 10^{-8}$ mbar. As a result we observe good single crystalline and free of contaminants EuO thin films. Only sample A334 and A333, grown at higher presures, show the presence of higher oxidation states in XPS valence band spectra while LEED and RHEED patterns revealed the presence of policrystals in the films.

- The doping concentration has huge effect on transport properties of EuO in general. Even resistance at room temperature varies a lot depending on the growth conditions. As the defects concentration is inversely proportional to P_{O2} and T_S values, similarly resistance decreases while increasing the oxygen vacancy concentration.

- A large oxygen deficiency concentration gives rise to Fermi foot in XPS valence band spectra, indicating the metallic character of those films which are also showing MIT below T_C. On the other side, those samples with a low oxygen deficiency concentration present no fermi food and a considerable charging effect during photoemission measurements, which is more pronounced, the lower the doping level is.

- Magnetic properties seem not to be affected significantly from the oxygen vacancy concentration. Curie temperature is measured to be about 69 K for all the samples. Only the intensity of the saturation magnetization varies with the stoichiometry of the film. In particular the higher is T_S the more stoichiometric is the rilm and thus the closer is the magnetization to the ideal value of 7 μ_B per unit cell.
  Moreover for samples grown at low P_{O2} and low T_S we see the presence of tails in M(T) curves at 1000G up to 150 K. This could arise from the Eu metal cluster which are forming in the films due to the lack of oxygen and the very difficult re-evaporation of Eu adatoms.

[2] data from sample A343

As a direct consequence therefore we can infer that to see metal insulator transition in Eu-rich EuO thin films it is required an oxygen deficiency level of about 20%. This value was found first in the oxygen pressure dependent measurements and confirmed later by the more precise substrate temperature dependent one.

No enhancement in T_C instead is expected for Eu-rich EuO doped by oxygen vacancy, while huge influence on the resistance value depending on the doping level is observed, with differences of up to 10 orders of magnitude. Moreover the jump in resistance due to MIT is more pronounced for those samples with an oxygen vacancy concentration slightly above the critical value.

Moreover, as a general conclusion, the region in the growth condition space where Eu-rich EuO is expected to grow is depicted in Figure 6.1.

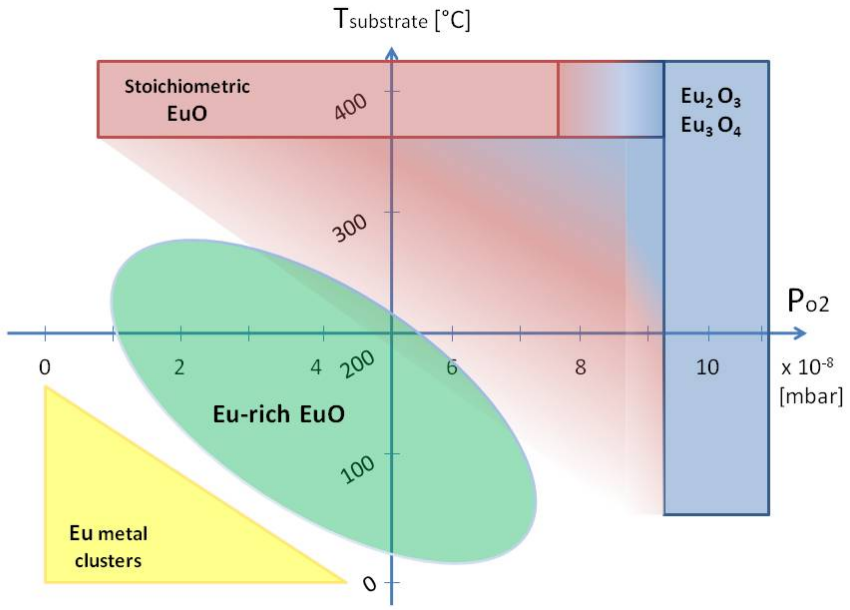

Figure 6.1: Schematic representation of EuO growth conditions including Eu-rich region.

Appendix A

MATLAB code for Background Fitting

Here we report the matlab code of the M-file function used to integrate and remove the background from the XPS spectra for chemical composition analysis of the films. Stoichiometry and oxygen vacancy level is thus determined.

The command line used to import datas into Matlab workspace is the following:

```
data import ('Folder/XPS2010_XXXX.txt', ' ', 44)
```

where `Folder` indicates the path where the SCIENTA file is located, `XXXX` the number of the scan to be analyzed, and `44` is the number of header strings to be skipped before getting the data ones.

M-file for O1s peak

```
function[v] = int1s(d, step, sweeps, m)

x=d.data(1:500,1)';
y=d.data(1:500,2)';
d=d.data(1:500,2)';

n=length(y);

d=d-d(n);
y=y-y(n);

for j=1:m

   for i=0:n-1
       b(n-i)=trapz(y(n-i:n));
   end

   b=step*b;
   a=d(1)/b(1);
   s=d-a*b;

   y=s;

end

plot(x,s)
hold on
plot(x,d, 'r')
plot(x', zeros)

v=(step*trapz(s))/sweeps;
```

M-file for Eu4d peak

```
function[v] = int4d(d, step, sweeps, m)

x=d.data(481:1101,1)';   % integration from 1334ev to 1365ev for Eu4d peak
y=d.data(481:1101,2)';
d=d.data(481:1101,2)';

n=length(y);

d=d-d(n);
y=y-y(n);

for j=1:m

    for i=0:n-1
        (n-i)=trapz(y(n-i:n));
    end

    b=step*b;
    a=d(1)/b(1);
    s=d-a*b;

    y=s;

end

plot(x,s)
hold on
plot(x,d, 'r')
plot(x', zeros)

v=(step*trapz(s))/sweeps;
```

Bibliography

Bibliography

[1] P. Wachter. emphHandbook of Physics and Chemistry of Rare Earths, volume 2. K. A. Gschneidner and L. R. Eyring, Amsterdam, North-Holland (1979)

[2] P. Wachter, Helv. Phys. Acta 37, 637 (1964)

[3] M.J. Freiser, F. Holtzberg, S. Methfessel, G. D. Pettit, M.W.Shafer and J. C. Suits, Helv. Phys. Acta 41 , 832 (1964)

[4] B. T. Matthias, R. M. Bozohrth, and J. H. van Vleck, Phys. Rev. Lett 7, 160 (1961)

[5] J. B. Torrance, J. W. Shafer, and T. R. McGuire, Phys. Rev. Lett. 29, 1168 (1962)

[6] J. Suits, Bull. Am. Phys. Soc. 8, 381 (1963)

[7] T. R. McGuire and M. W. Shafer, J. Appl. Phys. 35, 984 (1964)

[8] G.Bush, P. Junod and P. Wachter, Phys. Lett. 12:11, (1964)

[9] R. R. Heikes and C. W. Chen, Physics 1, 159 (1964)

[10] J. H. Greiner and G. J. Fan. emphLongitudinal Magneto-Optica Kerr Effect in EuO and EuS. Appl. Phys. Lett, 9(1):27 (1966)

[11] T. kasuya and A. Yanase. *Anomalous Transport Phenomena in Europium Chalcogenides Alloys.* Rev. Mod. Phys., 40(4):684 (1968)

[12] T. Kasuya, IBM J. Res. Develop 14, 214 (1970)

[13] M. R. Oliver, J. A. kafalas, J. O. Dimmock, and T. B. reed, Phys. Rev. Lett. 24, 1064 (1970)

[14] M. W. Schafer, J. B. Torrance and T. Penney, J. Phys. Chem. Solids 33, 2251 (1972)

[15] M. R. Oliver, J. O. Dimmock, A. L. MuWhorter, and T. B. Reed, Phys. Rev. B 5, 1078 (1972)

[16] M. R. Oliver et al. *Conductivity studies in Europium Oxide.* Phys. Rev. B , 5(3) (1972)

[17] O. Massenet, Y. Capiomont, and N. Van dang, J. Appl. Phys 45, 3593 (1974)

[18] O. W. dietrich, A. J. Henderson, Jr., and H. Meyer, Phys. Rev. B 12, 2844 (1975)

[19] N. W. Aschkroft and N. D. Mermin, *Solid State Physics.* Saunders College Publishing, USA (1976)

[20] H. A. Mook, Phys Rev. Lett. 46, 508 (1981)

[21] A. Mauger and C. Godart. *The magnetic, Optical, and Transport Properties of representatives of a Class of Magnetic Semiconductors: the Europium Chalcogenides* Phys. Rev.,141(2&3):51-176 Aug (1986)

[22] G. M. Roesler, Jr., Y. U. Idzerda, P.R. Broussard, and M.S. Osofsky, J.Appl. Phys. 75, 10 (1994)

[23] G. M. Roesler, Jr., M.E. Filipkowski, P. R. Broussard, Y.U. Idzerda, M. S. Osofsky and R. J. Soulen, Jr., *Superconducting Superlattices and Multilayers*, edited by I. Bozovic, SPIE Bellingham, Vol 2517 (1994)

[24] Y. Shapira, S. Foner, and T. Reed, Phys. Rev. Lett. B 64, 134409 (2001)

[25] P. G. Steeneken. *New light on EuO thin films: Preparation, transport, magnetism and spectroscopy o a ferromagnetic semiconductor.* Phd thesis, University of Groningen, The Netherlands (2002)

[26] H. Miyazaki, T. Ito, H. Im, K. Terashima, S. Yagi, M. Kato, K. Soda, and S. Kimura. *Singel Crystal Growth and Magnetic, Optical, and Photoelectrical Properties of EuO Thin Film* Jap. Journ. of Appl. Phys. 48 055504 (2009)

[27] M. Moretti. *Magnetic and Transport Propertiers of EuO thin Films* Master Thesis, Politecnico di Milano, Milan (2007)

[28] P. G. Steeneken, L. H. Tjeng, I. Elfimov, G. A. Sawatzky, G. Ghiringhelli, N. B. Brookes and D.-J. Huang, Phys. Rev. Lett. 88, 047201 (2002)

[29] H. von Kanel. *Semiconductor hetero- and nanostructures.* Lecture notes, Politecnico di Milano, Italy (2005)

[30] B. Coloru *Growth of Pure EuO on YSZ(100) substrate* Master Thesis, Politecnico di Milano, Milan (2009)

[31] S. Blundell. *Magnetism in Condensed Matter* University Lecturer in Condensed Matter Physics, University of Oxford. Oxford University Press, USA (2001)

[32] C. Caspers, *Magnetic and light induced properties of doped EuO thin films.* Master Thesis, University of Cologne, Institute of Physics II, Koln, Germany (2010)

[33] Ayahiko Ichimiya and Philip I. Cohen *Reflection High Energy Electron Diffraction.* Cambridge University Press (2004)

[34] N. J. C. Ingle and I. S. Elfimov. *Influence of epitaxial strain on the ferromagnetic semiconductor EuO: First-principles calculations* Phys. Rev. B, 77(12):121202 (2008)

[35] S. Hufner *Photoelectron Spectroscopy: principles and applications.* Springer (2003)

[36] S. Hufner. *Photoemission Spectroscopy.* Springer, Berlin, 3 edition (2003)

[37] *Low level measurements Handbook.* Keithley Instruments, Cleveland, Ohio USA, 6th edition (2004)

[38] N. Iwata, T. Morishita, and K. Kohn, J. Phys. Soc. Japan 69, 1745 (2000)

[39] S. von Molnar and S. Methfessel. *Giant negative Magnetoresistance in Ferromagnetic* $Gd_xEu_{1-x}Se$. J. Appl. Phys., 38(3) (1967)

[40] J. S. Smart, *Effective Field Theories of Magnetism*, W. B. Saunders Company, London (1966)

[41] P. M. Chaikin and T. C. Lubenski, *Principles of Condensed Matter Physics*, Cambridge University Press (2000)

[42] C. Kittel, *Introduction to Solid State Physics.* John Willey & Sons, Inc.(2005)

[43] T. Matsumoto et al. *preparation of Gd-doped EuO_{1-x} thin films and the magnetic and magneto-transport properties.* J.Phys. cond. Matter, 16:6017 (2004)

[44] S. Santos and J. S. Moodera *Observation of spin filtering with a ferromagnetic Eu tunnel barrier* Phys. Rev. B 69, 241203 (2004)

[45] P. Sinjukow and W. Nolting, Phys Rev. B 68, 125107 (2003)

[46] A.G. Swartz, J. Ciraldo, J. J. I. Wong, Yan Li, Wei Han, Tao Lin, S. Mack, J. Shi, D. D. Awschalom, and R. K. Kawakami, *Epitaxial EuO thin films on GaAs* Appl. Phys. Lett. 97, 112509 (2010)

[47] A. Schmehl et al. *Epitaxial integration of the highly spin-polarized ferromagnetic semiconductor EuO with silicon and GaN*, Nature vol.6 nov. (2007)

[48] T. S. Santos, J.S. Moodera, K.V. Raman, E. Negusse, J. Holroyd, J. Dvorak, M.Liberati, Y.U Idserda, and R. Arenholz *Determining Exchange Splitting in a Magnetic Semiconductor by Spin-Filter Tunneling* Phys. Rev. Lett. 101' 147201 (2008)

[49] R. P. Panguluri, T. S. Santos, E. Negusse, J. Dvorak, and Y. Idzerda, J. S. Moodera, B. Nadgorny (2008)

[50] R. Sutarto *EuO and Gd-doped EuO thin films: epitaxial growth and properties* PhD thesis, University of Cologne, insitute of Physics II, Koln, Germany (2009)

[51] R.Sutarto, S. G. Altendorf, B. Coloru, M. Moretti Sala, T. Haupricht, C. F. Chang, Z. Hu, C. Schussler-Langheine, N. Hollmann, H. Kierspel, H. H. Hsieh, H.-J. Lin, C. T. Chen, and L. H. Tjeng, *Epitaxial and*

layer-bylayer growth of EuO thin films on yttria-stabilized cubic zirconia (001) using MBE distillation. 79(20) Physical Review B, 205318 (2009)

[52] R.Sutarto, S. G. Altendorf, B. Coloru, M. Moretti Sala, T. Haupricht, C. F. Chang, Z. Hu, C. Schussler-Langheine, N. Hollmann, H. Kierspel, H. H. Hsieh, H.-J. Lin, C. T. Chen, and L. H. Tjeng. *Epitaxy, stoichiometry and magneti properties of Gd-Doped EuO films on YSZ(001)* Physical Review B 80(8),085308 (2009)

Aknowledgments

The entire work presented in this thesis was carried out in the laboratories of the II Institute of Physics of the University of Cologne, in collaboration with the Max Plank Institute of Dresden under the supervision of Prof. Liu Hao Tjeng. To him and to Prof. Giacomo Ghiringhelli from Politecnico di Milano I want to express my gratitude for making this wonderful experience possible. It has been a great opportunity for me to learn how to work in an advanced research laboratory, to experience a new lifestyle, and to grow once againg.

In particular I wish to deeply thank Prof. Tjeng for the precious time he dedicated to me, for the passion and energy he was able to convey in me and in people working with him and for his fashinating way of making physics. In the same way I want to thank Prof. Ghiringhelli, which helped and supported me from the beginning of this adventure and during the whole period, encouraging and providing me with useful suggestions for the development of the work.

I want to say very big "thank you" to the people I worked in the lab with: Simone Altendorf, Anna Efimenko and Fabio Strigari. With those guys I have spent the most of my time, in the University of Cologne and in NSRRC Syncrotron facility during the Taiwan beam time. I will never forget the endless daytimes and nightimes in the labs, the efforts in mounting, backing and venting the chambers, preparing samples, performing experiments (and yes, tuning the oxygen leak valve!).

Another very big "thank you" to Diana Rata, for her big disposability and attention to the relation between people in the group, and also for correcting me the hundred pages of this work in so few time.

A big big "thank you" to Johnas and Stefano for the logistic support in starting my new life in Germany, for sharing the offices of two different cities, and for the unforgettable week in Japan.

A special thank you to Nicola and to the other friend meet in Cologne for the (unfortunately few) time we spent together and they only know how precious was their support to me.

"Thank you" to my parents, Elisa and Stefano, and to my sister Beatrice. This work is dedicated to them for the continuous support they gave me in 5 years of university studies, thus making it possible to achieve this important

result.

Last but not least a huge "thank you" to Alessandra, for her courage and affection. Even at 1000 km of distance, even half-way around the world she was able to make me feel her closeness and I knew that for any reason she would always been there.

"Thank you" to my friends and to all those people who helped me during this year, through this experience, from home or from abroad, with thousand or few words.

THANK YOU